Melting and differentiation of early-formed asteroids: The perspective from high precision oxygen isotope studies

Journal Item

Chemie der Erde 77 (2017) 1–43

Contents lists available at ScienceDirect

Chemie der Erde

journal homepage: www.elsevier.de/chemer

Invited Review

Melting and differentiation of early-formed asteroids: The perspective from high precision oxygen isotope studies

Richard C. Greenwood[a,*], Thomas H. Burbine[b], Martin F. Miller[a], Ian. A. Franchi[a]

[a] Planetary and Space Sciences, School of Physical Sciences, The Open University, Walton Hall, Milton Keynes MK7 6AA, United Kingdom
[b] Astronomy Department, Mount Holyoke College, South Hadley, MA 01075, USA

ARTICLE INFO

Article history:
Received 25 January 2016
Received in revised form
22 September 2016
Accepted 22 September 2016
Editorial handling - Klaus Keil

Keywords:
Oxygen isotopes
Achondrites
Laser fluorination
Chondrites
Early Solar System processes
Solar nebula
Mass independent variation

ABSTRACT

A number of distinct methodologies are available for determining the oxygen isotope composition of minerals and rocks, these include laser-assisted fluorination, secondary ion mass spectrometry (SIMS) and UV laser ablation. In this review we focus on laser-assisted fluorination, which currently achieves the highest levels of precision available for oxygen isotope analysis. In particular, we examine how results using this method have furthered our understanding of early-formed differentiated meteorites. Due to its rapid reaction times and low blank levels, laser-assisted fluorination has now largely superseded the conventional externally-heated Ni "bomb" technique for bulk analysis. Unlike UV laser ablation and SIMS analysis, laser-assisted fluorination is not capable of focused spot analysis. While laser fluorination is now a mature technology, further analytical improvements are possible via refinements to the construction of sample chambers, clean-up lines and the use of ultra-high resolution mass spectrometers.

High-precision oxygen isotope analysis has proved to be a particularly powerful technique for investigating the formation and evolution of early-formed differentiated asteroids and has provided unique insights into the interrelationships between various groups of achondrites. A clear example of this is seen in samples that lie close to the terrestrial fractionation line (TFL). Based on the data from conventional oxygen isotope analysis, it was suggested that the main-group pallasites, the howardite eucrite diogenite suite (HEDs) and mesosiderites could all be derived from a single common parent body. However, high precision analysis demonstrates that main-group pallasites have a $\Delta^{17}O$ composition that is fully resolvable from that of the HEDs and mesosiderites, indicating the involvement of at least two parent bodies. The range of $\Delta^{17}O$ values exhibited by an achondrite group provides a useful means of assessing the extent to which their parent body underwent melting and isotopic homogenization. Oxygen isotope analysis can also highlight relationships between ungrouped achondrites and the more well-populated groups. A clear example of this is the proposed link between the evolved GRA 06128/9 meteorites and the brachinites.

The evidence from oxygen isotopes, in conjunction with that from other techniques, indicates that we have samples from approximately 110 asteroidal parent bodies (~60 irons, ~35 achondrites and stony-iron, and ~15 chondrites) in our global meteorite collection. However, compared to the likely size of the original protoplanetary asteroid population, this is an extremely low value. In addition, almost all of the differentiated samples (achondrites, stony-iron and irons) are derived from parent bodies that were highly disrupted early in their evolution.

High-precision oxygen isotope analysis of achondrites provides some important insights into the origin of mass-independent variation in the early Solar System. In particular, the evidence from various primitive achondrite groups indicates that both the slope 1 (Y&R) and CCAM lines are of primordial significance. $\Delta^{17}O$ differences between water ice and silicate-rich solids were probably the initial source of the slope 1 anomaly. These phases most likely acquired their isotopic composition as a result of UV photo-dissociation of CO that took place either in the early solar nebula or precursor giant molecular cloud. Such small-scale isotopic heterogeneities were propagated into larger-sized bodies, such as asteroids and planets, as a result of early Solar System processes, including dehydration, aqueous alteration, melting and collisional interactions.

* Corresponding author.
E-mail address: r.c.greenwood@open.ac.uk (R.C. Greenwood).

http://dx.doi.org/10.1016/j.chemer.2016.09.005

There is increasing evidence that chondritic parent bodies accreted relatively late compared to achondritic asteroids. This may account for the fact that apart from a few notable exceptions' such as the aubrite-enstatite chondrite association, known chondrite groups could not have been the parents to the main achondrite groups.

Contents

1. Introduction

Solar System formation began when a dense molecular cloud underwent gravitational collapse to produce an active protostar embedded in an extended disc of gas and dust (Adams, 2010; Boss et al., 2010). Such protoplanetary nebulae evolve rapidly and relatively large planetesimals, with diameters on the order of ~100 km, would have formed on timescales of 10^3–10^4 years (Weidenschilling and Cuzzi, 2006; Weidenschilling, 2011). Dating studies based on the decay of extinct ^{182}Hf ($t_{½}$ = 8.9 Myr) to ^{182}W support such rapid accretion rates and indicate that the parent bodies of the magmatic iron meteorites formed as little as 100,000 years after calcium aluminium-rich inclusions (CAIs), which are the earliest dated Solar System solids (Kruijer et al., 2014). As a result of heating, principally due to the decay of short-lived radionuclides, such as ^{26}Al ($t_{½}$ = 0.73 Myr), these early-formed planetesimals melted and underwent differentiation, producing layered bodies comprising a metallic core, a thick olivine-dominated mantle and a relatively thin "basaltic" crust (Righter and Drake, 1997; Hevey and Sanders, 2006; Sahijpal et al., 2007; Mandler and Elkins-Tanton, 2013). But these first generation differentiated bodies would not have remained intact for long; asteroid 4 Vesta being a notable exception (McSween et al., 2011, 2013; Russell et al., 2012). As a consequence of collisional reprocessing, the vast majority were rapidly disrupted and underwent fragmentation, with the debris being swept up by larger-sized protoplanets (Asphaug et al., 2006).

With the dispersion of nebular gas and/or migration of the outer gas giant planets, the collisional environment became even more energetic and resulted in an era of giant impacts; the end stage being the formation of the present-day terrestrial planets (Chambers, 2004; Walsh et al., 2011; O'Brien et al., 2014).

Achondrites, meteorites that have experienced variable degrees of melting, are predominantly derived from the very earliest generation of differentiated asteroids and so provide a unique insight into the initial stages of terrestrial planet formation. However, the fragmentary character of this record makes it difficult to interpret. In particular, potential genetic relationships between the diverse groups of achondritic meteorites are often difficult to decipher due to the obscuring effects of later events, including parent body metamorphism, impact processes and terrestrial weathering. Oxygen isotope analysis is one technique that has proved to be particularly important in understanding such links (e.g. Clayton and Mayeda, 1996; Greenwood et al., 2005, 2006; Franchi, 2008). Here we focus on the results from recent high-precision oxygen isotope studies of achondrites using the laser fluorination technique and examine their implications for our understanding of early Solar System processes. However, the results from a single technique cannot be viewed in isolation and so in discussing these recent findings we attempt to integrate the information they provide into a wider geochemical context.

Mainly as a result of the pioneering studies of Robert Clayton and co-workers at the University of Chicago, oxygen isotope analysis now plays a central role in almost all areas of cosmochemical research. Before looking in detail at achondrites, we first examine the reasons why oxygen isotope analysis has proved to be such an important tool in the study of meteorites and discuss various aspects of the laser fluorination technique, which currently provides the highest levels of precision available for sample analysis.

2. Oxygen isotope analysis

2.1. Oxygen – the magic element!

It will come as little surprise to learn that oxygen is a uniquely important element. After all, life as we know it, including scientific research, would be impossible without oxygen! It is perhaps less obvious why oxygen should arguably have become the single most powerful tool available to the cosmochemist studying the origin and evolution of the early Solar System.

Oxygen is a highly reactive non-metal that readily forms compounds with other elements. It is the first element in group 16 of the periodic table, has an electronic configuration of $1s^2, 2s^2, 2p^4$ and so readily forms a double covalent bond with another oxygen atom, with pure oxygen being a colourless, odourless gas with the formula O_2. Credit for the discovery of oxygen is controversial, being split three ways between the Swedish apothecary Carl Scheele, the English chemist Joseph Priestley and the French chemist Antoine Lavoisier; the latter generally considered to be the founder of modern chemistry (Lane, 2002). Scheele appears to have been the first to have made the discovery in 1773, or sometime before. However, Priestly published his results first, in 1774 and so is generally given priority. Oxygen was named by Lavoisier, who demonstrated that it was the reactive constituent of air and the element responsible for both combustion and respiration. In fact, Lavoisier was actively undertaking experiments on air when he was dragged off to a tribunal by a revolutionary mob and subsequently beheaded in May 1794 on an obscure charge relating to soldier's tobacco! (Lane, 2002).

Oxygen is the third most abundant element in the Solar System after hydrogen and helium, as determined by spectroscopic measurements of the Solar Photosphere (Fig. 1) (Lodders, 2003).

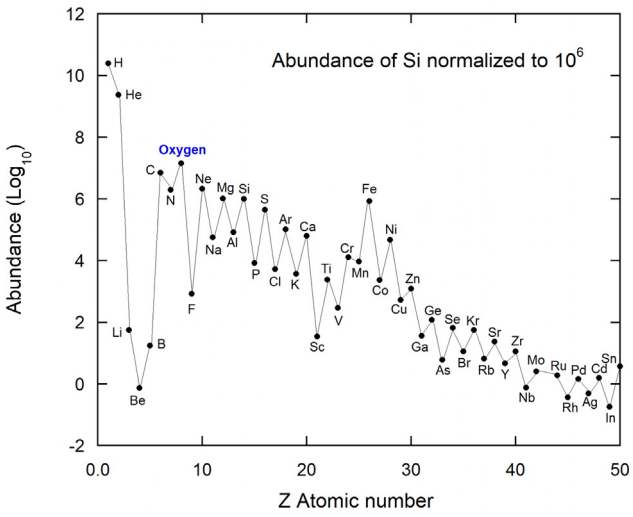

Fig. 1. Elemental Solar System abundances up to z = 50 illustrating that oxygen is the third most abundant element after hydrogen and helium (Data: Lodders, 2003).

However, more important than its high relative abundance is the fact that oxygen is a major mineral-forming element. Comprising close to 46 wt.% of the Bulk Silicate Earth (Javoy et al., 2010), oxygen is the most abundant element in the Earth's crust and mantle (Allègre et al., 1995). Even when the core is included to derive a total Bulk Earth composition, oxygen at 32.4 wt.% remains the most abundant element, just ahead of iron at 28.2 wt.% (Allègre et al., 1995). In the case of Venus and Mars, oxygen is also roughly in equal abundance to iron (both ~30 wt.%), whereas Mercury is anomalously iron-rich (Elser et al., 2012). But while its Solar System and Bulk Earth abundances may be important, perhaps the most critical feature of oxygen is the fact that it readily combines with hydrogen to form water. Water is the essential compound for life, is ubiquitous throughout the Solar System and undoubtedly played a major role in its early evolution. A significant proportion of the water in the solar nebula was inherited from the parent molecular cloud (Cleeves et al., 2014).

2.2. Oxygen isotopes – notation and mass fractionation

Unlike the other important light elements, nitrogen and carbon, which have only two stable isotopes, oxygen has three: ^{16}O (99.757 atom.%), ^{17}O (0.038 atom.%), ^{18}O (0.205 atom.%) (Rosman and Taylor, 1998). This is helpful because it means that two sets of isotope ratios ($^{17}O/^{16}O$ and $^{18}O/^{16}O$) can be measured and then plotted on what is generally referred to as an oxygen three-isotope diagram (Fig. 2). The oxygen isotope composition of a sample is measured with reference to the international reference standard VSMOW (Vienna Standard Mean Ocean Water) provided by the International Atomic Energy Agency (IAEA) in Vienna as a replacement for the earlier standard SMOW (Craig, 1961). In fact, SMOW never physically existed, but was an average of values for a number of ocean water samples that was then tied to the distilled water sample NBS-1, which was actually available for measurement. In reality, isotopic measurements of samples are made with reference to a working laboratory gas that has been nominally calibrated relative to VSMOW. In fact, direct calibration on the VSMOW scale is an analytically difficult procedure and the subject of current debate. The issues involved are beyond the scope of this review, the reader is referred to the paper by Pack and Herwartz (2014) and the subsequent comment by Miller et al. (2015) for further details on this topic.

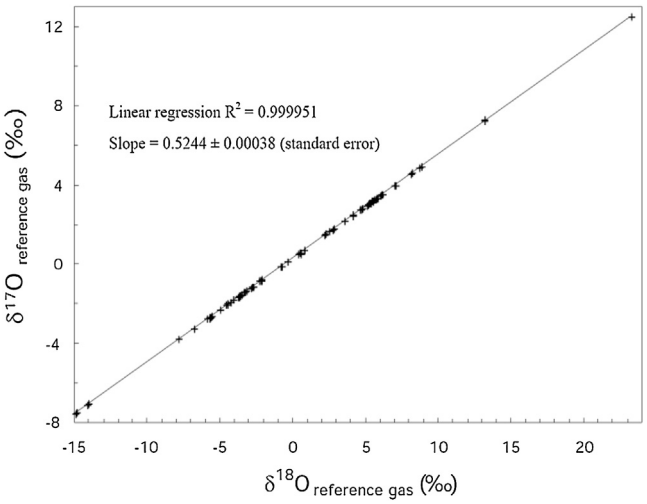

Fig. 2. Oxygen three-isotope diagram for 47 terrestrial whole-rock and mineral separates (Miller et al., 1999).

Oxygen isotope ratios are conventionally expressed using the delta notation first formally defined by McKinney et al. (1950) and recently revised by the Commission on Isotopic Abundance and Atomic Weights (CIAAW) (Brand, 2011):

$$\delta^{18}O = ({}^{18}R_{sample} - {}^{18}R_{VSMOW})/{}^{18}R_{VSMOW} \text{where} R = {}^{18}O/{}^{16}O$$

and

$$\delta^{17}O = ({}^{17}R_{sample} - {}^{17}R_{VSMOW})/{}^{17}R_{VSMOW} \text{where} R = {}^{17}O/{}^{16}O$$

Because delta values are very small and dimensionless, it is usual to express them as parts per thousand ('per mil'). Thus, a delta value of 0.01 would generally be written as 10 per mil (or 10‰).

In a similar manner to other light elements, oxygen is readily fractionated by a variety of chemical and physical processes. The magnitude of this variation is a function of the masses of the isotopes and is therefore referred to as mass-dependent fractionation. Thus, for a particular process the $^{18}O/^{16}O$ ratio will vary approximately twice as much as the $^{17}O/^{16}O$ ratio.

When oxygen isotope analyses of terrestrial silicate rocks and minerals are plotted on a three-isotope diagram, with $\delta^{18}O$ plotted as the abscissa (Fig. 2), the resultant line of slope ~0.52 (Matsuhisa et al., 1978) is commonly referred to as the terrestrial fractionation line (TFL) (e.g. Rumble et al., 2007). Deviations from this reference line are conventionally expressed as: $\Delta^{17}O = \delta^{17}O - 0.52\,\delta^{18}O$ (e.g. Clayton and Mayeda, 1988). As noted by Clayton and Mayeda (1996), the linear relationship between $\delta^{17}O$ and $\delta^{18}O$ is actually an approximation, derived from:

$$\left(\frac{{}^{17}R_{sample}}{{}^{17}R_{VSMOW}}\right) = \left(\frac{{}^{18}R_{sample}}{{}^{18}R_{VSMOW}}\right)^{\lambda}$$

with the exponent λ varying between ~0.5 and 0.5305 depending on the nature of the samples under investigation and whether a kinetic or equilibrium mass fractionation process is involved (Miller, 2002; Young et al., 2002; Pack and Herwartz, 2014). In delta notation, the equation becomes:

$$1 + \delta^{17}O = (1 + \delta^{18}O)^{\lambda}$$

This provides the basis of a more accurate and robust formulation of $\Delta^{17}O$, as proposed by Miller (2002):

$$\ln(1 + \Delta^{17}O) = \ln(1 + \delta^{17}O) - \lambda\ln(1 + \delta^{18}O)$$

where λ corresponds to the slope of a reference fractionation line. For $\Delta^{17}O$ values of less than 3‰, which includes the vast majority of the samples considered in this review, $\Delta^{17}O$ can be defined as:

$$\Delta^{17}O = \ln(1 + \delta^{17}O) - \lambda\ln(1 + \delta^{18}O)$$

without loss of accuracy. With regard to an appropriate value of λ: some authors have selected a value based on the actual fractionation line given by a collection of terrestrial samples (e.g. Miller, 2002; Spicuzza et al., 2007; Pack et al., 2013); others have assigned it as the high temperature equilibrium limit value of 0.5305 (Wiechert et al., 2004; Pack and Herwartz, 2014). There is, as yet, no consensus on which reference line should be chosen for defining $\Delta^{17}O$. This can lead to misleading comparisons, if care is not taken to ensure that all $\Delta^{17}O$ values are defined consistently. An additional complication is that it has recently been shown (Tanaka and Nakamura, 2013; Miller et al., 2015) that terrestrial rocks and minerals form fractionation arrays which are slightly offset (by ~30–70 ppm) from the VSMOW reference material.

For much of the past decade or so, $\Delta^{17}O$ measurements made at the Open University laboratory have been reported in the format proposed by Miller (2002) and with reference to a line of slope 0.5247 passing through VSMOW. This format and slope are generally used throughout this review unless otherwise stated. However, as a result of the extensive studies undertaken by the Chicago group, a large database of analyses in the literature, collected using the nickle "bomb" technique (Section 2.3), are quoted using the conventional version of $\Delta^{17}O$ i.e. $\Delta^{17}O = \delta^{17}O - 0.52\,\delta^{18}O$. It would be misleading to recalculate these analyses using the format of Miller (2002), therefore in some instances $\Delta^{17}O$ values for laser fluorination data have been calculated using a slope factor of 0.52 to aid comparison with this earlier dataset.

2.3. *Oxygen isotope analysis of meteorites – a brief historical perspective*

Quantitatively liberating oxygen from silicate and oxide minerals is no easy task in view of the strength of the Si–O bond. The early development of oxygen isotope cosmochemistry essentially involved the quest for the most appropriate (and safe) reagents and the optimal analytical conditions required to release oxygen and then measure its isotopic composition. All successful methodologies involved the use of either halogens, or halogen-bearing compounds, to displace oxygen from the silicate/oxide structure. However, the highly reactive character of these compounds brings with it significant health and safety issues. One of the first attempts to analyze oxygen from meteorites was undertaken by Manian et al. (1934) using a resistance wound electric furnace heated to 1000 °C. The meteorite samples were mixed with graphite, and carbon tetrachloride was used as the chlorinating agent. The attempt was unsuccessful due to yield problems, the presence of interfering compounds and the poor resolving power of the mass spectrometers available at that time. The problem of inconsistent and poor yields was improved with the development of externally heated, sealable, nickel reaction tubes (Baertschi and Silverman, 1951), which are sometimes affectionately referred to as "bombs". In the study of Baertschi and Silverman (1951) rock samples, including a eucrite, were treated using mixtures of chlorine trifluoride and hydrogen fluoride at 430 °C, or fluorine and hydrogen fluoride at 420 °C, for periods ranging from 6 to 20 hours. Apart from the obvious problem of having to deal with extremely dangerous compounds, the "bomb" technique suffers from the fact that the maximum reaction temperatures attainable are comparatively low and so reaction times must be long. This results in high system blank levels and even with the long reaction times involved, complete fluorination is rarely achieved, resulting in variable yields

and mass fractionation of the liberated gas. Significant analytical and safety improvements were obtained using the reagent bromine pentafluoride (BrF_5) (Clayton and Mayeda, 1963). A colourless liquid at room temperature (M.P. −61.3 °C, B.P. 40.5 °C) and hence inherently easier to handle in the laboratory than fluorine gas, BrF_5 could be heated in nickel bombs to temperatures as high as 700 °C, thus ensuring more consistent yields (Clayton and Mayeda, 1963).

Until the early 1970s oxygen isotope analysis of extraterrestrial materials was little different to its terrestrial counterpart. While a significant amount of work was undertaken on lunar rocks following the Apollo landings (e.g. Clayton et al., 1971, 1972) and in the application of oxygen isotopes to geothermometry (Onuma et al., 1972), there were few major surprises. This all changed in 1973, the year oxygen isotope cosmochemistry was kick started by the discovery of mass-independent variation in carbonaceous chondrites (Clayton et al., 1973). This work was undertaken following the recognition that calcium, aluminium-rich inclusions (CAIs) in carbonaceous chondrites had a mineralogy similar to the predicted early condensates from a cooling gas of solar composition (Grossman, 1972). What Clayton and his co-workers found when they analyzed these CAIs was that their $\delta^{18}O$ and $\delta^{17}O$ ratios, rather than defining a slope ~0.5, plotted along a line of slope close to 1. As this variation is not due to mass dependency it has come to be known as mass-independent fractionation. At the time of their discovery Clayton et al. (1973) suggested that this variation was due to the injection of a component of almost pure ^{16}O early in Solar System history. An alternative mechanism was subsequently suggested by Thiemens and Heidenreich (1983), who showed experimentally that ozone formation was associated with a slope 1 oxygen isotope anomaly. More recently, the slope 1 variation first identified by Clayton et al. (1973) has been explained in terms of a self-shielding mechanism associated with photodissociation of CO, either in the early solar nebula (Clayton, 2002; Lyons and Young, 2005), or earlier still in the molecular cloud from which the Solar System formed (Yurimoto and Kuramoto, 2004). In the years since the pioneering study of Clayton et al. (1973), detailed analysis of different meteorite groups and their components has demonstrated that they show significant, systematic variations with respect to $\delta^{18}O$ and $\delta^{17}O$ (Clayton, 2003, 2006; Franchi, 2008). The interpretation of such variation for differentiated meteorites is the subject of the latter part of this review.

The availability of affordable and reliable laser systems in the 1980s led to the development of a wide range of microanalytical techniques for both bulk compositional and isotopic studies. Although there had been earlier published descriptions of laser techniques with the potential to undertake oxygen isotope analysis (Franchi et al., 1986), the first working laser fluorination system was developed by Sharp (1990). Compared to early methodologies, laser fluorination has the considerable advantage of operating at high temperatures (>1200 °C), thus ensuring more consistent yields and due to the more rapid rate of reaction (generally just a few minutes) has much lower system blanks. As a result of these advantages, laser fluorination consistently achieves higher levels of precision than were obtainable using the nickel "bomb" technique and it is now routinely used in a large number of stable isotope laboratories worldwide (Sharp, 1990; Elsenheimer and Valley, 1992; Mattey and Macpherson, 1993; Rumble and Hoering, 1994; Miller et al., 1999; Macaulay et al., 2000; Kusakabe et al., 2004; Pack et al., 2007). A description of a typical laser fluorination system is given in the next section.

2.4. Analytical procedures and instrumentation

2.4.1. Laser fluorination and related techniques: overview

Laser fluorination currently provides the highest levels of precision available for oxygen isotope analysis of both terrestrial and extraterrestrial materials. It is routinely possible to analyze 0.5 to 2 mg mineral and whole-rock samples with a precision of at least ±0.08‰ for $\delta^{17}O$, ±0.16‰ for $\delta^{18}O$, and ±0.05‰ for $\Delta^{17}O$ (2σ) (Miller et al., 1999; Valley and Kita, 2005; Greenwood et al., 2014; Starkey et al., 2016). A notable success of the technique has been the measurement of mass fractionation lines (average $\Delta^{17}O$ values) for the Earth, Mars, Vesta and various achondrite parent bodies to a precision of better than ±0.03‰ (2σ) (Franchi et al., 1999; Wiechert et al., 2004; Greenwood et al., 2005, 2006). Under favourable conditions, the levels of precision obtained by secondary ion mass spectrometry (SIMS) techniques can be close to those achieved by laser fluorination (Kita et al., 2009a). However, due to the lower amounts of material being analyzed and the influence of various instrumental and matrix effects, SIMS oxygen isotope analyses are normally of significantly lower precision than can be routinely achieved by laser fluorination.

While the process of reacting samples and then cleaning-up the released oxygen gas is an essential part of all laser fluorination systems, the analytical protocols and apparatus that have been developed are generally quite diverse (Rumble et al., 2007). It is certainly the case that no two laser fluorination lines are the same. While the description given here is based primarily on the Open University system (Miller et al., 1999), we also draw on information available in published descriptions from other laboratories. In this section we also look briefly at UV laser ablation systems.

2.4.2. General system configurations

Most laser fluorination systems consist of four principal components (Fig. 3a and b): (1) an infrared, or near-infrared, laser and beam delivery system, (2) a sample chamber, (3) a sample gas clean-up line, and (4) an isotope-ratio mass spectrometer.

2.4.3. Laser systems and sample chamber configurations

CO_2 lasers are used in most laser fluorination systems (10.6 μm, 12–50 W max. power output) (Miller et al., 1999; Kusakabe et al., 2004). Near infrared Nd:YAG lasers (1.064 μm, 60 W max. power output) have also been employed (Mattey and MacPherson, 1993). The laser is sometimes fixed, with the static laser beam delivered to the sample chamber via an optic system of half-silvered mirrors and prisms. In this configuration the sample chamber is mounted on a motorized X-Y-Z stage. However, it is now more normal to use commercially available X-Y-Z gantry mounted lasers (e.g. esi MIR 10 system, or Teledyne Photon Machines Fusion CO2 system) in association with a fixed sample chamber. In either configuration the sample is viewed by video camera through a BaF_2 window (for CO_2 lasers) in the top of the chamber.

Sample chamber configurations vary enormously from system to system. The arrangement described by Miller et al. (1999) consists of a two-part chamber, made vacuum tight using a compression seal with a copper gasket and quick-release KFX clamp. In terms of maintaining a high vacuum, and hence low blank levels, the sample chamber is a particularly problematic component in any laser fluorination system. This results from the fact that, during sample loading, this portion of the line needs to be opened to the atmosphere. To facilitate this, either a gasket system, or fluoroelastomer O-rings, or both, are employed (e.g. Sharp, 1990; Miller et al., 1999; Kusakabe et al., 2004). Such seals invariably have non-trivial leak rates and the fluoroelastomer O-rings inevitably outgas hydrocarbons. In addition, exposure of the sample chamber surfaces to the atmosphere means that they become coated in a layer of moisture, which further increases the blank once BrF_5 is introduced into the chamber. As a consequence of these problems, the sample chamber undoubtedly makes the largest contribution to the overall system blank.

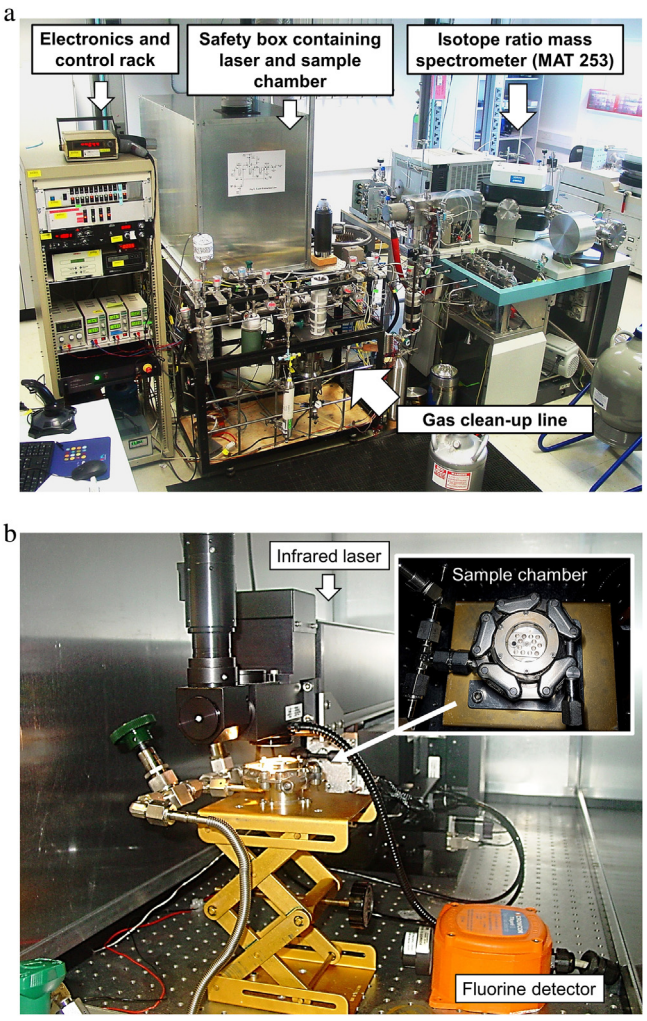

Fig. 3. Laser fluorination line at the Open University. (a) Photo showing the main component sections of the line (see text for further details). (b) The sample chamber and infrared laser are housed within the laser safety box. Inset: Two-part chamber with the upper half incorporating a BaF_2 window for simultaneous viewing and laser-heating of samples. The two halves of the chamber (lower half not visible) are kept vacuum tight by a compression seal involving an internal copper gasket and external quick-release KFX clamp. Samples are loaded in a removable Ni block with drilled wells (14 are present in the example shown in Fig. 3b).

2.4.4. Sample gas clean-up line

Following reaction with excess BrF_5 (F_2 gas is used as the fluorinating agent in some systems), the product gases are expanded into a cleanup-line, which generally consists of at least two liquid nitrogen "U" tube traps, separated by a bed of heated KBr. The first liquid nitrogen trap removes the majority of condensable gases. The bed of heated KBr serves to remove any F_2 gas by reaction to form KF, with the displaced Br_2 removed in the second liquid nitrogen trap. Following these clean-up procedures, the purified O_2 gas is trapped down on 13X molecular sieve pellets cooled to liquid nitrogen temperatures. The molecular sieve is then isolated from the clean-up line and heated up, with the released O_2 gas expanded into the inlet system of the mass spectrometer. In some systems additional clean-up steps are employed based on gas chromatography technology, with the aim of eliminating any potential residual traces of NF_3 (Pack and Herwartz, 2014).

2.4.5. Isotope-ratio mass spectrometer

In most systems, the mass spectrometer used is either a ThermoFisher MAT 253 (or the earlier 251 and 252 models), or a Micromass Prism III. Both of these instruments have relatively high mass resolution ($m/\Delta m = \sim 250$). However, lower resolution mass spectrometers, such as the Finnigan-MAT Delta^{plus} ($m/\Delta m = \sim 95$) are sometimes used.

2.4.6. How laser fluorination differs from UV laser ablation

It is a common misconception that laser fluorination is capable of undertaking *in situ* spot analysis. While infrared lasers can be focused to a limited extent, significantly better spatial resolution is achieved by shorter wavelength lasers and hence ultraviolet (UV) laser ablation was developed as a technique to undertake spot analysis (Wiechert and Hoefs, 1995; Rumble et al., 1997; Farquhar and Rumble, 1998; Young et al., 1998; Wiechert et al., 2002). In terms of the nature of their interaction with the analysis substrate, UV and infrared lasers operate in fundamentally different ways (Farquhar and Rumble, 1998; Young et al., 1998). Infrared lasers essentially act as a narrow diameter heat source, allowing the fluorinating agent to react rapidly with the hot mineral surface. In contrast, UV lasers produce a superheated plume of material from a well-constrained spot, with minimal heating of the surrounding material. Thus, in the case of the infrared laser, the fluorination reactions take place on the mineral surface itself, whereas for the UV laser, these reactions take place within the superheated plume. These differences mean that infrared laser fluorination is essentially a bulk analysis technique with relatively poor spatial resolution, whereas UV laser ablation is capable of spot analysis. F_2 gas is normally used as the fluorinating agent in UV laser ablation as BrF_5 gives less precise results (Rumble et al., 1997). Both laser fluorination and UV laser ablation are capable of achieving comparable levels of accuracy and precision (Farquhar and Rumble, 1998). However, the relatively small amounts of material reacted during spot analysis by UV laser ablation results in lower levels of precision than are routinely achieved by laser fluorination (Young et al., 1998; Wiechert et al., 2002). The UV laser ablation technique has been applied successfully in a wide range of extraterrestrial analysis studies (e.g. Young and Russell, 1998; Wang et al., 2004; McCoy et al., 2011; Dyl et al., 2012).

2.4.7. Future developments

Due to the high levels of precision that can be routinely achieved, at the time of writing, laser fluorination is the technique of choice to undertake bulk oxygen isotope analysis of extraterrestrial materials. Where materials are limited by mass, or spatially resolved analysis of individual phases is required, SIMS techniques are now generally employed (Kita et al., 2009a). Refinement and innovation in a number of areas of laser fluorination technology would significantly help to improve overall levels of precision. As discussed above, the sample chamber is the component that most influences the overall system precision. Airlock shuttle systems have been developed, but are not yet in routine use (e.g. Spicuzza et al., 1998). The capability of changing samples without bringing the chamber up to air would be a major improvement. The system clean-up line certainly also causes fractionation during gas handling. Reducing the overall size of the components involved in the clean-up procedure should also result in improved precision. Finally, the fluorinating reagent itself, BrF_5, probably traps down a fraction of oxygen when it is frozen onto the first liquid nitrogen trap. Controlling the freeze-down process in terms of temperature and duration may help to reduce this potential source of fractionation. The use of mass spectrometers with very high resolving power is a further development that, in conjunction with refined clean-up procedures (e.g. Pack and Herwartz, 2014; Young et al., 2016a), is likely to result in improved system precision (Young et al., 2016b).

3. Oxygen isotope analysis of achondritic meteorites

3.1. Introduction

In this section we look in detail at what information high precision oxygen isotope studies can provide concerning the origin of achondritic meteorites. As we are primarily interested in early Solar System processes, we specifically excluded groups that have a planetary origin, such as martian or lunar meteorites. Achondrites experienced variable degrees of melting and mobilization in an asteroidal setting, such that primary, "chondritic" components (chondrules, CAIs, amoeboid olivine aggregates (AOAs), matrix) are no longer present (Krot et al., 2014; Scott et al., 2015). Achondrites are generally divided into two broad classes: (i) primitive achondrites, and (ii) differentiated achondrites (Weisberg et al., 2006; Krot et al., 2014; Scott et al., 2015). Primitive achondrites are those that exhibit near-chondritic bulk compositions and non-chondritic textures and as a consequence are considered to be the products of relatively low degrees of partial melting and mobilization (Weisberg et al., 2006; Krot et al., 2014). In contrast, differentiated achondrites have more evolved compositions and generally display well-developed igneous textures (Mittlefehldt et al., 1998; Krot et al., 2014). Differentiated achondrites are considered to be derived from sources that experienced moderate to high degrees of partial melting, resulting in large-scale differentiation (Krot et al., 2014; Scott et al., 2015). Along with the differentiated achondrites we also examine the origin of the stony-iron meteorites and provide a brief summary of what has been learnt from oxygen isotope studies concerning the formation of iron meteorites.

There is complete gradation in degrees of melting and mobilization between primitive and differentiated achondrites, such that there is some disagreement as to which category certain meteorite groups should be assigned (Krot et al., 2014; Scott et al., 2015). Weisberg et al. (2006) consider the primitive achondrite "classic core groups" to be the acapulcoites, lodranites, winonaites and silicate-bearing IAB and IIICD irons. These authors also include the brachinites and ureilites as primitive achondrites, but point out that there is continuing uncertainty about whether these groups are residues or cumulates. In contrast, Hutchison (2004) suggests that the high-degree of crystal-liquid fractionation indicated by ureilite mineralogy does not support their designation as primitive achondrites. A cumulate origin for the ureilites, as well as the brachinites, is also proposed by Mittlefehldt (2005a, 2008). In this paper, in addition to the "classic core groups" of Weisberg et al. (2006), we have included both ureilites and brachinites amongst the primitive achondrites. There are a number of reasons for considering the brachinites to be *bone fide* primitive achondrites; these include the near-chondritic, lithophile element abundances displayed by Brachina (Weisberg et al., 2006) and the oxygen isotope heterogeneity of the group as a whole (Section 3.2.2) (Greenwood et al., 2012). Despite the uncertainty concerning the origin of ureilites we include them with the primitive achondrites in this review on account of their extreme oxygen isotope heterogeneity (Table 1, Fig. 25), which indicates that their parent body did not experience melting on a scale similar to the HEDs (Section 3.2.3).

3.2. Primitive achondrites

3.2.1. Acapulcoite-lodranite clan

Acapulcoites are relatively fine-grained (150–230 μm), with an equigranular texture and an essentially chondritic mineralogy, consisting of olivine ($Fa_{4\text{-}13}$) (all mineral compositions in mol%), low-Ca pyroxene ($Fs_{1\text{-}9}$), Ca-rich pyroxene ($Fs_{46\text{-}50}$, $Wo_{43\text{-}46}$), plagioclase ($An_{12\text{-}31}$), metal and troilite (McCoy et al., 1996, 1997a; Mittlefehldt 2005a, 2008; Weisberg et al., 2006). Relict chondrules have been reported in a number of acapulcoites (Schultz et al., 1982; McCoy et al., 1996; Rubin, 2007). In comparison, lodranites are coarser-grained (540–700 μm), but similarly have equigranular textures and nearly identical mineral compositions to the acapulcoites (McCoy et al., 1997a,b). However, in contrast to the acapulcoites, they are depleted in troilite and plagioclase (McCoy et al., 1997a,b; Mittlefehldt, 2005a, 2008; Weisberg et al., 2006). In terms of their grain-size and mineralogy, a number of meteorites are transitional between the acapulcoites and lodranites (i.e., EET 84302, GRA 95209, FRO 93001). In view of their similar mineralogy, geochemistry and isotopic composition, there is a general consensus that the acapulcoites and lodranites are derived from a single parent body (McCoy et al., 1997a; Mittlefehldt, 2008). In recognition of their common characteristics, acapulcoites and lodranites have been given "clan" status (Weisberg et al., 1995, 2006).

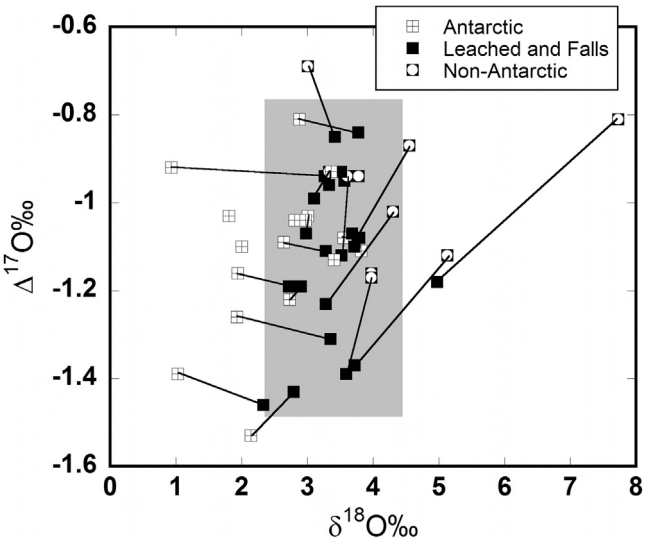

Fig. 4. Oxygen isotopic composition of untreated acapulcoite and lodranite finds compared to falls and EATG-treated residues. Tie lines link untreated samples with their respective EATG residues. Antarctic finds are systematically displaced to lower $\delta^{18}O$ values compared to their EATG residues and non-Antarctic finds are shifted to higher $\delta^{18}O$ values. The diagram also shows that untreated samples are generally displaced to less negative $\Delta^{17}O$ values than falls or EATG residues, consistent with the source of the contamination being terrestrial in origin. The light grey shaded box shows the 2σ variation on the mean $\delta^{18}O$ and $\Delta^{17}O$ values for the EATG residues and fall samples. As it is based on samples that have had terrestrial weathering effects at least partially removed, the grey box provides an indication of the primary oxygen isotope variation in the acapulcoite-lodranite clan. All data from Greenwood et al. (2012).

Acapulcoites and lodranites, being relatively metal and sulphide rich, are particularly susceptible to the effects of terrestrial weathering, which can significantly disturb their oxygen isotope compositions (Clayton and Mayeda, 1996; Greenwood et al., 2012). In order to define primary levels of oxygen isotope heterogeneity in these lithologies it is generally necessary to leach meteorite finds to remove weathering products. When this is done some samples show shifts of nearly 3‰ with respect to $\delta^{18}O$ between leached and unleached pairs (Greenwood et al., 2012) (Fig. 4). At the Open University samples are leached using a solution of ethanolamine thioglycollate (EATG) (Greenwood et al., 2014). Washing in HCl of various strengths is also commonly undertaken in other laboratories as a means of removing terrestrial weathering products (Clayton and Mayeda, 1996; Rumble et al., 2008).

In contrast to $\delta^{18}O$, variation in $\Delta^{17}O$ is only slightly decreased in the EATG residues compared to untreated finds, varying from about −0.8 to −1.5‰ (Fig. 4). The average $\Delta^{17}O$ value of the EATG-treated acapulcoites and lodranites is -1.12 ± 0.36‰ (2σ) (Table 1). This level of heterogeneity is greater than that found in any of the ordinary chondrite groups (Clayton et al., 1991) (Table 1) and

Table 1
Oxygen isotope variation in chondrites and achondrites. See Table S1 for references and additional data.

	$\delta^{17}O‰$	2σ	$\delta^{18}O‰$	2σ	$\Delta^{17}O‰$	2σ
Differentiated Achondrites						
Angrites	2.04	0.18	4.02	0.33	−0.07	0.01
Aubrites	2.84	0.17	5.40	0.34	0.01	0.01
Eucrites and diogenites	1.65	0.32	3.60	0.60	−0.24	0.02
Main-group pallasites	1.36	0.13	2.96	0.24	−0.19	0.02
Mesosiderites	1.77	0.36	3.84	0.70	−0.25	0.02
Planets						
Lunar rocks	2.94	0.13	5.64	0.24	−0.01	0.02
Martian meteorites	2.75	0.35	4.68	0.67	0.32	0.03
Terrestrial – high He olivines	2.60	0.27	4.98	0.52	−0.01	0.01
Primitive Achondrites						
Acapulcoite-lodranite clan						
EATG residue and falls	0.66	0.72	3.41	1.02	−1.12	0.36
Untreated samples	0.63	1.58	3.22	2.68	−1.06	0.38
Brachinites						
EATG residue (inc. Brachina)	2.01	0.70	4.30	1.10	−0.25	0.18
EATG residue (ex. Brachina)	2.14	0.32	4.48	0.54	−0.23	0.14
Untreated samples	2.12	0.64	4.48	1.02	−0.22	0.16
Winonaites						
EATG residues and fall	2.01	1.36	4.81	2.56	−0.51	0.08
Untreated samples	1.43	2.16	3.54	4.14	−0.42	0.16
Ureilites	2.45	1.85	6.54	2.10	−0.96	1.00
Ordinary Chondrites						
H equilibrated	2.85	0.30	4.08	0.44	0.73	0.18
L equilibrated	3.52	0.28	4.70	0.48	1.07	0.18
LL equillibrated	3.88	0.32	5.04	0.48	1.26	0.24
LL3 unequilibrated	4.01	0.34	5.60	0.66	1.10	0.20
Enstatite Chondrites						
EH chondrites	2.76	0.83	5.31	1.25	0.00	0.35
EL chondrites	2.87	0.42	5.48	0.79	0.02	0.13
Carbonaceous Chondrites						
CK3-6 chondrites	−4.25	1.86	−0.28	2.11	−4.10	0.95
CM1-2 chondrites	0.24	2.42	5.65	3.52	−2.70	1.03
CO3 chondrites	−6.89	1.67	−4.02	3.05	−4.80	0.35
CR2 chondrites	−1.00	3.66	1.81	5.33	−1.94	0.99
CV3 chondrites (Ox. & Red.)	−3.56	3.01	0.67	3.44	−3.91	1.27

was most likely inherited from their precursor materials, which were presumably chondritic in composition. Rubin (2007) suggests that the precursor to the acapulcoite-lodranite clan was similar in composition to the CR chondrites, but more enriched in metal and sulphide. When oxygen isotope compositions are plotted according to their respective groups there is almost complete overlap between the acapulcoites and lodranites, consistent with their derivation from a single source (Fig. 5). The cosmic ray exposure ages of the acapulcoites and lodranites show a tight cluster, evidence which is also consistent with a unique asteroidal source for these meteorites (Krot et al., 2014).

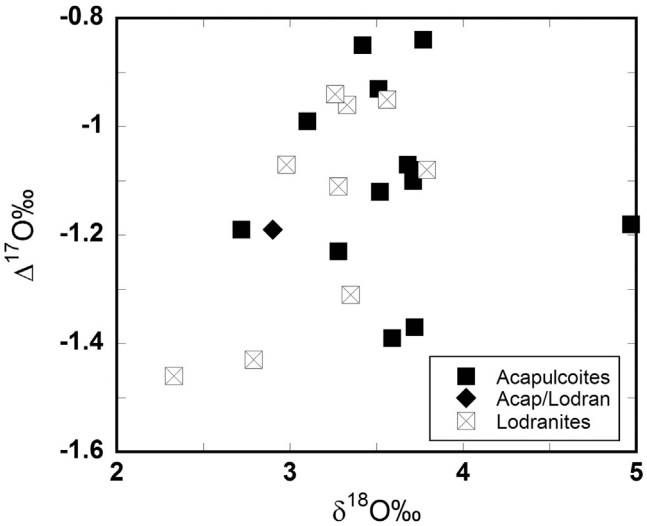

Fig. 5. Oxygen isotopic composition of acapulcoite and lodranite EATG residues plotted in terms of their group designations. It is clear from the plot that there is no systematic difference between the acapulcoites and lodranites and as a consequence both groups are probably derived from a single asteroidal source. All data from Greenwood et al. (2012).

3.2.2. Brachinites

Brachinites are a diverse group of equigranular, olivine-rich achondrites, which can have variable grain-sizes, ranging from 100 to 2700 μm (Mittlefehldt et al., 1998; Weisberg et al., 2006; Keil, 2014). Olivine (Fa_{28-37}), generally homogeneous in individual meteorites, is present in amounts between 80 and 95 vol.%. Ca-rich pyroxene (Fs_{9-16}, En_{38-49}, Wo_{38-48}) is present in variable amounts (3–15 vol.%) in almost all brachinites. Ca-poor pyroxene (Fs_{25-31}) is either present at very low abundance levels, or absent. A notable exception is NWA 595, which contains 10–15 vol.% modal Ca-poor pyroxene. With the exception of Brachina (see below), plagioclase (An_{15-41}) is either present in only small amounts, or absent. Brachinites also typically contain trace to minor amounts of sulphide, metal, chromite and Ca-phosphate.

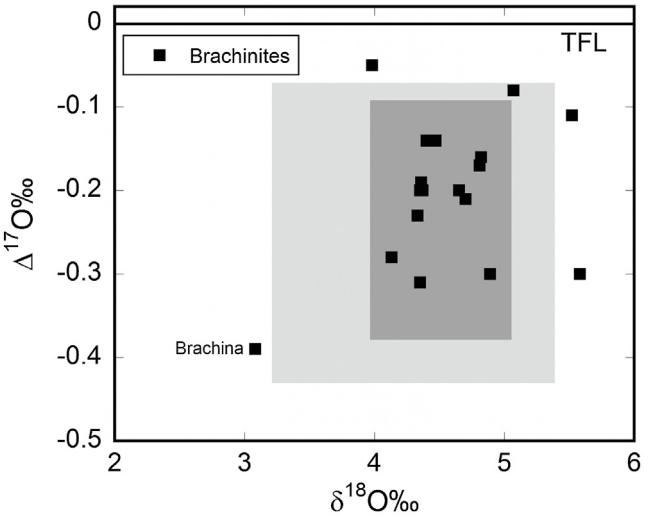

Fig. 6. Oxygen isotopic composition of brachinites. Light grey shaded box shows the 2σ variation on the mean $\delta^{18}O$ and $\Delta^{17}O$ values for EATG residues of 18 brachinites, including Brachina. Darker grey box is for the same group of EATG residues excluding Brachina. Data: Rumble et al. (2008); Day et al. (2012a); Greenwood et al. (2012) and Met Bull Database (NWA 6152, NWA 6474, NWA 7388, NWA 7605, NWA 7904, RaS 309).

There are currently 40 officially classified brachinite specimens listed on the Meteoritical Bulletin Database. All of these are finds and it is clear from the descriptions given that many are significantly weathered. However, brachinites contain only trace amounts of metal and sulphide (the most easily oxidized phases) and as a consequence the shifts in oxygen isotope composition between untreated and EATG residues are much less than seen in the acapulcoites, lodranites or winonaites (Greenwood et al., 2012). Oxygen isotope analyses for 18 EATG-treated brachinites are plotted in Fig. 6 in relation to the fields defined by Greenwood et al. (2012) (see figure caption for further details). The majority of brachinite analyses plot within the inner box in Fig. 6, with a few scattering outside the outer box. Brachina plots away from the inner core brachinite group in Fig. 6. Brachina is known to show some compositional differences when compared to the other brachinites, in particular having a relatively high plagioclase content (~10%) (Nehru et al., 1983, 1992). However, in terms of its major and trace elements, Brachina is close to being chondritic in composition, with other brachinites being more fractionated (Mittlefehldt et al., 2003; Goodrich et al., 2010; Shearer et al., 2010; Day et al., 2012a). Thus, Brachina is probably the most primitive brachinite sample available. There seems no real justification for excluding Brachina, or any of the other samples that scatter at the edge of the outer box in Fig. 6, from the brachinite group. The outer box in Fig. 6 therefore provides an indication of the oxygen isotopic heterogeneity of the group as a whole. The EATG treated brachinites (including Brachina) have an average $\Delta^{17}O$ value of -0.25 ± 0.18‰ (2σ) (Table 1), which is twice the level of $\Delta^{17}O$ variation displayed by the winonaites and equivalent to that found in the H and L group ordinary chondrites (Clayton et al., 1991; Greenwood et al., 2012). Despite the lack of features such as relict chondrules, the $\Delta^{17}O$ variation displayed by the brachinites supports their designation as primitive achondrites.

3.2.3. Ureilites

Ureilites are ultramafic achondrites predominantly composed of olivine and pyroxene, and characteristically contain a significant amount of elemental carbon (up to 5.5 wt.%) (Mittlefehldt et al., 1998; Downes et al., 2008; Barrat et al., 2016a). With 431 specimens currently listed on the Meteoritical Bulletin database, ureilites are the second largest achondrite group after the HEDs. Ureilites are now generally considered to be mantle-derived samples from a single disrupted parent body (Mittlefehldt et al., 1998; Downes et al., 2008; Bischoff et al., 2014; Barrat et al., 2016a).

As a result of the pioneering studies of Clayton and Mayeda (1988, 1996), oxygen isotope evidence has played a critical role in deciphering the origin and early evolution of this enigmatic group (Clayton, 2003; Franchi, 2008). Clayton and Mayeda (1988) showed that ureilites display a much greater level of oxygen isotope variation than any other group of achondrites (Fig. 7). They also demonstrated that ureilites do not fall on a mass-dependent fractionation line, as is the case for most other achondrite groups, but instead define a trend similar to Allende CAIs (Figs. 7 and 8). In addition, they showed that there is a clear correlation between ureilite $\Delta^{17}O$ whole-rock values and olivine and pyroxene iron contents (Fig. 9). On the basis of this evidence, Clayton and Mayeda (1988) suggested that the oxygen isotope heterogeneity displayed by the ureilites was inherited from the group's nebular precursor materials and that this variation was not significantly modified by later parent body processes. The implication of this observation is that the ureilite parent asteroid did not experience a large-scale melting event similar to that proposed for the HEDs (Section 3.3.3).

Detailed studies of polymict ureilites, both by SIMS (Kita et al., 2004; Downes et al., 2008) and laser fluorination (Bischoff et al., 2010, 2014; Rumble et al., 2010; Horstmann et al., 2012) have provided additional insights into the evolution of the ureilite parent body (UPB), and in general have added further support to the original findings of Clayton and Mayeda (1988, 1996). Polymict ureilites are regolith breccias from the near-surface layers of ureilitic asteroids (Downes et al., 2008) and have the advantage over monomict ureilites of containing a range of clast types and hence may be more representative of the UPB as a whole. Both the studies of Kita et al. (2004) and Downes et al. (2008) found that the oxygen isotope compositions of polymict ureilite clasts are identical to those of monomict types and define a relatively tight trend close to the CCAM line. The results from a number of laser fluorination studies of the spectacular Almahata Sitta polymict fall (Jenniskens et al., 2009; Bischoff et al., 2010, 2014; Rumble et al., 2010; Horstmann et al., 2012) are plotted in Figs. 7 and 8. While the oxygen isotope results from Almahata Sitta are very similar to those obtained by SIMS techniques, these laser fluorination analyses define a trend that is offset to the left of the CCAM line, although the slope of both is identical (Fig. 8). It is conceivable that this slight offset from the CCAM line is genuine, alternatively it may reflect a slight analytical difference between laser fluorination and conventional oxygen isotope techniques; the position of the CCAM line being originally defined using the latter methodology (Clayton et al., 1977; Clayton and Mayeda, 1999).

It was suggested by Franchi et al. (1998, 2001), on the basis of laser fluorination analyses of a comprehensive suite of samples (Table S2), that ureilites might be subdivided into four discrete subgroups, each characterized by having a relatively shallow slope on an oxygen three-isotope diagram. Although some subsequent studies (Rumble et al., 2010) have found evidence for clumping of oxygen isotope compositions in ureilites, the discrete series defined by Franchi et al. (1998, 2001) appear to have been replaced by a continuum as more high precision data have been acquired (Figs. 7 and 8) (Downes et al., 2008; Bischoff et al., 2010; Rumble et al., 2010; Horstmann et al., 2012). This evidence suggests that ureilites were originally derived from a single heterogeneous asteroid (Downes et al., 2008).

Due to their lack of plagioclase, superchondritic Ca/Al ratios and depletion in incompatible lithophile elements, ureilites are generally considered to have lost a basaltic component (Mittlefehldt et al., 1998; Kita et al., 2004; Goodrich et al., 2007; Downes et al., 2008). Basaltic material from the UPB may have been lost to space

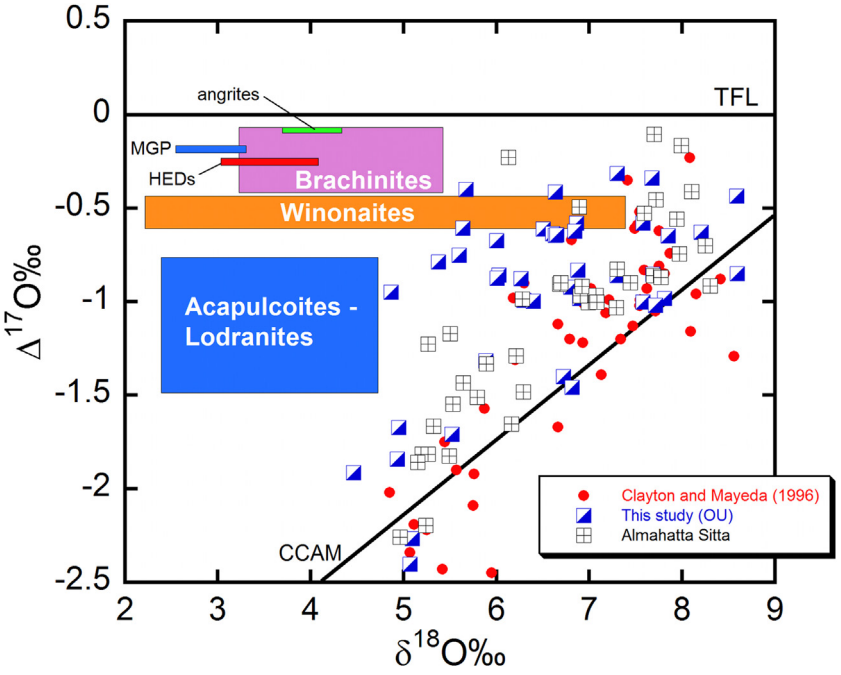

Fig. 7. Oxygen isotopic composition of ureilites shown in relation to other major achondrite groups. Conventional oxygen isotope data from Clayton and Mayeda (1996). Laser fluorination data collected at the Open University are given in Table S2. Laser fluorination data for Almahatta Sitta from Bischoff et al., 2010, 2014; Rumble et al., 2010; Horstmann et al., 2012. Fields for primitive and differentiated achondrites from Greenwood et al. (2012).Abbreviations: MGP: main-group pallasites, HEDs: howardite-eucrite-diogenite suite, TFL: terrestrial fractionation line, CCAM: carbonaceous chondrite anhydrous minerals line (Clayton et al., 1977; Clayton and Mayeda, 1999).

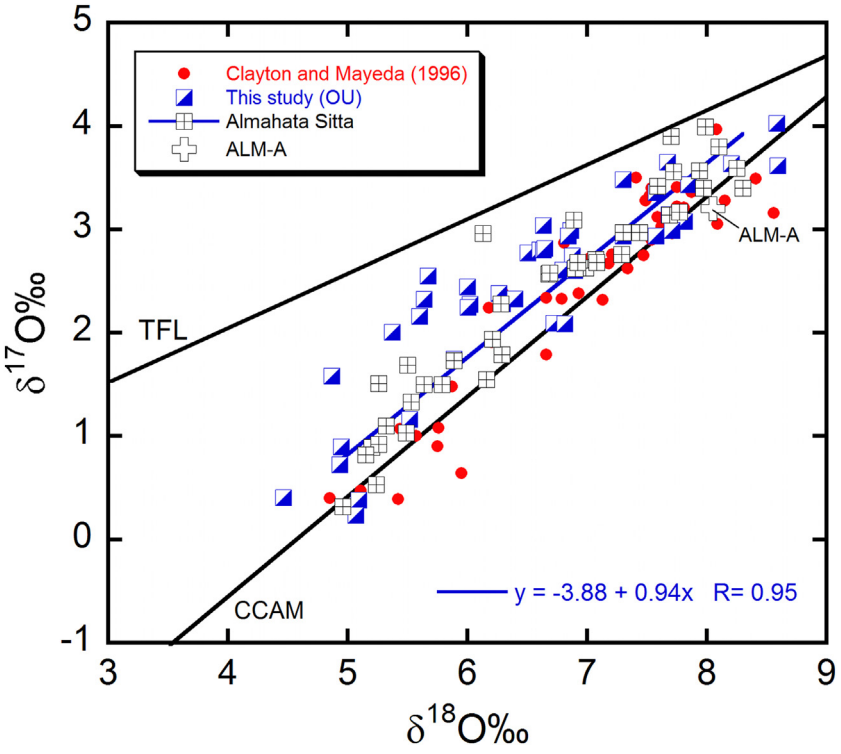

Fig. 8. Oxygen isotopic composition of ureilites. Conventional oxygen isotope data from Clayton and Mayeda (1996). Laser fluorination data this study (Table S2). Almahata Sitta laser fluorination data: see caption to Fig. 7. Best fit line through Almahata Sitta data only. Data for ALM-A trachyandesitic clast from Bischoff et al. (2014). Abbreviations: TFL: terrestrial fractionation line, CCAM: carbonaceous chondrite anhydrous minerals line (Clayton et al., 1977; Clayton and Mayeda, 1999).

during explosive volcanism triggered by low pressure reduction of FeO leading to the formation of CO and CO_2 from graphite entrained in the melt (Wilson et al., 2008). Traces of this missing basaltic component are present in polymict ureilites in the form of plagioclase-bearing clasts (Kita et al., 2004). A unique trachyandesitic clast in the Almahata Sitta ureilite, ALM-A, has a ureilitic oxygen isotope composition (Fig. 8) and appears to show that the UPB was capable of producing highly evolved lavas (Bischoff et al., 2014). REE abundance data for ureilites suggests that at least two distinct magma types were produced during melting of the

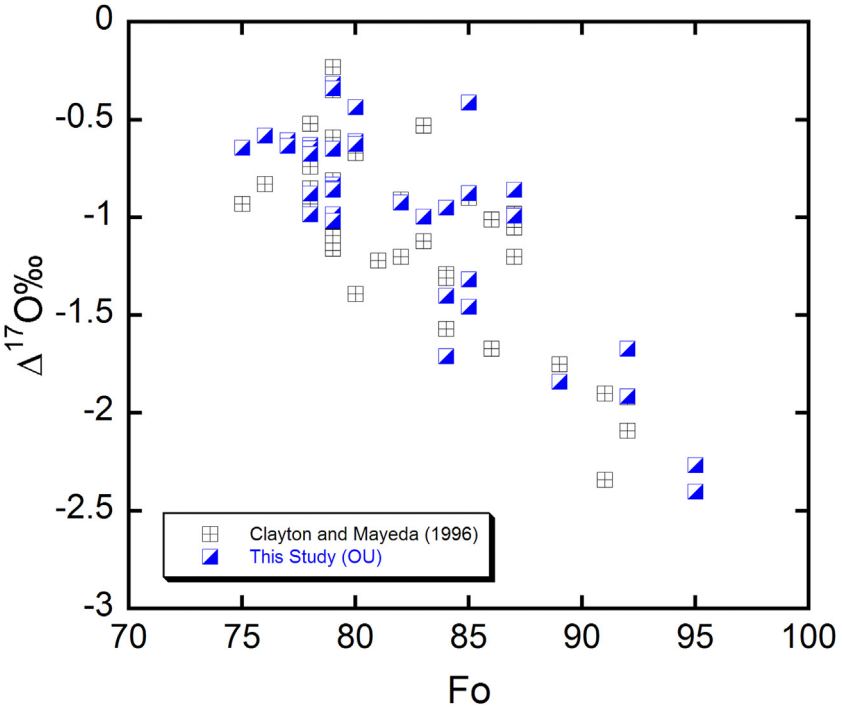

Fig. 9. Plot showing the relationship between olivine and whole-rock oxygen isotope compositions. Oxygen isotope data: Calyton and Mayeda (1996) and Open University (Table S2). Olivine compositions from Mittlefehldt et al. (1998).

UPB, one aluminous and the other Al and alkali-poor (Barrat et al., 2016a).

Despite the oxygen isotope evidence that appears to link ureilites to carbonaceous chondrites, ^{54}Cr isotope systematics seemingly exclude any direct genetic relationship between the two (Fig. 10) (Warren, 2011a,b). If correct, this poses something of a conundrum for the interpretation of primary oxygen isotope variation in the solar nebula. Young and Russell (1998) have proposed that a line of exactly slope 1 defines the primordial variation and that this was modified by later parent body processes to form the CCAM line. However, if carbonaceous chondrites and ureilites are unrelated, the fact that both plot along the CCAM line might suggest that this line is more than just a secondary artifact (see Section 4.2 for further discussion).

3.2.4. *Winonaites and IAB-IIICD irons*

Winonaites are a relatively small group of primitive achondrites which, in terms of their textures and mineralogy, show some similarities to the acapulcoites and lodranites. Benedix et al. (1998) proposed three classification criteria for the group: (1) a highly reduced mineralogy (i.e., olivine typically $Fa_{1\text{-}10}$), (2) an oxygen isotopic composition within the range $\Delta^{17}O = -0.40$ to -0.73‰ (Clayton and Mayeda, 1996), and (3) a relatively high content of metal and troilite. Metal contents in the winonaite fall Pontlyfini and the relatively unweathered winonaite Yamato 74025 range from 1.5 to 12.3 vol.%, while troilite contents range from 9.1 to 19.9 vol.% (Benedix et al., 1998).

Winonaites display variable average grain-sizes, generally in the range 75–230 μm, but millimeter-sized grains can also be present (Hutchison, 2004). They display equigranular textures, with grain boundaries that meet at 120° triple junctions and have broadly chondritic mineral abundances (Benedix et al., 1998; Floss et al., 2008). Mineral compositions are: olivine ($Fa_{1\text{-}10}$), low-Ca pyroxene ($Fs_{1\text{-}9}$), Ca-rich pyroxene ($Fs_{2\text{-}4}$, $Wo_{44\text{-}45}$) and plagioclase ($An_{11\text{-}22}$) (Mittlefehldt, 2005a, 2008; Weisberg et al., 2006). Relict chondrules have been recognized in a number of winonaites, including NWA 725, NWA 1052, NWA 1463, Pontlyfni, Dhofar 1222, Mount Morris (Wisconsin) (Benedix et al., 1998, 2003; Rubin, 2007). Dhofar 1222, NWA 725 and NWA 1052 are currently classified as acapulcoites (Meteoritical Bulletin Database, 2016), but their oxygen isotope compositions indicate that they are winonaites (Greenwood et al., 2012).

As a result of their high metal and sulphide content, untreated winonaite finds display significantly greater levels of oxygen isotope variation than their EATG residues (Greenwood et al., 2012) (Fig. 11). In a similar manner to the acapulcoites and lodranites, untreated Antarctic winonaites are shifted to lower $\delta^{18}O$ values and slightly displaced to less negative $\Delta^{17}O$ values compared to their EATG residues (Fig. 11). Y-791058 is the most extreme case, with the untreated sample being nearly 7‰ lighter with respect to $\delta^{18}O$ than the EATG residue (Fig. 11). Unlike the acapulcoites and lodranites, non-Antarctic winonaite finds do not show a consistent shift to higher $\delta^{18}O$ values compared with their EATG residues (Fig. 11). However, this may reflect the relatively limited number of samples involved, and in particular the behaviour of the two extremely weathered North American finds, Winona and Tierra Blanca (Fig. 11). The apparently anomalous behaviour of these two samples may reflect past weathering in a colder climate, or more speculatively in the case of Winona, transport by Native Americans from more northerly latitudes (Greenwood et al., 2012).

On an oxygen three-isotope diagram, EATG-treated winonaite samples show much less scatter than the acapulcoite-lodranite clan, with an average $\Delta^{17}O$ of -0.51 ± 0.08‰ (2σ) (Table 1) and essentially define a mass fractionation line with a slope of 0.53 ± 0.01 and a y-axis intercept of -0.53 ± 0.04 ($R^2 = 1$) (Fig. 12) (Greenwood et al., 2012). This evidence suggests that the winonaite parent body experienced a greater level of isotopic homogenization than that of the acapulcoites and lodranites. Based on their similar petrographies (Benedix et al., 2000) and oxygen isotope compositions (Clayton and Mayeda, 1996), the winonaites have been linked to silicate inclusions in the well-populated IAB-complex iron group (currently showing 289 individual Meteoritical Bulletin Database

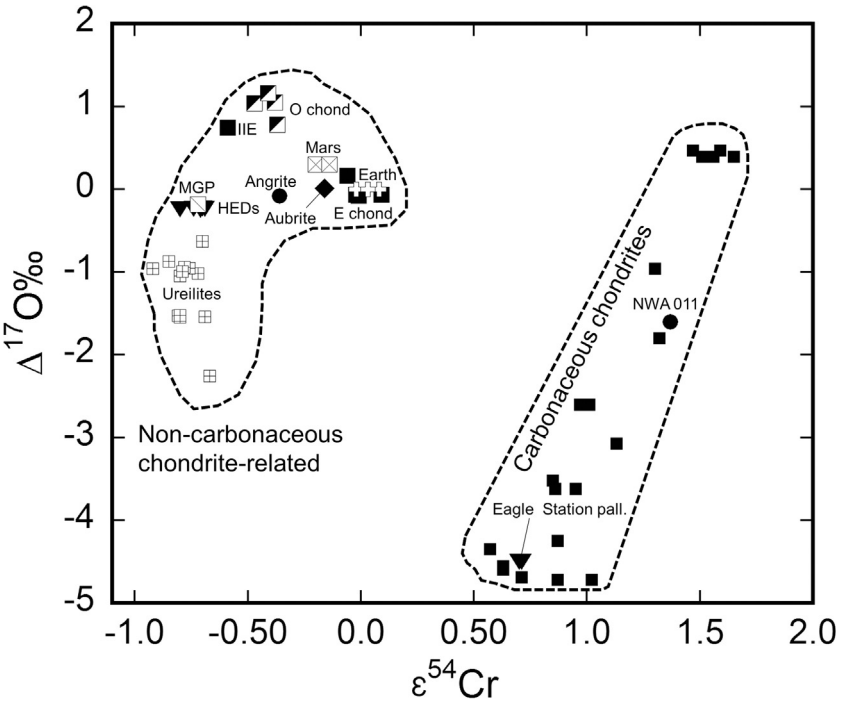

Fig. 10. ε^{54}Cr vs Δ^{17}O diagram for a range of planetary materials. Eagle Station pallasites plot within the carbonaceous chondrite grouping, whereas main-group pallasites (MGPs) plot in the same field as the ordinary and enstatite chondrites and the majority of achondrite groups. Data from Clayton et al. (1991); Clayton and Mayeda (1999); Newton et al. (2000); Trinquier et al. (2007); Shukolyukov and Lugmair, (2006); Ueda et al. (2006); Qin et al. (2010a,b); Yamakawa et al. (2010); Greenwood et al. (2012) Diagram modified after Warren (2011a).

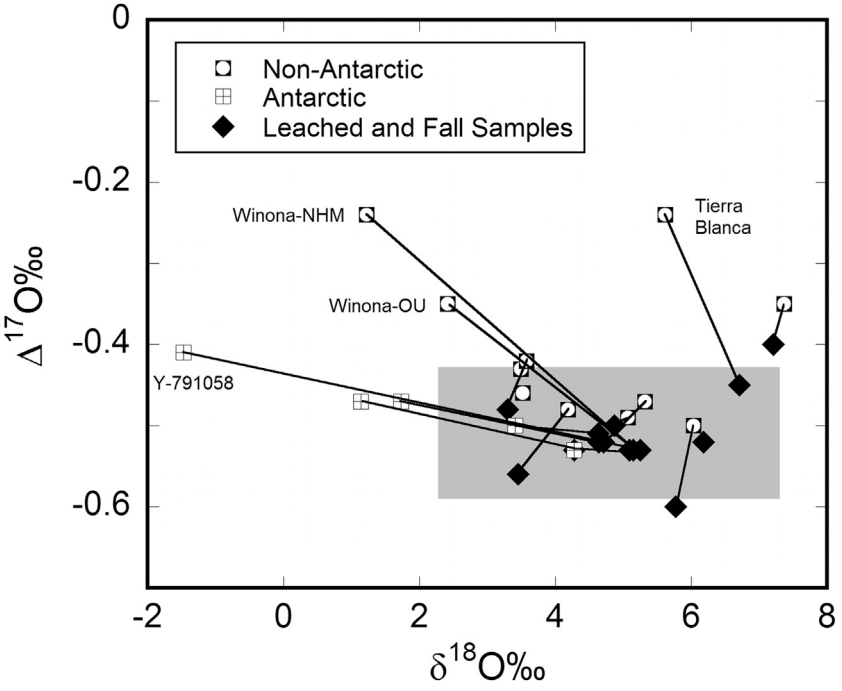

Fig. 11. Oxygen isotopic composition of winonaites. Antarctic finds are displaced to lower δ^{18}O values and less negative Δ^{17}O values than their EATG residues. Non-Antarctic finds show less distinct trends than seen in the acapulcoites and lodranites (Fig. 4) with Winona and Tierra Blanca showing anomalous behaviour (see text for further discussion). The light grey shaded box shows the 2σ variation on the mean δ^{18}O and Δ^{17}O values for the EATG residues and Pontlyfni, the only fall in the group. All data from Greenwood et al. (2012).

entries). In particular, the winonaites appear to be closely related to the abundant angular silicate inclusions in IAB irons, and a single parent body source for both groups has been proposed (Benedix et al., 2000). Oxygen isotope analyses for IAB and IIICD silicate inclusions are also plotted in Fig. 12 (Clayton and Mayeda, 1996). While the IAB and IIICD data show slightly greater scatter than the winonaite analyses, the two datasets display considerable overlap, consistent with a single source for both (Bild, 1977; Clayton and Mayeda, 1996; Benedix et al., 1998; Greenwood et al., 2012).

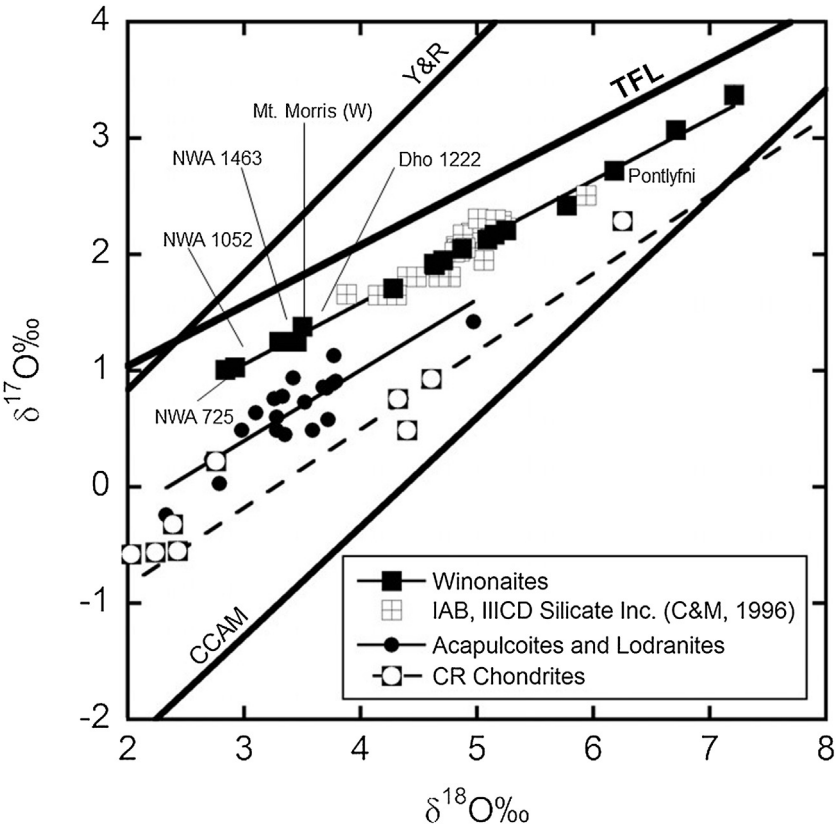

Fig. 12. Oxygen isotopic composition of winonaites, acapulcoite-lodranite clan, IAB, IIICD silicate inclusions and CR chondrites. Named winonaite samples are those which contain relict chondrules. Winonaite and acapulcoite-lodranite data (Greenwood et al., 2012), IAB, IIICD data (Clayton and Mayeda, 1996), CR chondrite data (Clayton and Mayeda, 1999; Schrader et al., 2011). TFL: Terrestrial Fractionaton Line; Y&R: slope 1 line (Young and Russell, 1998); CCAM: carbonaceous chondrite anhydrous mineral line (Clayton et al., 1977; Clayton and Mayeda, 1999).

Both the IAB silicate inclusions and winonaites display evidence of heterogeneous heating to at least the Fe,Ni-FeS cotectic (~950 °C), and possibly to as high as ~1450 °C (Benedix et al., 2005). An interesting feature of the winonaite oxygen isotope data is the fact that chondrule-bearing samples plot at lower $\delta^{18}O$ values than other members of the group. The sole exception to this is the winonaite fall Pontlyfni ($\delta^{18}O = 6.18‰$). However, the chondrule structures in Pontlyfni appear to be less well-developed than in the other chondrule-bearing winonaites and there also seems some doubt about their interpretation. If the chondrule-bearing winonaites that plot at low $\delta^{18}O$ values (Fig. 12) are indicative of the oxygen isotope composition of the precursor material then this suggests that the bulk of the winonaites, IAB and IIICD samples that plot at higher $\delta^{18}O$ values are either depleted in a mafic component (low $\delta^{18}O$), or conversely enriched in feldspathic material (high $\delta^{18}O$). This evidence is consistent with the suggestion that, prior to catastrophic disruption, the original winonaite-IAB-IIICD parent body underwent early-stage differentiation (Benedix et al., 1998).

3.3. Differentiated achondrites, stony-iron and iron meteorites

3.3.1. Angrites

Angrites are a relatively small group of ancient, essentially unshocked meteorites with a broadly basaltic composition, and are characterized by extreme levels of alkali depletion and refractory element enrichments, in particular Ca and Ti (Keil, 2012). Despite the small number of specimens (28 currently listed on the Meteoritical Bulletin Database), angrites show considerable textural and mineralogical diversity and are subdivided into volcanic and plutonic sub-types (Keil, 2012) (Table 2). Within the volcanic sub-type, some samples show evidence for rapid crystallization and so are generally referred to as "quenched" angrites. Due to their old ages and the fact that they are relatively unbrecciated and unshocked, angrites have proved to be key samples in early Solar System dating studies (Keil, 2012). Volcanic and plutonic angrites give well-resolved mean ages of 4562.1 ± 0.4 Myr and 4557.7 ± 0.7 Myr respectively (Keil, 2012).

Clayton and Mayeda (1996) were the first to determine the oxygen isotope composition of the angrites, using a conventional analysis technique. At the time of their study only four angrite samples had been identified: Angra dos Reis, Asuka 881371, LEW 86010 and LEW 87051. They obtained a mean $\Delta^{17}O$ value for the group of $-0.15 \pm 0.12‰$ (2σ), which showed considerable overlap with their HED value of $-0.25 \pm 0.16‰$ (2σ). Greenwood et al. (2005) undertook a laser fluorination study of five angrites (Angra dos Reis, LEW 86010, D'Orbigny, NWA 1296 and NWA 1670) and obtained a group mean $\Delta^{17}O$ value of $-0.072 \pm 0.014‰$ (2σ) (Table 2), which was fully resolved from their mean HED $\Delta^{17}O$ value of $-0.239 \pm 0.014‰$ (2σ). This provided confirmation that both groups were derived from separate parent bodies; a result in keeping with their distinct compositions and mineralogies (Mittlefehldt et al., 1998; Keil, 2012). Laser fluorination analysis of main-group pallasites (Greenwood et al., 2006, 2014) demonstrates that this group is also fully resolved from the angrites (Fig. 13).

Laser fluorination analyses of five additional angrites are available in various abstracts and in the Meteoritical Bulletin Database: NWA 2999, NWA 4590 (Irving et al., 2006), NWA 4801, NWA 7812, NWA 8535 (Agee et al., 2015). The mean $\Delta^{17}O$ value of these five analyses is $-0.076 \pm 0.028‰$ (2σ) (Fig. 13) (Table 2), with the lower

Table 2
Oxygen isotopic composition of angrites.

Sample	Lithology	Data source	N	$\delta^{17}O$	1σ	$\delta^{18}O$	1σ	$\Delta^{17}O^*$	1σ
Open University angrite analyses									
NWA 1296	Volcanic – Quenched	Greenwood et al. (2005)	2	2.086	0.048	4.126	0.097	−0.077	0.003
NWA 1670	Volcanic – Quenched	Greenwood et al. (2005)	2	1.966	0.116	3.884	0.142	−0.070	0.042
Angra dos Reis	Plutonic	Greenwood et al. (2005)	4	1.945	0.053	3.864	0.087	−0.080	0.009
LEW 86010	Plutonic	Greenwood et al. (2005)	2	2.016	0.109	3.980	0.190	−0.070	0.009
D'Orbigny	Volcanic – Quenched	Greenwood et al. (2005)	2	2.167	0.031	4.253	0.052	−0.062	0.003
		AVERAGE		**2.036**	**0.091**	**4.021**	**0.166**	**−0.072**	**0.007**
Other angrite laser fluorination analyses[a]									
NWA 2999	Plutonic	Met. Bull Database	3	2.041	0.062	4.029	0.167	−0.071	0.028
NWA 4590	Plutonic	Irving et al. (2006)	2	1.947	0.028	3.863	0.025	−0.078	0.015
NWA 4801	Plutonic	Met. Bull Database	2	1.816	0.010	3.570	0.036	−0.055	0.029
NWA 7812	Volcanic – Quenched	Met. Bull Database	3	2.003	0.047	3.978	0.104	−0.083	0.015
NWA 8535	Dunite	Met. Bull Database	3	1.703	0.352	3.425	0.729	−0.093	0.031
		AVERAGE		**1.902**	**0.140**	**3.773**	**0.264**	**−0.076**	**0.014**

[a] $\Delta^{17}O$‰ values have been recalculated using a slope value of 0.5247 (see Miller, 2002 for details).

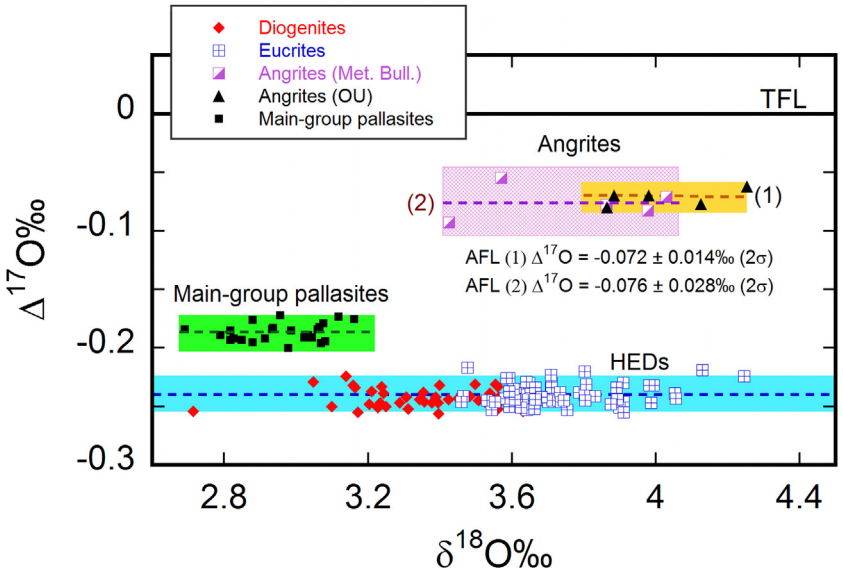

Fig. 13. Oxygen isotopic composition of angrites shown in relation to the HEDs (excluding howardites and polymict eucrites) and main-group pallasites. HED data: Table S4; main-group pallasite data: Greenwood et al. (2015a); angrite data (1): Greenwood et al. (2005); angrite data (2) from Meteoritical Bulletin Database. AFL: angrite fractionation line. All $\Delta^{17}O$ values calculated relative to a slope of 0.5247. See text for further discussion.

precision of this data, compared to that of Greenwood et al. (2005), at least in part reflecting inter-laboratory calibration differences. However, as can be seen from Fig. 13, the mean $\Delta^{17}O$ values of both sets of data are within error of each other, supporting the proposition that angrites are relatively homogeneous with respect to $\Delta^{17}O$.

It was suggested by Greenwood et al. (2005) that the oxygen isotope homogeneity of angrites points to an early, large-scale melting event on their parent body, possibly leading to the development of a magma ocean. The suggestion that magma oceans may have existed on asteroids in the early Solar System has been criticized in general terms by Wasson (2013a), and in the specific case of the angrite parent body by Keil (2012). There is no doubt that the term "magma ocean" is probably a poor one when applied to asteroids that may not have been any larger than about 500 km diameter, i.e., Vesta-sized. However, this term is really just shorthand for the concept that early-formed asteroids experienced large-scale melting events, probably driven be decay of short-lived radionuclides, such as ^{26}Al (i.e., Hevey and Sanders, 2006). The evidence cited by Greenwood et al. (2005) in favour of early, large-scale melting on the angrite parent body comes from the extremely uniform mean $\Delta^{17}O$ value of -0.072 ± 0.014‰ (2σ) (Table 2; Fig. 13).

The homogeneous $\Delta^{17}O$ composition displayed by angrites has to be set against the significantly more heterogeneous values measured in achondrite groups that appear to have experienced relatively low degrees of partial melting, the ureilites show the highest levels of oxygen isotope heterogeneity of any achondrite group, with a mean $\Delta^{17}O$ value of -0.96 ± 1.00‰ (2σ) (Table 1). Ureilites are commonly considered to represent partial melt residues that must have experienced at least 15% melting to eliminate plagioclase, and as much as 30% to satisfy REE and Eu constraints (Mittlefehldt et al., 1998; Wilson et al., 2008; Barrat et al., 2016b). The acapulcoite-lodranite clan is also extremely heterogeneous with respect to $\Delta^{17}O$, with a mean value of -1.12 ± 36‰ (2σ) (Table 1) (Greenwood et al., 2012), and are estimated to have experienced extremely variable levels of whole-rock partial melting of <1 vol.% to probably >20 vol.% (McCoy et al., 1997a) (Table S1). This evidence suggests that to attain oxygen isotopic equilibration, an asteroidal body must have undergone at least 40% partial melting and probably in excess of 50% (Greenwood et al., 2005, 2014).

As pointed out by Keil (2012), an underlying assumption of this model is that the angrite precursor material was heterogeneous with respect to oxygen isotopes, an assumption which he suggests is unsubstantiated. This is certainly true. As a result of the exten-

sive thermal processing experienced on the angrite parent body all evidence concerning the heterogeneity of the starting material has been completely obliterated. However, in view of the high levels of oxygen isotope heterogeneity present in all chondrite groups (e.g. Clayton et al., 1991; Clayton and Mayeda, 1999; Franchi, 2008) (Table 1), this assumption would seem to be reasonable.

Independent of the oxygen isotope evidence, siderophile element depletions (Righter, 2008; Shirai et al., 2009) and paleomagnetic analysis (Weiss et al., 2008) are consistent with the formation of a small core on the angrite parent body. Both the high level of oxygen isotope homogeneity displayed by the angrites and evidence for core formation on their parent body would seem to be consistent with an early phase of large-scale melting. Based on Hf-W data, Kleine et al. (2012) also invoke early, large-scale melting of the angrite parent body driven by decay of live ^{26}Al. However, they also suggest that the data indicates that core formation was not a single event and may have been disrupted by multiple impacts which constantly removed insulating crust and hence caused rapid cooling of the magma ocean. The suggestion by Kleine et al. (2012) that the angrite mantle was not sufficiently well-mixed to account for the observed oxygen isotope homogenization, is not supported by Baghdadi et al. (2015). Instead these latter authors suggest that the mantle heterogeneity discussed by Kleine et al. (2012) is a secondary feature that postdates core-mantle separation and reflects the incorporation of various amounts of exogenous iron impactor material.

3.3.2. Aubrites

Aubrites are highly reduced achondritic meteorites, predominantly composed of Mg-rich enstatite, with minor albitic plagioclase, Mg-rich diopside, olivine, metal, sulphide and a variety of rare accessory minerals (Keil, 2010). In terms of their compositional variation, mineralogy and oxidation state, aubrites show a close affinity to the EH and EL chondrites and as a result it is generally accepted that they formed from enstatite chondrite-like parent materials (Keil, 1989, 2010; Barrat et al., 2016b). Enstatite chondrites and aubrites also have closely similar oxygen isotope compositions and plot on, or close to, the terrestrial fractionation line (Clayton et al., 1984; Clayton and Mayeda, 1996; Newton et al., 2000; Miura et al., 2007; Barrat et al., 2016b) (Fig. 14). The EH chondrites show a larger compositional range than the EL chondrites with respect to both δ^{18}O and Δ^{17}O (Fig. 14) (Table 3, Table S3). With the exception of Cumberland Falls, the aubrites define a relatively restricted field in Fig. 14, which is more-or-less central to both the EH and EL fields. Cumberland Falls is a polymict breccia that consists of chondritic fragments in an enstatite-rich cataclastic matrix (Keil, 2010). These chondritic fragments are LL ordinary chondrite-like (Keil, 2010) and their presence is the likely reason that Cumberland Falls has a relatively heavy Δ^{17}O composition and plots away from the other aubrites in Fig. 14. The aubrite data of Newton et al. (2000) shows more scatter than the recent analyses of Barrat et al. (2016b), which probably reflects both improvements

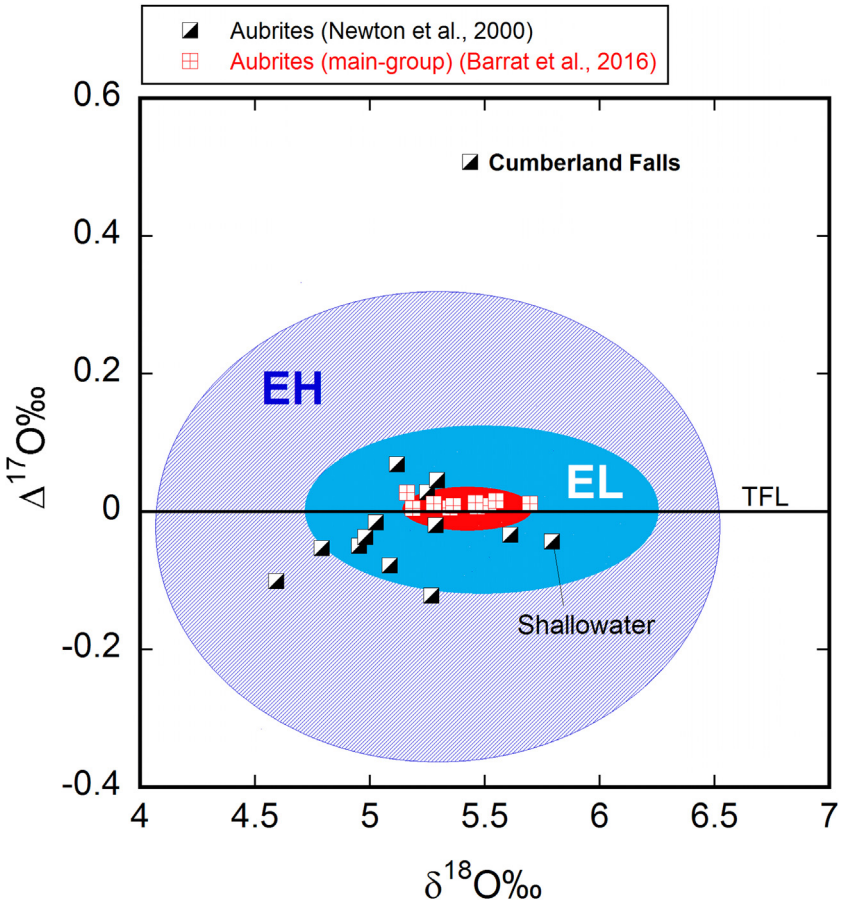

Fig. 14. Whole-rock oxygen isotope analyses of aubrites and enstatite chondrites. Data from Newton et al. (2000) and Barrat et al. (2016b). Elipses show the 2σ variation of mean δ^{18}O and Δ^{17}O values for the EH, EL and aubrite groups. All Δ^{17}O values are linearized using a slope value of 0.5247 (Miller, 2002). Full data given in Table S3.

Table 3
Summary of aubrite and enstatite chondrite oxygen isotope analyses.

SAMPLE	N	$\delta^{17}O$‰	1σ	$\delta^{18}O$‰	1σ	$\Delta^{17}O$‰	1σ
EH chondrites*	18	2.760	0.417	5.309	0.626	−0.022	0.172
EL chondrites*	21	2.871	0.211	5.485	0.395	−0.003	0.064
Aubrites with C. Falls*	14	2.720	0.257	5.177	0.315	0.007	0.153
Aubrites without C. Falls*	13	2.671	0.187	5.157	0.318	−0.031	0.055
Aubrites (main-group)**	10	2.844	0.086	5.404	0.167	0.012	0.007

A full listing of aubrite and enstatite chondrite data is given in Table S3. *Newton et al. (2000); **Barrat et al. (2016b). C. Falls = Cumberland Falls.

in analytical precision and a slightly higher number of weathered finds in the earlier study (Table 3, Table S3). Barrat et al. (2016b) conclude that the samples they analyzed were derived from two parent bodies, one for the "regular" main-group aubrites and a second for the anomalous samples Mount Egerton and Larned.

As a result of their overlapping oxygen isotope compositions, there has been general agreement that the enstatite chondrites and aubrites are in some way genetically related (e.g., Rubin, 1983; Clayton and Mayeda, 1996; Keil, 1989, 2010; Keil et al., 1989), although there is discussion about the exact nature of this relationship. Rubin (1983) suggested that the aubrites represented melted EL chondrite material, but from a distinct asteroid to that of the EL chondrites. Keil et al. (1989) proposed that, although related to the enstatite chondrites, the aubrites come from two parent bodies, one represented by Shallowater, with the remaining aubrites from a second body. Shallowater appears to have experienced a unique three-stage cooling history, which may have been the result of a collision between two enstatite-rich bodies, one molten and one solid (Keil et al., 1989). Barrat et al. (2016b) suggest that Mount Egerton and Larned may be derived from the same parent body as Shallowater. The derivation of aubrites and enstatite chondrites from the same nebular reservoir is supported by their similar isotopic variation for a range of elements, including Ca (Dauphas et al., 2014), Ti (Zhang et al., 2012) and Cr (Warren, 2011a).

As pointed out by Clayton and Mayeda (1996), one of the intriguing features of the aubrites and enstatite chondrites is their close similarity in oxygen isotope composition to that of the Earth and Moon. Based on the analysis of 76 peridotite xenoliths, Mattey et al. (1994) calculated a $\delta^{18}O$ value for the Earth's mantle of 5.5‰. This is clearly very close to the $\delta^{18}O$ composition of the EH, EL and aubrites, which have values of 5.309 ± 1.253 (2σ), 5.485 ± 0.789 (2σ) and 5.404 ± 0.334 (2σ) respectively (Table 3). Based on this evidence and overlapping isotopic variation for a range of other elements, enstatite chondrites have been proposed as suitable precursor materials for the Earth (Javoy, 1995; Javoy et al., 2010). However, based on Si isotope differences between the silicate Earth and enstatite meteorites, Savage and Moynier (2012) exclude the possibility of a direct genetic relationship between the two.

3.3.3. Howardite-Eucrite-Diogenite suite (HEDs)

The Howardite, Eucrite, Diogenite suite (HEDs) is the most abundant group of differentiated meteorites arriving on Earth today, comprising roughly 6% of all witnessed falls (statistics from Meteoritical Bulletin Database; see also Burbine et al., 2002a). Eucrites are basaltic rocks that formed either as lava flows or intrusions, diogenites are orthopyroxene-rich, coarser-grained igneous cumulates, and howardites are complex impact breccias containing both diogenitic and eucritic fragments (Mittlefehldt et al., 1998; Mittlefehldt, 2015; Barrat et al., 2008, 2010; Yamaguchi et al., 2009; McSween et al., 2011). A range of evidence, including spectral data, orbital dynamics and recent remote sensing observations by the NASA Dawn spacecraft indicates that the HEDs originate from the asteroid 4 Vesta, the second largest body in the main belt (McCord et al., 1970; Binzel and Xu, 1993; De Sanctis et al., 2012; McSween et al., 2011, 2013; Mittlefehldt, 2015; McCoy et al., 2015).

Despite showing significant mineralogical and geochemical diversity (Mittlefehldt et al., 1998; McSween et al., 2011, 2013), the majority of diogenites and monomict eucrites display relatively restricted variation with respect to $\Delta^{17}O$ (Wiechert et al., 2004; Greenwood et al., 2005, 2014). A compilation of 144 published and unpublished HED analyses performed at the Open University is given in Table S4 and a summary of this data in Table 4. Diogenite and eucrite falls (n = 26) display a high level of isotopic homogeneity with respect to $\Delta^{17}O$, with a mean value of −0.240 ± 0.014‰ (2σ) (Table 4, Table S4). A much larger dataset of eucrite and cumulate eucrite falls and finds (n = 61) has the same mean $\Delta^{17}O$ value, but with a slightly lower precision i.e. −0.240 ± 0.018‰ (2σ) (Table 4, Table S4). Likewise, analyses of diogenite falls and finds (n = 44) have a mean $\Delta^{17}O$ value that is only slightly more negative than that of the falls only data, i.e., −0.243 ± 0.016‰ (2σ) (Table 4, Table S4). The diogenite data in Table S4 includes the analyses of Greenwood et al. (2014) (n = 22), which were all leached in EATG. The slightly more negative mean $\Delta^{17}O$ value obtained in that study, i.e., −0.246 ± 0.014‰ (2σ), compared to the larger diogenite dataset given in Table S4 is presumably due to the effects of terrestrial weathering in the latter. It is clear from these results that the diogenites and eucrites have virtually identical compositions with respect to their mean $\Delta^{17}O$ values, and this evidence is consistent with their derivation from a single isotopically homogeneous parent body. This is further illustrated by the fact that the precision of the combined diogenite and eucrite (n = 105) mean $\Delta^{17}O$ value of −0.241 ± 0.018‰ (2σ) is almost identical to that of the eucrites alone (Table 4, Table S4).

Compared to the diogenites and monomict eucrites, the howardites and polymict eucrites (n = 39) are significantly more heterogeneous with respect to $\Delta^{17}O$, as reflected by the much

Table 4
Summary of HED oxygen isotope data.

Lithology		N	$\delta^{17}O$‰	1σ	$\delta^{18}O$‰	1σ	$\Delta^{17}O$‰	1σ
Eucrite, falls and finds (inc. Stannern trend and cumulate eucrites)	A	61	1.732	0.132	3.761	0.250	−0.240	0.009
Diogenites, falls and finds	B	44	1.527	0.106	3.377	0.201	−0.243	0.008
Eucrites and diogenites, falls only		26	1.642	0.112	3.591	0.219	−0.240	0.007
Eucrites and diogenites, falls and finds		105	1.646	0.158	3.600	0.299	−0.241	0.009
Howardites and polymict eucrites	C	39	1.715	0.147	3.744	0.279	−0.247	0.025
	TOTAL (A + B + C)	**144**						

$\Delta^{17}O$‰ linearized using a slope of 0.5247 (see Section 2.2 for further details). All analyses undertaken at the Open University.
A full listing of Open University HED data is given in Table S4.

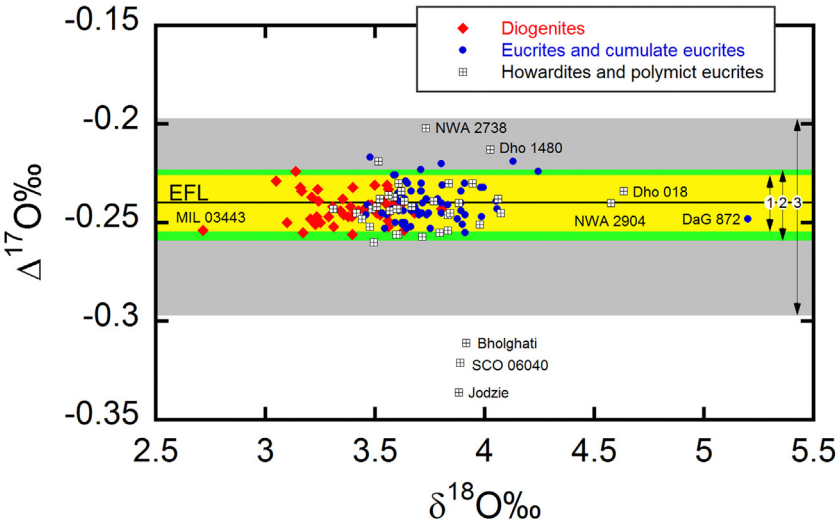

Fig. 15. Oxygen isotopic composition of HEDs (n = 144). Central zone (labelled "1"): ±2σ precision for eucrite and diogenite falls only (n = 26). Intermediate zone (labelled "2"): ±2σ precision for eucrite, cumulate eucrite and diogenite falls and finds (n = 105). Outer zone (labelled "3"): ±2σ precision for howardites and polymict eucrites (n = 39). EFL = Eucrite Fractionation Line: average $\Delta^{17}O$ value for 26 eucrite and diogenite falls = −0.240 ± 0.014 (2σ) (All data: Table S4).

greater 2σ variation of their mean value: −0.247 ± 0.050‰ (2σ) (Table 4, Table S4) (Fig. 15). Howardites and polymict eucrites are heterogeneous breccias which, in addition to indigenous clast and matrix material, often contain a significant non-HED component (Mittlefehldt et al., 1998). In particular, a number of howardites contain a significant fraction of carbonaceous chondrite-related material. In the case of Jodzie and Bholghati this can be up to 5 vol.% (Fig. 15) (Zolensky et al., 1996). The coarse howardite breccia SCO 06040 contains abundant CM2-related clasts (Herrin et al., 2011) and this is reflected in its $\Delta^{17}O$ composition, which plots close to that of Jodzie and Bholghati in Fig. 15. Much higher concentrations of CM2-like material (~40–50% in places) are present in the howardite PRA 04401 (Herrin et al., 2011; Greenwood et al., 2015b). Carbonaceous chondrite material in howardites is generally believed to result from impact mixing in a regolith environment and is probably related to the dark material located by the Dawn spacecraft on Vesta's surface (McCord et al., 2012; Reddy et al., 2012; Turrini et al., 2014).

The presence of carbonaceous chondrite material in howardites and polymict eucrites will have the effect of displacing their $\Delta^{17}O$ compositions to more negative values compared to the mean value for diogenites and monomict eucrites (Fig. 15). On the other hand, impactor material with $\Delta^{17}O$ values more positive than the HED mean value, such as ordinary chondrite-related compositions, will move the $\Delta^{17}O$ value in the opposite sense. This is one possibility to explain the compositions of howardite NWA 2738 or the polymict eucrite Dho 1480 (Fig. 15). However, terrestrial weathering will also result in shifts in $\Delta^{17}O$ values towards the TFL. Possible scenarios for the formation of HED-like compositions that plot outside the normal HED $\Delta^{17}O$ range defined in Fig. 15 are discussed further in Section 3.4.2.

As is clear from Fig. 15 and Tables 4 and S4, all of the main HED lithologies, with the exception of howardites and polymict eucrites, have virtually identical $\Delta^{17}O$ compositions and display a high level of isotopic homogeneity. In fact, the level of $\Delta^{17}O$ homogeneity shown by diogenites and monomict eucrites (n = 105) (±0.018‰ (2σ)) (Table 4) is comparable to that of other bodies that have experienced high levels of melting i.e., the angrites (±0.014‰ (2σ)) (Greenwood et al., 2005), lunar rocks (±0.021‰ (2σ)) (Hallis et al., 2010) and SNCs (±0.026‰ (2σ)) (Franchi et al., 1999) (Table 1). In contrast, primitive achondrite groups, which experienced lower degrees of melting, have more heterogeneous $\Delta^{17}O$ values e.g., ±1.00‰ (2σ) in the case of the ureilites, and ±0.36‰ (2σ) in the case of the acapulcoites and lodranites (Greenwood et al., 2012) (Table 1). This evidence suggests that both the diogenites and monomict eucrites are derived from a single source that was extremely homogeneous with respect to $\Delta^{17}O$. Such high levels of oxygen isotope homogeneity suggest that the HED parent body underwent a phase of large-scale melting (Greenwood et al., 2005, 2014).

Based on moderately siderophile element abundances (Ni, Co, Mo, W and P), it has been suggested that the HED parent body experienced an early global-scale melting event (Righter and Drake, 1997). The extremely low abundances of highly siderophile elements (HSE) (Os, Ir, Ru, Pt, Pd, Re) in HEDs are also consistent with early large-scale melting, resulting in rapid core formation (Dale et al., 2012; Day et al., 2012b). Using a range of possible chondritic source compositions, Righter and Drake (1996, 1997) calculated a percentage core mass for the HED parent body of between 5 and 25%. Modelling by Toplis et al. (2013) derived values of between 10 and 30%. The preferred HED precursor composition of Toplis et al. (2013) (75% H chondrite: 25% CM chondrite mix) gives a calculated core radius of 114.2 km, which is a close match to that derived from Dawn observations (110 ± 3 km) (Russell et al., 2012). Based on the results of laboratory studies, Ashcroft and Wood (2015) also conclude that the eucrites and diogenites can be derived by partial melting of a chondritic body with a core size of between 15 and 20% the mass of Vesta.

While moderately and highly siderophile element abundance data indicate that the HED parent body underwent core formation, this evidence alone does not unambiguously demonstrate that a phase of global melting was involved. Taylor (1992) concluded that high degrees of partial melting (~50%) were required for metal "to drain away and form a core". While partial melting exceeding 50% has been generally accepted by most recent modelling studies (Hevey and Sanders, 2006; Moskovitz and Gaidos, 2011), core formation at lower degrees of melting may also be possible (Neumann et al., 2012). The magma ocean model developed by Righter and Drake (1997) indicates that the HED mantle may have been between 65%–77% molten (1500–1530 °C) and would have undergone turbulent convection during its initial stages. Under such conditions, global-scale homogenization of oxygen isotopes would have been an efficient and rapid process (Greenwood et al., 2005, 2014). However, while magma ocean models have had some

success in explaining the larger-scale features of Vesta's differentiation (Righter and Drake, 1997; Mandler and Elkins-Tanton, 2013), there remain significant problems with our understanding of many aspects of HED magmatic evolution, in particular, the relationship between diogenites and eucrites (Barrat et al., 2008, 2010; Barrat and Yamaguchi, 2014).

3.3.4. Mesosiderites

Mesosiderites are breccias consisting of silicate-rich material enclosed in Fe,Ni metal (plus troilite), with both fractions being present in roughly equal proportions (Weisberg et al., 2006). As a consequence, like the pallasites, mesosiderites are generally classified as stony-irons (Krot et al., 2014). In the mesosiderites the silicate fraction is predominantly composed of basaltic, gabbroic and orthopyroxene-rich clasts. In contrast to pallasites, olivine-rich material is rare in the mesosiderites (Mittlefehldt et al., 1998; Scott et al., 2001; Greenwood et al., 2015a). So while pallasites appear to represent a mix of core and mantle-derived materials, the mesosiderites appear to represent a core-crust mix. Mixing materials derived from an asteroidal core with those from the outer layers of a differentiated body, without also sampling significant amounts of olivine-rich mantle material, necessarily implies complex formation conditions (Mittlefehldt et al., 1998). A further complicating factor is the two-stage thermal history of the mesosiderites, which cooled extremely rapidly at high temperatures (0.1–100 °C per year at 850–1150 °C) and much more slowly at lower temperatures (0.2–0.5 °C/Myr at ~500 °C) (Delaney et al., 1981; Ruzicka et al., 1994; Hopfe and Goldstein, 2001).

Although a wide range of models have been put forward to explain the origin of the mesosiderites (Hewins, 1983), it is now generally agreed that their metal fraction must have been largely molten at the time of its emplacement (Wasson and Rubin, 1985; Hassanzadeh et al., 1990; Rubin and Mittlefehldt, 1993; Scott et al., 2001). The main evidence in favour of emplacement of molten metal comes from the fact that the mesosiderite metal fraction is so homogeneous in composition and that it is difficult to solidify an asteroidal core without causing significant elemental variation (Wasson and Rubin, 1985; Hassanzadeh et al., 1990). Emplacement of molten metal is also consistent with the extensive metamorphism and partial melting experienced by the mesosiderite silicate fraction. Recent discussions concerning the formation of the mesosiderites have focused on whether the metal and silicate-rich fractions were derived from the same, or two distinct asteroids, as well as the extent of parent body disruption i.e., total or local. Thus, Hassanzadeh et al. (1990) put forward a model involving the impact of a denuded molten core into the surface layers of a second differentiated asteroid, whereas Scott et al. (2001) consider that only a single disrupted asteroid is required to explain the formation of the mesosiderites.

Conventional oxygen isotope analysis (i.e., using the externally-heated "bomb" technique) indicated that the average $\Delta^{17}O$ value of the mesosiderites was indistinguishable within error from that of the HEDs and so consistent with a single source for both groups (Clayton and Mayeda, 1996). However, conventional analysis also suggested that the HEDs and main-group pallasites had indistinguishable isotopic compositions (Clayton and Mayeda, 1996). Deriving the HEDs, mesosiderites and main-group pallasites from the same parent body is problematic in view of the evidence that both the HEDs and mesosiderites lack a significant mantle component, whereas the main-group pallasites are essentially a core-mantle mix (Section 3.3.5.1).

The higher precision provided by laser-assisted fluorination, when compared to the conventional technique (Section 2.3), has given an important new perspective on the relationship between the two major stony-iron groups. In a study of 12 main-group pallasites and 17 mesosiderites, Greenwood et al. (2006) found that they had fully distinguishable average $\Delta^{17}O$ values of -0.183 ± 0.018 (2σ) and -0.245 ± 0.020 (2σ) respectively. The average $\Delta^{17}O$ value for the main-group pallasites changed only slightly to -0.187 ± 0.016 (2σ) in a more recent study, with an increased suite of 24 individual samples (103 replicates) (Greenwood et al., 2015a) (Fig. 16) (Table 1). Laser fluorination data for the main-group pallasites and mesosiderites show no overlap with respect to $\Delta^{17}O$ and indicate that both groups form distinct populations derived from separate parent bodies. In contrast, laser-fluorination data for mesosiderites and HEDs show complete overlap with respect to $\Delta^{17}O$ (Greenwood et al., 2015a) and therefore confirm the findings of earlier studies (Clayton and Mayeda, 1996; Clayton, 2006) (Fig. 16).

Although more abundant than in the HEDs, olivine-rich materials are still rare in mesosiderites, making up between 0 and 6 vol.% of total silicates (Ruzicka et al., 1994; Kong et al., 2008). However, as pointed out by Mittlefehldt (1980), there are compositional and textural similarities between olivine in pallasites and mesosiderites. This raises the possibility that such materials may be co-genetic with the proposed metal-rich impactor, rather than the crustal units from which the bulk of the silicate fragments were derived. However, recent analysis of olivine-rich materials from the Vaca Muerta, Mount Padbury and Lamont mesosiderites and from the mesosiderite-related dunites NWA 2968 and NWA 3329 shows that these samples have $\Delta^{17}O$ values identical within error to the average mesosiderite $\Delta^{17}O$ value (Greenwood et al., 2006, 2015a) (Fig. 16). The most likely explanation for these data is that the olivine-rich material in mesosiderites was not derived from the metal-rich impactor, but instead originates from the same source as the other silicate clasts. However, this interpretation is dependent on the proposed impactor and target having distinct oxygen isotope compositions that are detectable at the levels of precision available using the laser fluorination technique.

3.3.5. Pallasites

Pallasites are stony-iron meteorites that consist of coarse-grained silicates, predominantly olivine, enclosed in Fe,Ni metal, with the silicates and metal being present in roughly equal proportions (Mittlefehldt, 2008; Krot et al., 2014). Pallasites are sub-divided into three main types on the basis of their mineralogy and oxygen isotope composition: (i) main-group, (ii) Eagle Station group and (iii) the pyroxene pallasites (Krot et al., 2014).

3.3.5.1. Main-group pallasites. Olivine in main-group pallasites is generally very coarse-grained, displaying both rounded and angular morphologies (Scott, 1977a). In most samples it has a very uniform composition ($Fo_{88\pm1}$), although a few examples contain more Fe-rich olivines, which may be as low as Fo_{82} (Mittlefehldt, 2008; Krot et al., 2014). In addition to olivine, main-group pallasites contain minor amounts of calcium pyroxene, chromite, various phosphates, troilite and schreibersite (Buseck, 1977a,b; Krot et al., 2014).

Until recently, there was general agreement that main-group pallasites were derived from the core-mantle interface of a single, differentiated asteroid (Scott and Taylor, 1990; Ulff-Møller et al., 1998; Wasson and Choi, 2003). To explain the angular morphology of many pallasitic olivines (Scott, 1977a), an impact event was generally invoked involving crushing of mantle olivine into an underlying molten core (Scott and Taylor, 1990; Ulff-Møller et al., 1998; Wasson and Choi, 2003). However, based on Ni profiles across taenite lamellae, Yang et al. (2010) showed that main-group pallasites display evidence for variable cooling rates; a feature that is inconsistent with a core-mantle boundary origin. Instead, Yang et al. (2010) suggested that main-group pallasites originated in an asteroid that had experienced disruption in a hit-and-run style

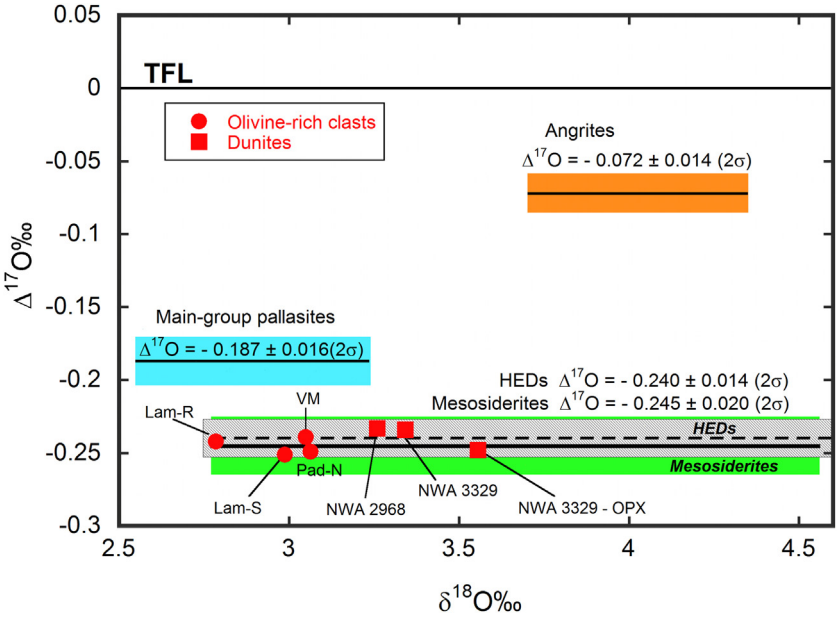

Fig. 16. Oxygen isotopic composition of olivine-rich clasts in mesosiderites compared to main-group pallasites, HEDs (Greenwood et al., 2015a; Table S4) and data for other mesosiderite samples (Greenwood et al., 2006). ±2σ variation on the HED group mean value is represented by the narrower zone (diagonal-rule ornament), which is fully enclosed by the slightly wider ±2σ zone for the mesosiderites. The thick continuous line represents the mesosiderite fractionation line. The dashed line represents the HED fractionation line. Lam = Lamont, VM = Vaca Muerta, Pad = Mount Padbury. TFL = terrestrial fractionation line.

collision. Based on paleomagnetic measurements, Tarduno et al. (2012) suggested that main-group pallasites formed at depths as shallow as 10 km, when liquid metal from the core of an impactor was injected into the shallow mantle of an ~200 km radius body. They also proposed that this body retained a partially liquid core for tens of millions of years after the impact event. In contrast to an impact origin, Boesenberg et al. (2012) suggest that the main-group pallasites may have formed on a single parent body by fractional-melting of a chondritic precursor, followed by fractional crystallization of residual metal and silicate liquids.

The silicate fraction of main-group pallasites is generally considered to be derived from a single parent body (Wasson and Choi, 2003). However, a number of recent oxygen isotope studies of olivine from main-group pallasites have reported evidence for a bimodal $\Delta^{17}O$ distribution, suggesting that these silicates might be derived from multiple parent bodies (Ziegler and Young, 2007, 2011; Ali et al., 2013, 2014). These finding are in contrast to those of Greenwood et al. (2006, 2015a) who found no evidence for bimodality in olivines from a suite of 24 main-group pallasites, which instead display a high level of isotopic homogeneity, with a mean $\Delta^{17}O$ value of −0.187 ± 0.016‰ (2σ) (Figs. 16 and 17) (Table 1). The level of $\Delta^{17}O$ homogeneity in the main-group pallasites reported by Greenwood et al. (2006, 2015a) is comparable to that of other bodies that have experienced high levels of melting, including the HEDs (±0.014‰ (2σ)) (Greenwood et al., 2014), angrites (±0.014‰ (2σ)) (Greenwood et al., 2005), lunar rocks (±0.021‰ (2σ)) (Hallis et al., 2010) and SNCs (±0.026‰ (2σ)) (Franchi et al., 1999) (Table 1). In contrast, primitive achondrite groups, which experienced much lower degrees of partial melting, have much more heterogeneous $\Delta^{17}O$ values i.e. ±0.36‰ (2σ) in the case of the acapulcoites and lodranites (Greenwood et al., 2012). This evidence suggests that main-group pallasites are derived from a single source that was extremely homogeneous with respect to $\Delta^{17}O$.

In terms of their $\Delta^{17}O$ values, as determined by laser fluorination analysis (Greenwood et al., 2006, 2015a), main-group pallasites show no overlap with the HEDs (Figs. 13 and 17), indicating that they represent distinct populations and were derived from distinct parent bodies. The proposal by Wasson (2013b) that main-group pallasites, IIIAB irons and HEDs all originate from a single parent body is incompatible with this oxygen isotope evidence.

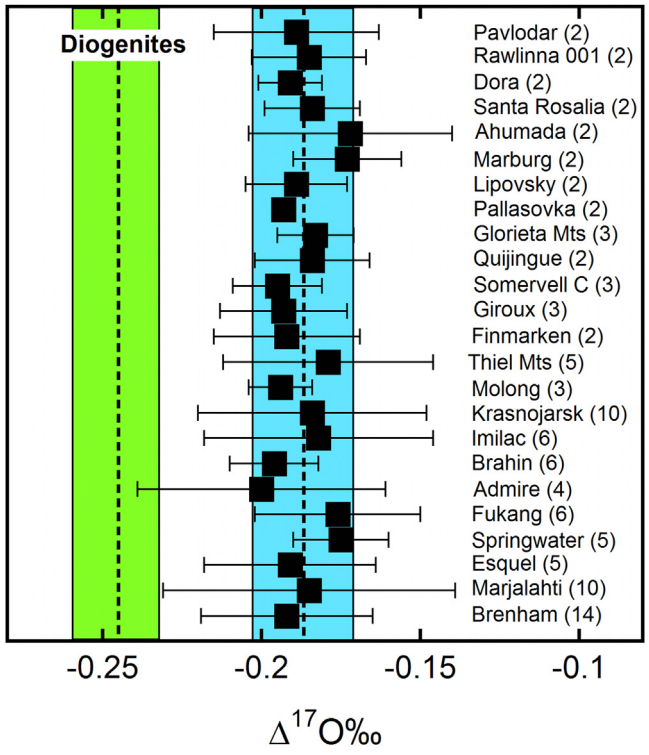

Fig. 17. Oxygen isotopic composition of 24 main-group pallasites (Greenwood et al., 2015a) compared to the diogenite data of Greenwood et al. (2014). Shaded zones represent the ±2σ variation on the group mean $\Delta^{17}O$ values. Error bars shown for individual pallasite samples represent the ±2σ variation of the analyzed replicates for that sample. Vertical dashed lines represent the mean $\Delta^{17}O$ values for the main-group pallasites (Greenwood et al., 2015a) and diogenites (Greenwood et al., 2014).

With respect to their possible precursor materials, main-group pallasites have distinct ε^{54}Cr, ε^{50}Ti and ε^{62}Ni compositions compared to carbonaceous chondrites and distinct ε^{54}Cr values compared to the Eagle Station pallasites (Warren, 2011a) (Section 3.3.5.2) (Fig. 10). The main-group pallasites also show deficits in μ^{26}Mg* compared to both chondrites and the Earth (Larsen et al., 2016). This evidence is interpreted by Larsen et al. (2016) as indicating that the main-group formed as olivine-rich, partial melt residues, within a planetesimal that accreted in the inner hot protoplanetary disc while ^{26}Al was "live". From their data they calculate that the main-group precursor material had a reduced initial abundance $(^{26}Al/^{27}Al)_0$ of $\sim 1–2 \times 10^{-5}$, compared to the CAI determined value of $\sim 5.3 \times 10^{-5}$ (Section 4.4).

3.3.5.2. Eagle station pallasites. With the identification in 2014 of a fifth member, Oued Bourdim 001, the Eagle Station pallasites passed the threshold required to be recognized as a group (Weisberg et al., 2006); the four other members being: Cold Bay, Eagle Station, Karavannoe and Itzawisis. Eagle Station pallasites have a similar mineralogy to the main-group, but contain more Fe-rich olivine (Fo_{80} compared to Fo_{88}) and additionally their metal has a higher Ni and Ir content (Scott, 1977a; Wasson and Choi, 2003; Korochantsev et al., 2013; Humayun et al., 2014; Krot et al., 2014). In terms of their oxygen isotope compositions, main-group and Eagle Station pallasites are also quite distinct. The main-group plot close to the terrestrial fractionation line, whereas the Eagle Station group are significantly more ^{16}O-rich and plot close to the CCAM line, in the region where the CO3 and CK-CV chondrite fields overlap (Fig. 18). A possible genetic link between the Eagle Station group and CV chondrites has been postulated on the basis siderophile element patterns (Humayun and Weiss, 2011; Humayun et al., 2014). Main-group and Eagle Station pallasites are also distinct with respect to their ε^{54}Cr compositions, with the Eagle Station group plotting close to the CO3, CV3, CK carbonaceous chondrites on a Δ^{17}O vs. ε^{54}Cr diagram (Fig. 10) (Warren, 2011a). This evidence suggests that the Eagle Station pallasites are from a distinct source to the main-group and that prior to differentiation their parent body had a close compositional affinity to the CO3, CV3, CK chondrites (Figs. 10 and 18). Larsen et al. (2016) come to similar conclusions, suggesting, on the basis of variable μ^{26}Mg* excesses, that the Eagle Station pallasites formed from a melted carbonaceous chondrite precursor that was undergoing fractional crystallization during the period when ^{26}Al was "live".

3.3.5.3. Pyroxene pallasites and Milton. The pyroxene pallasites NWA 1911, Vermillion, Yamato 8451 and Zinder are distinguished from the main-group and Eagle Station pallasites by the presence of millimeter-sized pyroxenes (Krot et al., 2014). In terms of their oxygen isotope compositions NWA 1911 and Zinder plot close to the main-group (Bunch et al., 2005), whereas Vermillion and Yamato 8451 are more ^{16}O-rich (Clayton and Mayeda, 1996) (Fig. 18). Milton is a unique pallasite (Jones et al., 2003) that plots at the ^{16}O-poor end of the CV-CK array in Fig. 18. Like the main-group, the pyroxene pallasites Yamato 8451, Vermillion and Zinder all show deficits in μ^{26}Mg*, whereas Milton does not and has a value similar to some grains from Eagle Station (Larsen et al., 2016). In keeping with their oxygen isotope compositions, these relationships suggest affinities between the main-group and pyroxene pallasites and between Milton and the Eagle Station group (Fig. 18). In particular, based on its oxygen isotope composition Milton seems to have formed from a carbonaceous chondrite-like precursor, but on a distinct asteroid to that of the Eagle Station group.

3.3.5.4. How many pallasite parent bodies?. Scott (2007) estimated that pallasites could be derived from as many as seven separate parent bodies (four for the pyroxene pallasites, plus one each for Milton, the main-group and Eagle-station group). However, Vermillion and Yamato 8451 have almost identical oxygen isotope compositions (Clayton and Mayeda, 1996) and may be samples from the same parent body. Thus, the presently identified pallasites would appear to be samples from six distinct parent bodies.

3.3.6. Iron meteorites

Oxygen isotope analysis of iron meteorites is limited to those specimens that contain silicate inclusions, or other oxygen-bearing phases, such as chromite and phosphate. While generally present in only minor proportions, such inclusions or phases are found in samples from almost half the iron meteorite groups (Franchi, 2008). Here we present a brief overview of oxygen isotope studies of iron meteorites (see also Clayton and Mayeda, 1996; Franchi, 2008). General reviews of iron meteorite geochemistry and genesis are provided by Goldstein et al. (2009) and Benedix et al. (2014b). A detailed review of silicate-bearing irons is given by Ruzicka (2014). Table 5 provides a summary of the results of oxygen isotope analysis of the various iron meteorite groups.

The IIIAB magmatic irons are the most abundant iron group, although only a relatively limited number are known to contain oxygen-bearing phases. Based on similarities in their metal compositions, a genetic link with the main-group pallasites has been proposed (Scott, 1977b; Wasson and Choi, 2003). However, Yang et al. (2010) argue, on the basis of cooling rate evidence, that both groups sample separate parent bodies. Clayton and Mayeda (1996) suggested that the oxygen isotope composition of the IIIABs was consistent with a genetic relationship with the main-group pallasites. Analysis of chromites from four IIIAB specimens by Franchi et al. (2013) yielded an average Δ^{17}O value of -0.18 ± 0.02‰ (2σ), which is within error of the main-group pallasite average of -0.187 ± 0.016‰ (2σ) obtained by Greenwood et al. (2015a). In contrast, chromite from the Cape York iron analyzed by Franchi et al. (2013) gave a Δ^{17}O value of −0.27‰, raising the possibility that chromites in IIIAB irons may have multiple sources.

Silicates, primarily tridymite and orthopyroxene, are abundant in a number of IVA magmatic irons and have an oxygen isotope composition that overlaps the range measured in L and LL chondrites (Clayton and Mayeda, 1996; Wang et al., 2004). On the basis of this evidence it has been suggested that the IVAs may be derived from the same parent body as either the L or LL chondrites (Clayton and Mayeda, 1996). Wang et al. (2004) undertook a high precision *in situ* laser fluorination study of silicates in four IVA specimens and found evidence of isotopic heterogeneity between samples. They concluded that this reflected precursor material heterogeneity rather than evidence that the IVAs were derived from multiple parent bodies. Cooling rate estimates for the IVAs (Wang et al., 2004) are consistent with breakup and reassembly models for the IVA parent body (Scott et al., 1994; Haack et al., 1996). In agreement with earlier studies, McCoy et al. (2011) concluded that the IVAs originated within an ~150 km radius molten metal body that was separated from a larger body during a catastrophic collision.

The non-magmatic IAB and IIICD irons were classified by Choi et al. (1995) as a single group, later termed the "IAB complex" by Wasson and Kallemeyn (2002). The IABs and associated meteorites represent the largest group of non-magmatic irons and characteristically contain chondritic silicate inclusions. Silicate inclusions in IABs show significant textural and mineralogical similarities to the winonaites and have overlapping oxygen isotope compositions (Section 3.2.4) (Clayton and Mayeda, 1996). It is generally accepted that both the winonaites and IABs sample a single parent body, which according to the model of Benedix et al. (1998, 2000, 2005), experienced early catastrophic disruption while undergoing partial melting and differentiation.

The IIE irons are also classified as a non-magmatic group, with silicate inclusions identified in about half of all the known speci-

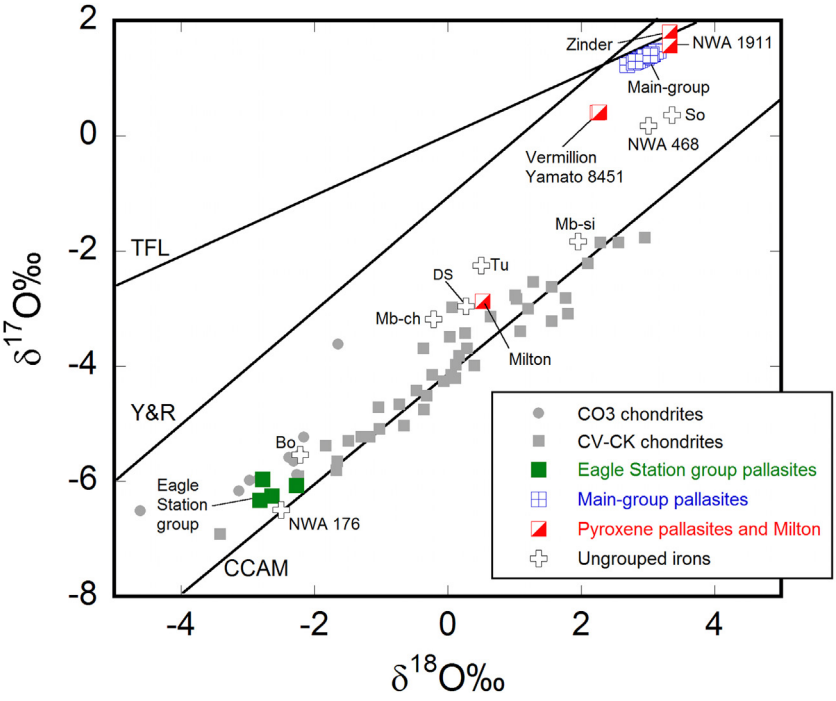

Fig. 18. Oxygen isotopic composition of pallasites and various ungrouped irons. Data sources: main-group pallasites: Greenwood et al. (2015a); Eagle Station pallasite group: Clayton and Mayeda (1996), Korochantsev et al. (2013); pyroxene pallasites: Clayton and Mayeda (1996), Bunch et al. (2005); Milton: Jones et al. (2003); CO3 chondrites: Greenwood and Franchi (2004); CV3 and CK chondrites: Greenwood et al. (2010); Ungrouped irons: Clayton and Mayeda (1996) and Meteoritical Bulletin Database. Key: TFL: Terrestrial Fractionation Line; Y&R: slope 1 line (Young and Russell, 1998); CCAM: Carbonaceous Chondrite Anhydrous Mineral line (Clayton et al., 1977; Clayton and Mayeda, 1999). Ungrouped irons: Mb-si: Mbosi silicates; Mb-ch: Mbosi chromite; Tu: Tucson; DS: Deep Springs; Bo: Bocaiuva; So: Sombrerete.

Table 5
Iron meteorites.

Group	Classification	mean $\Delta^{17}O$	Possible affinities	reference
IAB-IIICD	non-magmatic	−0.48 ± 0.20‰ (2σ) (1)	Winonaites	1
IIE	non-magmatic	0.69 ± 0.20‰ (2σ) (5)	H/HH chondrites	1, 3, 4, 5
IIIAB	magmatic	−0.18 ± 0.02‰ (2σ) (2)	Main-group pallasites	1,2
IVA	magmatic	1.16 ± 0.18‰ (2σ) (6)	L or LL chondrites	1, 6
Guin	Ungrouped	1.13	L or LL (IVA-related)	1
EET 83230	Ungrouped	1.134 ± 0.034‰ (2σ) (8)	L or LL (IVA-related)	8
Kendall County	Ungrouped	−0.3	IAB-related	1
NWA 6583	Ungrouped	−0.44	IAB-related	7
ALH 77255	Ungrouped	−0.48	IAB-related	1
LEW 86211	Ungrouped	−0.59	unknown	1
Sombrerete	Ungrouped	−1.39	unknown	1
NWA 468	Ungrouped	−1.39	unknown	Met Bull
Tucson	Ungrouped	−2.51	CV/CK/Milton pallasite	1
Mbosi	Ungrouped	−3.07; −2.84	CV/CK/Milton pallasite	1
Deep Springs	Ungrouped	−3.1	CV/CK/Milton pallasite	1
Bocaiuva	Ungrouped	−4.39	CV/CK/CO/Eagle Station Pall.	1
NWA 176	Ungrouped	−5.2	CV/CK/CO/Eagle Station Pall.	Met Bull

Notes: (1) Clayton and Mayeda (1996); (2) Franchi et al. (2013); (3) Franchi (2008); (4) Van Roosbroek et al. (2015); (5) McDermott et al. (2016); (6) Wang et al. (2004); (7) Fazio et al. (2013); (8) McCoy et al. (2011).

mens. In contrast to those in the IAB complex, silicate inclusions in IIEs are compositionally and texturally diverse, ranging from primitive chondritic to highly differentiated, although individual IIE meteorites characteristically contain only a single inclusion type (Van Roosbroek et al., 2015; McDermott et al., 2016). Silicate inclusions within individual IIE meteorites show only limited $\Delta^{17}O$ variability, whereas a relatively wide range of values is seen in the IIE suite as a whole, with a mean value of 0.69 ± 0.20‰ (2σ) (McDermott et al., 2016). A genetic link between the IIEs and H chondrites was supported by Clayton and Mayeda (1996) on basis of overlapping oxygen isotope variation, although this was later questioned by Franchi (2008), due to an offset between newer high-precision H chondrite data and the earlier IIE analyses. A detailed study of the chondrule-bearing Mont Dieu IIE iron by Van Roosbroek et al. (2015) yielded a $\Delta^{17}O$ value for its inclusions of 0.71 ± 0.02‰ (2σ), which falls within the H chondrite range of Clayton et al. (1991). Recent high precision oxygen isotope data for both the IIEs and H chondrites shows complete overlap and thus provides additional evidence for a genetic link between the two groups (McDermott et al., 2016). Both Van Roosbroek et al. (2015) and McDermott et al. (2016) favour an origin for the IIEs involving impact deformation of an H chondrite-related parent body.

As pointed out by Clayton and Mayeda (1996), ungrouped irons show a more extreme range in $\Delta^{17}O$ than the regular iron groups (IAB-complex, IIE, IIIAB, IVA), with values that extend to −5.2‰ (NWA 176) (Table 5) (Fig. 18). A potential genetic link between the C3 chondrites and the ungrouped irons with significantly negative $\Delta^{17}O$ values, such as Tucson, Mbosi, Deep Springs, Bocaiuva, and

NWA 176 was originally suggested by Clayton and Mayeda, 1996 (Fig. 18). The ungrouped irons NWA 176 and Bocaiuva also plot close to the Eagle Station group in Fig. 18, however, the evidence linking them to a single parent body is equivocal (Mittlefehldt et al., 1998; Franchi, 2008). Likewise, despite similar oxygen isotope compositions (Fig. 18), the ungrouped irons Deep Springs, Mbosi and Tucson do not appear to be related to the ungrouped pallasite Milton (Mittlefehldt et al., 1998; Franchi, 2008). NWA 468 and Sombrerete (Fig. 18) also appear to be unrelated to any other major group of meteorites. A number of the ungrouped irons have oxygen isotope compositions that overlap members of other iron groups, such as Kendal County, NWA 6583 and ALH 77244 with the IABs, Guin and EET 83230 with the IVAs. However, in most cases metal compositions and textures appear to exclude any direct relationships (Franchi, 2008). EET 83230 is an interesting example (McCoy et al., 2011). It has an oxygen isotope composition compatible with the IVAs, but has a higher Ni content and cooled faster. McCoy et al. (2011) conclude that EET 83230 may represent material that was ejected as a separate mass during the impact event that created the IVA parent body.

3.4. Ungrouped and anomalous achondrites

Ungrouped achondrites are of particular interest because they may be derived from unique parent bodies that would otherwise be unrepresented in the meteorite record. In a similar way to ungrouped irons, they have the potential to significantly expand the range of early Solar System bodies available for scientific investigation. Oxygen isotope analysis is an important technique in establishing possible links between such meteorites and the more well-defined groups for which we have larger sample suites.

3.4.1. Ungrouped primitive achondrites

An increasing number of ungrouped olivine-rich achondrites are being identified which show mineralogical, textural and oxygen isotopic affinities to the brachinites (Day et al., 2012a; Greenwood et al., 2012; Krot et al., 2014). These include: Al Huwaysah 010, Divnoe, NWA 1500, NWA 4042, NWA 4518, NWA 5400 (and pairs), Zag (b) (Table S5; Fig. 19). The nature of the relationship between the brachinites and these ungrouped olivine-rich achondrites is not always clear cut. In part this reflects the somewhat poorly defined characteristics of the brachinite group itself (Section 3.2.2). A few examples serve to illustrate the problems involved in deciding whether these meteorites are actually brachinites, or whether they are compositionally similar, but otherwise unrelated samples.

Divnoe is an ungrouped olivine-rich primitive achondrite, with an oxygen isotope composition that plots within the brachinite field (Fig. 19). The composition of olivine in Divnoe ($Fa_{20\text{-}28}$) just overlaps the brachinite range ($Fa_{27\text{-}36}$) (Petaev et al., 1994; Goodrich et al., 2010). It has been suggested by Delaney et al. (2000) that Divnoe may be related to the brachinites by a process involving reduction of iron-rich olivine of the type:

$$Fe_2SiO_4 + CO \rightarrow FeSiO_3 + Fe + CO_2$$

However, Divnoe plots off the redox trend defined by other brachinites (Goodrich et al., 2010) and consequently, despite showing mineralogical similarities to the brachinites, is probably derived from a distinct parent body. NWA 1500 was originally classified as a basaltic ureilite (Bartoschewitz et al., 2003), but has an oxygen isotope composition that plots in the main brachinite field (Fig. 19). More recent studies of the mineralogy and geochemistry of NWA 1500 have concluded that it should be reclassified as a brachinite (Kita et al., 2009b; Goodrich et al., 2010). In keeping with this suggestion, NWA 1500 was included within the brachinites discussed in Section 3.2.2. The olivine-rich achondrite NWA 4042 shows textural similarities to the brachinites and has an oxygen isotope composition that plots towards the edge of the brachinite field (Fig. 19). However, like Divnoe, the composition of olivine in NWA 4042 ($Fa_{20.3}$) (Meteoritical Bulletin Database) is less Fe-rich than that of the brachinites. Further work is required before NWA 4042 can be reclassified as a brachinite (Rumble et al., 2008). Zag (b) (currently classified as a winonaite) has an oxygen isotope composition indistinguishable from the brachinites (Delaney et al., 2000; Day et al., 2012a) (Fig. 19). It contains relatively magnesian olivines (Fa_{22}) compared to normal brachinites, but may be linked to the latter group via a similar redox process to that outlined for Divnoe (Delaney et al., 2000). Further evidence that such redox reactions may be an important factor in the genesis of olivine-rich achondrites is given by the olivine-rich ultramafic breccia NWA 4518 (Lorenz et al., 2007, 2011). The oxygen isotope composition of this meteorite plots on the edge of the brachinite field (Fig. 19). It contains two generations of olivine: the equigranular groundmass has a composition of Fa_{32}, whereas olivine inclusions in pyroxene megacrysts have a more Mg-rich composition of $Fa_{19.4}$ (Lorenz et al., 2007). NWA 5400 (and paired samples) (Table S5) is a coarse-grained, olivine-rich (~Fa_{30}) (79 vol.%) rock, which has a brachinite-like mineralogy, but an oxygen isotope composition which plots essentially on the terrestrial fractionation line (Fig. 19) (Irving et al., 2009; Day et al., 2012a, Meteoritical Bulletin Database). Thus, including NWA 5400 within the brachinites would further extend the group's oxygen isotope field (Fig. 19).

A number of meteorites which plot close to the brachinite field in Fig. 19, based on their mineralogy, are unrelated samples. NWA 8777 consists predominantly of orthopyroxene (88.6 vol.%), with subordinate olivine (9.0 vol.%) (~Fa_{31}) and minor calcic feldspar. The low olivine content and calcic plagioclase composition suggest that NWA 8777 is an ungrouped achondrite (Irving et al., 2015). NWA 2993 is a coarse-grained, metal-rich achondrite which has a reduced mineralogy that resembles that of the acapulcoite/lodranites and winonaites, but has an oxygen isotope composition that plots well away from either group and would appear to represent a unique sample (Bunch et al., 2007) (Fig. 19). Dho 1441 plots on the edge of the brachinite field in Fig. 19, but based on its Meteoritical Bulletin description appears to be an impact melt breccia containing a variety of clast types.

The unique, paired, sodic plagioclase-rich achondrites GRA 06128 and GRA 06129 (=GRA 06128/9) plot in the brachinite field in Fig. 19 (Day et al., 2009, 2011, 2012a; Shearer et al., 2010). Experimental and petrological studies indicate that melts with a composition similar to GRA 06128/9 are produced at temperatures between Fe,Ni sulphide melting (950–980° C) and the onset of basaltic melting (>1050° C) (Shearer et al., 2010). In this temperature interval, partial melting of between 13 and 30% of an oxidized chondritic source, followed by inefficient removal of the felsic melt, will leave a residue with a brachinite composition (Shearer et al., 2010; Day et al., 2011; Gardner-Vandy et al., 2013). On the basis of this evidence it has been suggested that GRA 06128/9 may represent evolved felsic crustal material from the brachinite parent body (Day et al., 2009, 2011).

LEW 88763 is still currently classified as a brachinite, however, a variety of evidence, including its oxygen and noble gas isotopic compositions, suggests that it is not a member of this group (Clayton and Mayeda, 1996; Swindle et al., 1998). LEW 88763 plots at the edge of the acapulcoite-lodranite field (Fig. 19), but has a mineralogy and geochemistry indicating that it is a unique, ungrouped achondrite (Swindle et al., 1998). LEW 88763 may be related to the metal-rich achondrite Tafassasset (Fig. 19) (Nehru et al., 2003, 2010; Gardner-Vandy et al., 2012). Two other brachinite-like, ungrouped achondrites NWA 6962 and NWA 7680 plot close to each other in Fig. 19 and are both composed predomi-

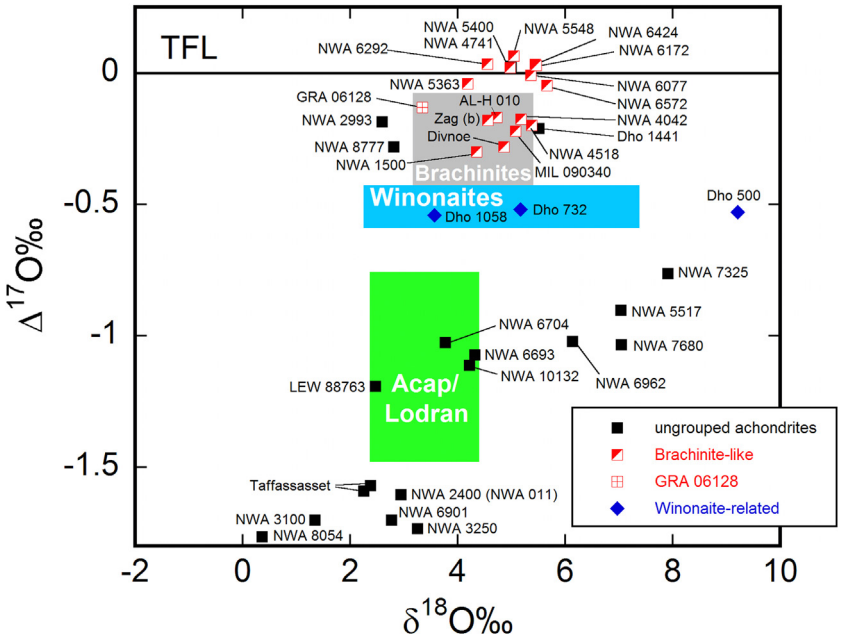

Fig. 19. The oxygen isotopic composition of anomalous and ungrouped primitive achondrites shown in relation to the main primitive achondrite groups (data: Table S5).

nantly of relatively Fe-rich olivine i.e., ~Fa_{47} and Fa_{45} respectively, suggesting that they may be related or paired (Hyde et al., 2013).

Dho 732 and NWA 1058 plot in the winonaite field in Fig. 19, while Dho 500 lies along the extension of the winonaite trend at higher $\delta^{18}O$ values. All three meteorites show mineralogical similarities to the winonaites, but further work is required to validate this classification (Lorenz et al., 2003; Greenwood et al., 2012).

Ungrouped achondrites with affinities to the acalpulcoite-lodranite clan appear to be rare. While the orthopyroxene-rich, highly oxidized achondrite NWA 6693, and related samples NWA 6704 and NWA 10132, plot in the acapulcoite-lodranite field in Fig. 19 mineralogical evidence suggests that they are not related to the latter group (Warren et al., 2013; Irving et al., 2015). The Meteoritical Bulletin entry for NWA 5517 suggests some affinities with the acapulcoites and lodranites on the basis of its similar oxygen isotope composition. However, NWA 5517 plots away from the acapulcoite-lodranite field in Fig. 19. The entry for NWA 5517 also points to its lack of orthopyroxene and paucity of metal as reasons for excluding a direct link with the acapulcoites and lodranites. NWA 7325, which plots relatively close to NWA 5517 in Fig. 19 is an unrelated sample based on its mineralogy; consisting of 56 vol.% calcic plagioclase ($An_{88.1\text{-}89.2}$), 27% diopside and 16% olivine (Fa_3) (Irving et al., 2013). It has been suggested that NWA 7325 is a possible candidate for being a meteorite from Mercury (Irving et al., 2013), and while this is unlikely (Barrat et al., 2015; Weber et al., 2016), there is evidence to suggest that it may represent a sample of one of the earliest asteroidal crusts so far studied (Barrat et al., 2015).

A number of samples which span the chondrite-achondrite transition (petrologic type 6 and above), and which sometimes contain relict chondrules, have been described as "metachondrites" and linked to the CR parent body (Bunch et al., 2008; Sanborn et al., 2014). In addition to NWA 6693, NWA 6704 and Taffassasset, this group also includes the primitive achondrites NWA 3100, NWA 3250, NWA 6901 and the ungrouped chondrite NWA 2994 (Sanborn et al., 2014). On the basis of its ^{54}Cr composition, the coarse-grained achondrite NWA 8054, which plots close to NWA 3100 in Fig. 19, appears to be an unrelated sample (Sanborn et al., 2014). However, in the case of NWA 6901 and the paired samples NWA 2994 and NWA 3250, Zipfel (2014) argues against a close affinity with the CR parent body on the basis of major element variation.

A number of ungrouped and primitive achondrites have very negative $\Delta^{17}O$ values and appear to be related to various carbonaceous chondrite groups (Fig. 20). While both of the ungrouped achondrites NWA 7822 and NWA 8186 are composed predominantly of olivine, and plot close to each other near the CCAM line in Fig. 20, they appear to be unrelated samples. NWA 8186 contains magnetite and no metal or troilite; this along with the presence of Cl-rich apatite and high Ni contents in olivine suggests an affinity with the CK chondrites (Agee et al., 2014; Srinivasan et al., 2015). In comparison, NWA 7822 contains accessory taenite and magnetite and shows affinities to the CV chondrites (Kuehner et al., 2013). The primitive achondrite NWA 3133 does not contain chondrules, has a recrystallized metamorphic texture with 120° triple grain junctions and may be related to the CV chondrite group (Irving et al., 2004; Schoenbeck et al., 2006).

Some ungrouped achondrites have oxygen isotope compositions that plot above the terrestrial fractionation line and show affinities with the ordinary chondrites (Fig. 21). NWA 2353, NWA 2635 and NWA 7835 show mineralogical affinities with the H chondrites according to their respective Meteoritical Bulletin entries. However, two of these samples, NWA 2353 and NWA 7835, plot somewhat away from the H chondrite field in Fig. 21. In the case of NWA 2353 this could reflect the influence of terrestrial weathering. NWA 7835 is a complex breccia and it is suggested that this may explain its very variable oxygen isotope results. Ungrouped and primitive achondrites showing affinities with the L (NWA 4284) and LL chondrites (NWA 5297, NWA 6698) are also recognized (Fig. 21).

3.4.2. *Ungrouped and anomalous basaltic achondrites*

As discussed in Section 3.3.3, the fact that the vast majority of diogenite, eucrite and cumulate eucrite samples have virtually identical $\Delta^{17}O$ values lends support to the view that all of the major HED lithologies are derived from a single parent asteroid (McSween et al., 2013). However, a relatively small group of basaltic achondrites have $\Delta^{17}O$ that lie at least 3σ outside the mean value defined by the HED falls, i.e., -0.240 ± 0.021‰ (3σ) (Fig. 22) (Scott et al., 2009). A list of currently identified anomalous basaltic achondrites is given in Table 6.

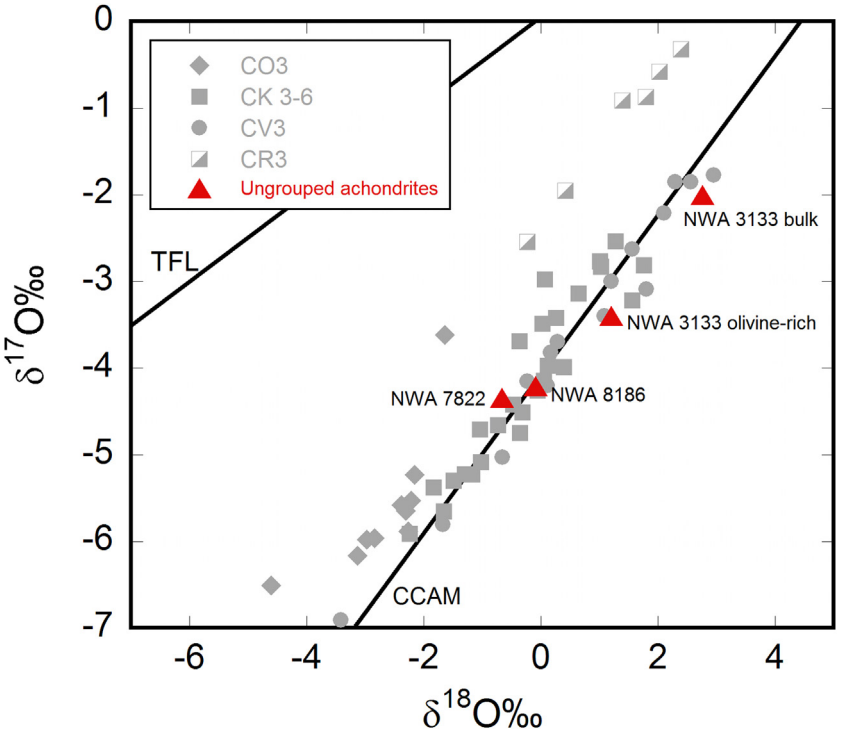

Fig. 20. Oxygen isotopic composition of ungrouped and primitive achondrites with carbonaceous chondrite affinities (data: Table S5).

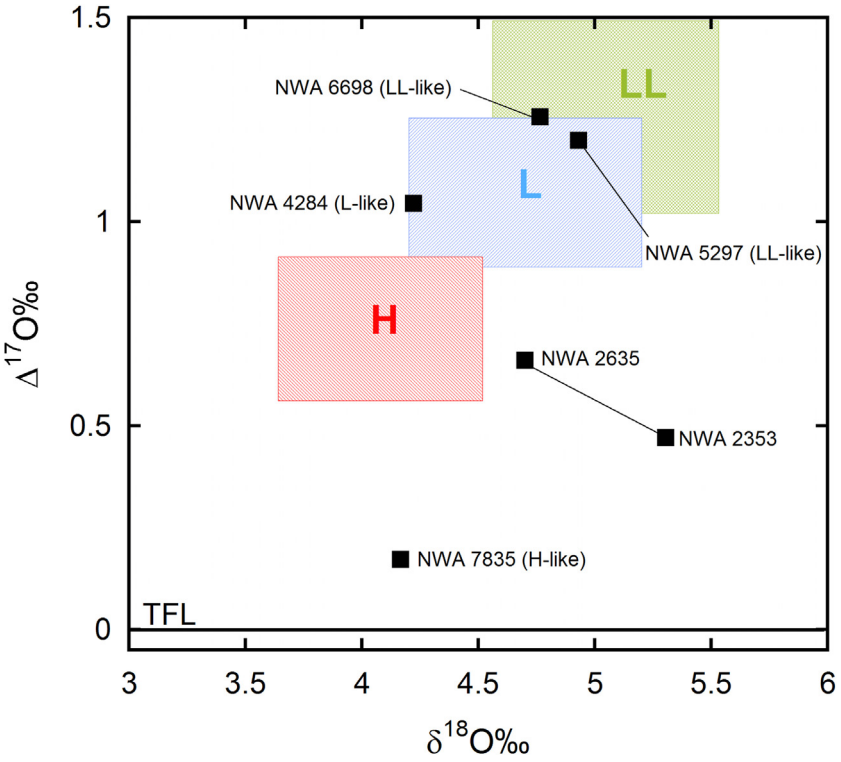

Fig. 21. Oxygen isotopic composition of ungrouped and primitive achondrites with ordinary chondrite affinities (data: Table S5).

With the exception of NWA 1240 and NWA 011 (and pairs e.g. NWA 2400 Fig. 19) all the known anomalous basaltic achondrites plot between the eucrite fractionation line (EFL) and the angrite fractionation line (AFL). NWA 011, despite its basaltic mineralogy (Yamaguchi et al., 2002), has a $\Delta^{17}O$ composition far removed from the other basaltic achondrites, i.e., −1.604‰ for the paired sample NWA 2400 (Table 6) and plots close to the acapulcoite-lodranite field in Fig. 19. The $\varepsilon^{54}Cr$ composition of NWA 011 places it in the same group as the carbonaceous chondrites (Fig. 10) (Warren, 2011a). As is clear from Fig. 15, the howardites Bholghatti, SCO 06040 and Jodzie also have anomalously bulk oxygen isotope composition when compared to other HEDs. However, this

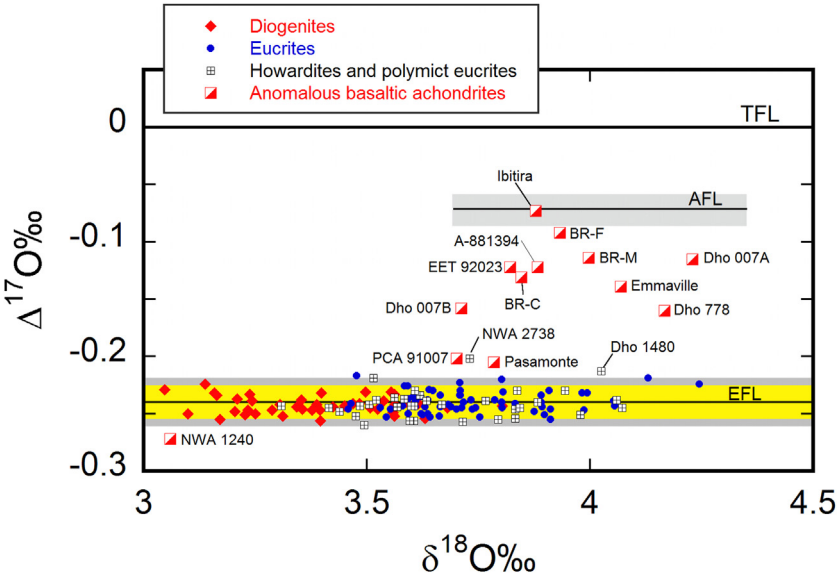

Fig. 22. Oxygen isotopic composition of anomalous basaltic achondrites shown in relation to the HED analyses plotted in Fig. 15 (Table S4). Central shaded zone: ±2σ precision for eucrite and diogenite falls only (n = 26). Outer shaded zone: ±3σ precision for eucrite and diogenite falls only (n = 26). References and data for the anomalous basaltic achondrites given in Table 6. Data for angrites from Greenwood et al. (2005) (Table 2). Abbreviations, EFL: eucrite fractionation line, AFL: angrite fractionation line, TFL: terrestrial fractionation line, BR-F: Bunburra Rockhole fine-grained lithology, BR-M: Bunburra Rockhole medium-grained lithology, BR-C Bunburra Rockhole coarse-grained lithology (BR analyses from Bland et al., 2009a,b).

Table 6
Oxygen isotopic composition of anomalous basaltic achondrites.

Sample Name	Classification	FALL?	N	References	$\delta^{17}O‰$	1σ	$\delta^{18}O‰$	1σ	$\Delta^{17}O‰$	1σ
A-881394	Cumulate eucrite	N	6	1	1.912	0.036	3.882	0.084	−0.122	0.015
Bunburra Rockhole	Eucrite	Y	9	2	1.945	0.049	3.925	0.073	−0.112	0.021
Dhofar 007 – Lithology A	Cumulate eucrite	N	2	This study	2.102	0.035	4.229	0.062	−0.115	0.002
Dhofar 007 – Lithology B	Cumulate eucrite	N	9	This study	1.772	0.130	3.711	0.248	−0.173	0.005
Dhofar 778	Diogenite	N	4	This study	2.024	0.019	4.167	0.068	−0.160	0.027
EET 92023	Unbrecciated eucrite	N	4	This study	1.881	0.044	3.821	0.097	−0.122	0.018
Emmaville	Monomict eucrite	Y	5	This study	1.993	0.036	4.069	0.093	−0.139	0.016
Ibitira	Monomict eucrite	Y	6	3	1.960	0.021	3.878	0.045	−0.073	0.015
NWA 2400 (pair of NWA 011)	ungrouped basaltic achondrite	N	1	This study	−0.060		2.947		−1.604	
Pasamonte	Polymict eucrite	Y	23	1,2, 4	1.778	0.052	3.785	0.098	−0.205	0.011
PCA 91007, 2	Brecciated eucrite	N	5	1	1.738	0.062	3.701	0.116	−0.202	0.011

Notes: 1: Scott et al. (2009); 2: Bland et al. (2009a,b); 3: Wiechert et al. (2004); 4; Greenwood et al. (2005).

reflects their relatively high content of impact-derived carbonaceous chondrite-related material (Section 3.3.3) and so the origin of these howardites will not be discussed further here. The howardite NWA 2738 and the polymict eucrite Dho 1480 also plot outside the 3σ envelope in Fig. 22. This might reflect the influence of terrestrial contamination, but based on their Meteoritical Bulletin entries both samples show only minimal weathering effects. Both samples require further detailed study, but one possible explanation for their anomalous isotopic compositions is that they may contain an impact-derived component in which the impactor had a $\Delta^{17}O$ value that was more positive than isotopically normal HEDs (see evidence from JaH 556 discussed below).

As pointed out by McSween et al. (2013) and Mittlefehldt (2015), the various explanations advanced to explain the origin of anomalous basaltic achondrites have significant consequences for the interpretation of HED oxygen isotope data as a whole. Thus, Wiechert et al. (2004) proposed that both normal and anomalous samples come from a single heterogeneous HED parent body. In contrast, Scott et al. (2009) suggested that the isotopically anomalous samples may have come from distinct asteroidal sources. This latter explanation implies that the HED parent body itself had a very homogeneous $\Delta^{17}O$ composition, consistent with magma ocean models (Greenwood et al., 2005). As an explanation for the origin of at least some anomalous basaltic achondrites, Greenwood et al. (2005) and Janots et al. (2012) highlighted the possible role of impact processes as a mechanism for producing isotopic heterogeneity.

In the case of a few anomalous basaltic achondrites, such as NWA 011 (Yamaguchi et al., 2002), Ibitira (Mittlefehldt, 2005b), and A-881394 (Nyquist et al., 2003), a range of evidence would seem to indicate that they are not from the same parent body as the majority of HED samples (Scott et al., 2009). However, the situation is less clear cut for the others, with at least some showing significant degrees of brecciation, e.g., Pasamonte (Metzler et al., 1995) and Dhofar 007 (Yamaguchi et al., 2006). In addition, extremely elevated siderophile element contents are observed in a number of anomalous basaltic achondrites, such as EET 92023 (Mittlefehldt and Lindstrom, 1996; Kaneda and Warren, 1998) and Dhofar 007 (Yamaguchi et al., 2006) and to a lesser extent, but still significantly higher than normal eucritic levels, in others, such as Pasamonte (Dale et al., 2012; Day et al., 2012b). While it is likely that some anomalous eucrites are derived from distinct parent bodies, a number may be the products of impact mixing on the surface of the HED parent body.

The highly shocked diogenite Dho 778 (shock stage S4) has an anomalous oxygen isotope composition (Fig. 22). Very little work has so far been undertaken on Dho 778, but as the only known anomalous diogenite this sample clearly merits further detailed

examination. Its anomalous composition may be due to contamination with impactor-derived material, or alternatively reflects a high degree of terrestrial weathering. This latter possibility seems unlikely in view of its relatively low weathering grade (W1) (Meteoritical Bulletin Database). Dhofar 007 was studied in detail by Yamaguchi et al. (2006) and it was concluded that it showed some affinities to the mesosiderites. Two separate fractions of this meteorite (Dho 007A and B, Fig. 22, Table 6) analyzed at the Open University have distinct $\Delta^{17}O$ compositions. Likewise, Bunburra Rockhole is composed of brecciated material of varying grain-sizes, which display significant levels of heterogeneity with respect to $\Delta^{17}O$ (Bland et al., 2009a; Benedix et al., 2014a).

The relatively constrained distribution of anomalous basaltic meteorites (with the notable exception of NWA 011), lying between the EFL and AFL (Figs. 22 and 23) could be interpreted as reflecting impact mixing between isotopically normal HED lithologies and material that has a heavier $\Delta^{17}O$ composition. An example of where this has actually taken place is provided by the anomalous howardite JaH 556 (Janots et al., 2012). This specimen is a weathered impact melt breccia, comprising highly shocked clasts set in a finely recrystallized, vesicular matrix. Its bulk oxygen isotope composition is anomalous, with a $\Delta^{17}O$ value of −0.11‰ (Fig. 23). In contrast, EATG-washed clasts in JaH 556 have normal HED $\Delta^{17}O$ values (Fig. 23). JaH 556 has a highly enriched siderophile element content and contains clasts that appear to be relict chondrules, with olivine compositions consistent with an H chondrite precursor. Both the siderophile element content of JaH 556 and its bulk oxygen isotope composition point to it containing a 10–15% H chondrite component. An impact origin for an anomalous HED could be overlooked when a lower percentage of impactor material is present, or was non-chondritic (i.e., low siderophile element content), such as would be the case if the impactor was an angrite, aubrite, or an ordinary chondrite-related achondrite.

It is clear from the preceding discussion that considerable uncertainty still exists concerning the origin of anomalous basaltic achondrites. The tightly constrained distribution of the bulk of these meteorites, lying between the EFL and AFL (Figs. 22 and 23), could be interpreted as supporting an impact origin. On the other hand, the relatively low siderophile element contents of some anomalous basaltic achondrites argues against impact-mixing as a general process in the formation of these meteorites (Scott et al., 2009). The possibility that they are simply samples of a heterogeneous HED parent body is not supported by their one-sided distribution in oxygen isotope space (Figs. 22 and 23). Clearly, further work is required to understand the origin of these anomalous meteorites.

4. Discussion

4.1. Understanding the meteorite record: an oxygen isotope/remote sensing perspective

Meteorites provide us with a great diversity of extraterrestrial materials that are capable of yielding fundamental insights into early Solar System evolution. However, in order to interpret the meteorite record effectively we need to evaluate its relationship, both to the contemporary asteroid population and also to how that population has evolved with time. This involves addressing a number of key issues. Firstly, it is important to evaluate how many asteroids/parent bodies are represented in the worldwide meteorite collection (e.g. Burbine et al., 2002a; Hutchison, 2004). Secondly, we need to assess how representative the meteorite record is both of the NEO and main belt populations (Burbine et al., 2002a; Vernazza et al., 2008; Thomas and Binxel, 2010). Finally, we need to address the question of just how useful contemporary meteorites and asteroids are as indicators of the composition and structure of the first generation planetesimals that populated the Solar System prior to the accretion of the terrestrial planets? Relevant to this final question are the proposals that: (i) migration of the giant planets played a critical role in controlling the present structure of the asteroid belt (Walsh et al., 2011); (ii) that existing differentiated asteroids, such as 4 Vesta, are secondary bodies (Consolmagno et al., 2015), and (iii) that early fragmentation of planetesimals resulted in differential loss of mantle materials (Bell et al., 1989; Burbine et al., 1996; Jacobson et al., 2016).

In this section, we look first at the evidence provided by oxygen isotopes concerning the likely number of differentiated parent bodies represented within the meteorite record. We then use remote sensing observations to assess how samples that arrive on Earth are related to the asteroids present in both the NEO and main belt

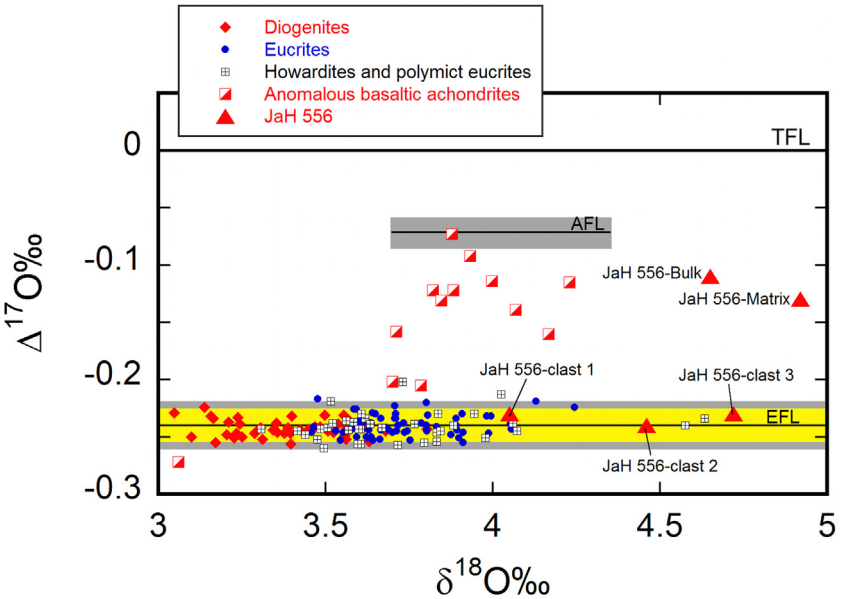

Fig. 23. Oxygen isotopic composition of clasts, matrix and bulk for the howardite JaH 556. All of the JaH 556 fractions were treated using EATG to mitigate the effects of terrestrial weathering (JaH 556 data: Janots et al., 2012). Abbreviations as Fig. 22.

populations. Finally, we evaluate the likely relevance of our existing samples to the population of planetesimals formed in the first few million years of Solar System history.

4.1.1. How many differentiated parent bodies are present in our meteorite collections?

It was estimated by Burbine et al. (2002a) that our meteorite collections could represent as few as ~100 asteroids (~27 chondritic, ~2 primitive achondritic, ~6 differentiated achondritic, ~4 stony-irons, ~10 iron groups, ~50 ungrouped irons). They suggested that this number could increase to ~150 depending on the interrelationships between ungrouped irons (117 ungrouped irons are currently listed on the Meteoritical Bulletin database). In line with these estimates, Hutchison (2004) suggested that meteorites are sourced from approximately 120 asteroids, with about 80 of these bodies being represented by ungrouped irons. However, Wasson (2013b) is more conservative and suggests that only 17 asteroids are sampled by the ungrouped irons, making a total of 26 asteroids represented by irons as a whole. As pointed out by Burbine et al. (2002a), estimates of how many distinct parent bodies are represented in our meteorite collections are evolving rapidly due to new finds, principally from Antarctica and the Sahara. As a consequence of their relatively high commercial value, achondrites are particularly sought after and so there is currently a high recovery rate of unique and unusual specimens from the Sahara. Here, we use the oxygen isotope evidence reviewed earlier (Sections 3.2, 3.3, 3.4) to assess the number of distinct parent bodies that were the source of the achondrites (Table 7).

In the case of the main primitive achondrite groups (acapulcoite-lodranite clan, brachinites, ureilites and winonaites) a minimum of 4 parent bodies is required. As discussed in Section 3.4.1, there is considerable uncertainty about which samples should be included in the brachinite group. We have essentially separated the brachinites and brachinite-like achondrites into two groups on the basis of olivine composition. One group we designate as "brachinites and brachinite-related samples" and a second group we have termed "Mg-rich, brachinite-like". This second group comprises samples such as Divnoe, which contain olivines with a relatively magnesian composition. Apart from the pallasites, which appear to be derived from six distinct parent bodies (Section 3.3.5.4) and the aubrites which are probably samples from two (see Section 3.3.2), all of the other main differentiated and stony-iron groups appear to be samples from just a single parent body. Greenwood et al. (2015a) have reviewed the evidence in favour of a single parent body for the mesosiderites and HEDs. However, here we have adopted the more conventional approach and assigned each to a distinct source asteroid. Based on the analysis presented in Section 3.4.1 ungrouped primitive achondrites and related samples would appear to be derived from about 16 parent bodies. There is considerable uncertainty associated with this figure, as the interrelationships between the various samples are, in many cases, speculative and require further detailed study to be fully evaluated. Finally, the ungrouped and anomalous basaltic achondrites could be derived from as few as 4 parent bodies (Section 3.4.2). The relationship between these samples is poorly understood and the subject of active research. An extreme position would be that each anomalous basaltic achondrite sample is derived from a distinct source, in which case about 10 different parent bodies are required. Alternatively, by solely invoking impact-related processes, or a highly heterogeneous composition for Vesta, only two parent bodies would be needed, one for NWA 011 and another (4 Vesta) for the remaining samples.

In summary, it would seem that silicate-rich achondrites (Table 7) are samples from approximately 35 parent bodies. This estimate lies within the range of 26 to 60 parent bodies thought to be represented by the iron meteorites (Scott, 1972; Burbine et al., 1996; Mittlefehldt et al., 1998; Haack and McCoy, 2005; Chabot and Haack, 2006; Wasson, 2013b; Benedix et al., 2014b). Assuming that irons are derived from a higher number of parent bodies than the achondrites, this may simply be a reflection of the greater space survivability of irons and stony-irons compared to stones (Burbine et al., 2002a).

An important question that now arises is whether irons and silicate-rich meteorites are derived from the same, or distinct asteroid populations. A range of evidence indicates that the parent bodies of the irons accreted over a very brief time interval and then heated up and differentiated rapidly (see Section 4.4). Contrary to the suggestion that such asteroids may have been surrounded by a chondritic shell (Elkins-Tanton et al., 2011; Weiss and Elkins-Tanton, 2013), it would seem that heating may have been too intense to have preserved anything other than a thin vestigial chondritic surface layer (Hevey and Sanders, 2006). Cooling rate studies of iron meteorites indicate that such early-formed bodies were the subject of rapid fragmentation, with the irons essentially losing most, if not all, of their silicate mantles and crust (Goldstein et al., 2009, 2014; The survivability of this silicate material is discussed further in Section (4.1.3.2).

Oxygen isotope studies provide some evidence to link silicate and iron meteorite groups, the most notable examples being the winonaites with the IAB-IIICD irons, IVA irons with L or LL group chondrites, IIE irons with H group chondrites, and possibly also main-group pallasites with the IIIAB irons (Section 3.3.6). However, apart from the disputed relationship between main-group pallasites and IIIABs, the other iron groups are in association with more primitive silicate material than would be produced by a fully differentiated asteroid. Without additional evidence to link them, it seems likely that the majority of irons are derived from separate parent bodies to the chondritic and achondritic meteorites. On this basis we can update the parent body inventory of Burbine et al. (2002a) as consisting of ~110 asteroids (~60 irons, ~35 achondrites, ~15 chondrites). In the main belt the number of asteroids with diameters >1, 50 and 100 km is 1.36×10^6, 680 and 220 respectively (Bottke et al., 2005). Provided meteorites are just sampling the larger bodies (e.g. diameters >100 km), then the figure of 110 asteroids might suggest that we have a representative sampling of the asteroid belt. However, the mechanisms involved in meteorite delivery from the main belt are complex and it is extremely unlikely that we have material from just the larger asteroids in our collections (Burbine et al., 2002a).

4.1.2. Asteroid – meteorite links: remote sensing observations

In the previous section we used the oxygen isotope evidence presented earlier in this review as a means of assessing how many distinct parent bodies we have samples of in our meteorite collections. Remote sensing observations provide an independent means of examining how representative the meteorite record is of the overall Solar System distribution of differentiated asteroids (Burbine, 2014, 2016a). Are we just sampling material from a few relatively recently-formed asteroid families, or do we have samples from a wider range of sources? V–type asteroids provide an interesting case study. The bulk of HEDs (V–types) appear to come from Vesta. However, oxygen isotope evidence suggests that a small subgroup have anomalous compositions (Section 3.4.2). Are these also from Vesta and hence is Vesta more heterogeneous than previously suggested by magma ocean models (Greenwood et al., 2005, 2006), or are there other sources of V types in the main belt?

Remote sensing observations of asteroids have identified possible meteorite parent bodies for all differentiated achondrites. The reflectance of powdered meteorite samples in the visible and near-infrared can easily be measured in the laboratory and compared to the reflectance spectra of asteroids measured at a telescope.

Table 7
Estimate of the number of parent bodies sampled by primitive and differentiated achondrites.

Meteorite groups	Related samples and pairs	Comments	Parent bodies (N)
Primitive achondrites			
Accapulcoite-Lodranite clan			1
Winonaites (plus IAB, IIICD irons)	Dho 500, Dho 732, Dho 1441, NWA 1058		1
Brachinites and brachinite-related samples	Al Huwaysah 010, GRA 06128/9, Mil 090206 (and pairs), NWA 4518, NWA 5400 (and pairs: 5363, 5548,6077,6172,6292,6424,6572)		1
Ureilites			1
Differentiated achon. and stony irons			
Pallasites			
Main-Group			1
Eagle-Station Group			1
Pyrox. pall. I	Vermillion, Y-8451		1
Pyrox. pall. II	NWA 1911		1
Pyrox. pall. III	Zinder		1
Milton			1
Mesosiderites			1
HEDs	Dho 778, Dho 1480, JaH 556, NWA 1240, NWA 2738		1
Angrites			1
Aubrites			2
Ungrouped primitive achondrites			
Mg-rich, brachinite-like	Divnoe, NWA 4042, NWA 4518, RBT 04255, RBT 04239, Zag(b),		1
NWA 8777			1
NWA 2993			1
LEW 88763		Brachinite-like mineralogy	1
Tafassasset		chondrule-bearing/primitve achondrite	1
NWA 6693	NWA 6704, NWA10132		1
NWA 5517			1
NWA 7325	NWA 8014, 8268, 8486	olivine gabbro	1
NWA 6962	NWA 7680	Brachinite-like mineralogy	1
NWA 3100	NWA 2994, NWA 3250, NWA 6901, NWA 8548	CR Chondrite-related	1
NWA 8054			1
NWA 3133	NWA 7822	CV Chondrite-related	1
NWA 8186		CK Chondrite-related	1
NWA 5297	NWA 6698	LL Chondrite-related	1
NWA 4284		L Chondrite-related	1
NWA 2353	NWA 2635, NWA 3145, NWA 7835	H Chondrite-related	1
Anomalous basaltic achondrites			
NWA 011 (and pairs)	NWA 2400, 2976, 4587, 4901, 5644, 7129, 8545		1
Ibitira			1
A-881394	Bunburra Rockhole, Emmaville, Dho 007, EET 92023		1
Pasamonte	PCA 91007		1
		TOTAL	35

Many minerals (e.g., olivine, pyroxene) have distinctive absorption features in this wavelength region (e.g., Burns, 1993).

Ureilites were traditionally linked with S-complex asteroids (Gaffey et al., 1993). However, this interpretation changed when near-Earth asteroid 2008 TC_3 collided with the Earth's atmosphere in October of 2008 and had fragments raining down over the Sudan (Jenniskens et al., 2009, 2010). These recovered meteorites (called Almahata Sitta) were primarily polymict ureilites (Zolensky et al., 2010; Bischoff et al., 2010). A visible reflectance spectrum of 2008 TC_3 was obtained (Jenniskens et al., 2009) before impact and was found to be a C-complex body. The asteroid was classified as an F-type, which is a class defined in the Tholen (1984) taxonomic system, due to its relatively flat reflectance spectrum. In hindsight, this should not have come as a surprise, since ureilites had been noted to be spectrally similar to C-complex asteroids due to their weak absorption features resulting from their high carbon contents (Cloutis and Hudon, 2004; Cloutis et al., 2010). However, some ureilites have stronger absorption bands (Cloutis et al., 2010) and their parent bodies could potentially be classified as K-types (Burbine, 2016b), or S-complex bodies.

Angrite spectra have been found (Burbine et al., 2006) to have a very broad 1 μm feature, but a weak to absent 2 μm band, consistent with a mineralogy of diopside-hedenbergite and olivine. S-complex Mars Trojan (5261) Eureka was identified by Rivkin et al. (2007) as having spectral properties similar to angrites. Cloutis et al. (2006) interpreted the reflectance spectrum out to ~1.65 μm of O-type (3628) Božněmcová to be consistent with an angrite-like mineralogy, but near-infrared spectra out to 2.5 μm of Božněmcová (DeMeo et al., 2009; Burbine et al., 2011) show a 2 μm band that is not consistent with an angrite mineralogy.

Aubrites have been traditionally linked to E-type asteroids (e.g., Zellner, 1975; Zellner et al., 1977), since both types of objects have high visual albedos and flat reflectance spectra. Aubrites are enstatite-rich, a white, virtually FeO-free, mineral. E-types are commonly found in the Hungaria region (Clark et al., 2004; Ćuk et al., 2014) of the inner asteroid belt. Bus and Binzel (2002a,b) identified a feature shortwards of 0.5 μm in a number of X-types (flat visible reflectance spectra) that has been attributed to oldhamite (Burbine et al., 2002b), a mineral commonly found in aubrites (Watters and Prinz, 1979; Mittlefehldt et al., 1998).

Due to spectral similarities in the visible (McCord et al., 1970) and near-infrared (Larson and Fink, 1975) HEDs have been linked to asteroid 4 Vesta. This compositional similarity was confirmed by the Dawn mission, which also found that Vesta's surface had elemental ratios from gamma ray analyses that are consistent with HEDs (Prettyman et al., 2012). Binzel and Xu (1993) had previ-

ously identified a number of small objects (called Vestoids) with HED-like spectra in the Vesta family and between Vesta and the 3:1 and ν_6 meteorite-supplying resonances. However, a number of Vestoids have been identified past the 3:1 resonance (e.g., Roig and Gil-Hutton, 2006; Roig et al., 2008) and it is unclear whether it is dynamically possible to derive all these bodies from Vesta. The most notable of these bodies is (1459) Magnya (Lazzaro et al., 2000; Hardersen et al., 2004), which is located at a semi-major axis of 3.14 AU, far from Vesta's location (2.36 AU). As discussed in Section 3.4.2, oxygen isotope evidence demonstrates that a small group of basaltic achondrites have anomalous compositions and may be derived from at least three parent bodies in addition to 4 Vesta. Is it possible that (1459) Magnya may be the source for at least some of these anomalous basaltic achondrites? Analysis of the fireball associated with the fall of the Bunburra Rockhole anomalous eucrite indicated that it originated in the inner main belt, far from Vesta (Bland et al., 2009a). This again suggests that we have basaltic achondrites within our collections derived from multiple parent bodies.

Mesosiderites and pallasites have suppressed silicate absorption features due to the presence of metallic iron (Burbine et al., 2007; Cloutis et al., 2015). Traditionally the parent bodies to these groups are thought to be found among the pyroxene-rich (mesosiderite-like) and olivine-rich (pallasite-like) S-complex asteroids (Gaffey et al., 1993). Fieber-Beyer et al. (2011) identified a number of S-complex Maria family members as having interpreted mineralogies similar to mesosiderites. Cloutis et al. (2015) identified a number of S-complex bodies as having spectral properties similar to pallasites, which would have weak olivine bands and red spectral slopes due to the presence of metallic iron.

Acapulcoites/lodranites and winonaites are typically linked with S-complex bodies (Gaffey et al., 1993; Burbine et al., 2001) since they have olivine-pyroxene mineralogies and most S-types have absorption features due to olivine and pyroxene. However, it is unclear how abundant these primitive achondrites are among main-belt bodies, since most observed S-complex asteroid have interpreted mineralogies similar to ordinary chondrites (Vernazza et al., 2014). Olivine-rich brachinites are commonly linked to some members of the A-type class (Sunshine et al., 2007; Sanchez et al., 2014), which have spectral properties dominated by olivine. Mothé-Diniz and Carvano (2005) noted the spectral similarity between Divnoe and the K-type asteroid (221) Eos.

Based on the above analysis it is clear that differentiated achondrites are derived from a wide range of asteroidal sources. However, most of the work so far undertaken is based on well-characterized meteorite groups. The recovery of increasing numbers of ungrouped and anomalous achondrites, principally from North Africa, represents a new challenge for remote sensing studies. Most of these samples have yet to be classified spectrally and their relationship to existing groups is largely unknown. The diverse olivine-rich brachinite and brachinite-like samples are of particular interest as it is unclear how many parent bodies these meteorites represent (Section 3.4.1).

4.1.3. Linking meteorites to early-formed planetesimals

4.1.3.1. Asteroid belt evolution. Dynamic models of early Solar System evolution indicate that, compared to the terrestrial planets, the gas giants formed rapidly and underwent an inward-then-outward migration (Walsh et al., 2011; O'Brien et al., 2014). It has been suggested that such a scenario can explain the present structure of the asteroid belt, so that migration initially cleans out the belt region but then repopulates its inner regions with planetesimals that accreted in the inner Solar System (1–3 AU) and its outer regions with bodies that formed between and beyond the orbits of the giant planets (Walsh et al., 2011; O'Brien et al., 2014). Even if the influence of the gas giants is neglected, modelling studies indicate that the planetesimals from which the iron meteorites were derived most likely accreted in the terrestrial planet region and, following intense collisional evolution, their remnants were subsequently scattered into the main belt (Bottke et al., 2006). Of course the bulk of this initial planetesimal population would have been consumed to form the terrestrial planets, including Earth (Chambers, 2004; Izidoro et al., 2014). A clear implication of these models is that the asteroid belt will contain material that accreted at widely varying heliocentric distances; an outcome that is compatible with the bimodality observed in a number of stable isotope systems (Section 4.4) (Warren, 2011a,b). In addition, the remnants of the planetesimals that are scattered into the main belt are likely to be highly deformed by virtue of multiple impact encounters (Asphaug et al., 2006). Even apparently intact asteroids such as 4 Vesta may be main belt interlopers (Bottke et al., 2006).

4.1.3.2. Do we have any samples from pristine planetesimals?. As is clear from the preceding section, samples of early-formed differentiated planetesimals, delivered to Earth as irons stony-irons and achondrites, are likely to have had complex deformation and impact histories. Collisional reprocessing is likely to have taken place both before and after emplacement into the main belt. While the evidence presented in this review clearly shows that we do have samples from the very earliest stages of planet building this record needs to be carefully evaluated. As an example of this, 4 Vesta, the archetypal intact protoplanet (Russell et al., 2012), may provide some valuable insights.

Prior to the Dawn mission, Hubble telescope and ground-based observation had suggested that some regions of Vesta may contain a substantial olivine component (Binzel et al., 1997; Gaffey, 1997). Such observations were in keeping with the protoplanetary paradigm, which hypothesized that Vesta was a left-over differentiated protoplanet (Russell et al., 2012). The basis of this model being that, given a "chondritic" bulk composition, and as a result of early heating by ^{26}Al, Vesta should have differentiated into a layered body comprising a metallic core, a thick olivine-dominated mantle and a relatively thin, predominantly basaltic crust (Righter and Drake, 1997; Ruzicka et al., 1997; Mandler and Elkins-Tanton, 2013; Toplis et al., 2013). In fact, the Dawn mission failed to detect any endogenous olivine on Vesta (Nathues et al., 2015). Olivine appears to be absent even in the deep southern crater where olivine-rich material should have been exposed if Vesta accreted from broadly chondritic precursor materials (Chenet et al., 2014). The HEDs also display extreme levels of alkali depletion, with values that are much lower than predicted on the basis of a chondritic precursor (Righter and Drake, 1997). Such non-chondritic characteristics have led to the suggestion that far from being a pristine protoplanet, Vesta is in fact a secondary body that experienced extreme post-formational collisional reprocessing (Consolmagno et al., 2015). Collisional processes have also been invoked to explain the formation of the main-group pallasites (Section 3.3.5.1), which show variable cooling rates and hence could not simply represent samples from the core-mantle boundary of their parent asteroid (Yang et al., 2010). Recent proposals involve formation in a hit-and-run style collision (Yang et al., 2010), or impact of a denuded asteroidal core into the mantle of a second differentiated body (Tarduno et al., 2012). Given that pallasites *sensu lato* appear to be derived from six distinct parent bodies (Section 3.3.5.4) such collisional processes were clearly commonplace in the early Solar System. A denuded and molten asteroidal core appears to be required to explain the genesis of the mesosiderites (Section 3.3.4). However, in contrast to the main-group pallasites, the mesosiderite silicate-rich fraction was derived from the regolith of the impacted body, rather than its mantle.

Cooling rate evidence from magmatic iron meteorites suggests that they formed as cores to differentiated asteroids that were then denuded of their silicate mantle and crust shortly after formation

(Goldstein et al., 2009). This raises the question of what happened to this silicate material?

In contrast to the irons that may be derived from the cores of ~60 parent bodies (4.4.1), olivine-rich mantle materials appear to be significantly underrepresented in both the meteorite and asteroid records (Chapman, 1986; Bell et al., 1989; Burbine et al., 1996; Mittlefehldt et al., 1998; Scott et al., 2010). Referred to by Bell et al. (1989) as the "Great Dunite Shortage", the basis of this problem is that complete melting of a chondritic asteroid should produce a layered body comprising a metallic core, a thick olivine-rich mantle and a relatively thin, predominantly basaltic crust (Righter and Drake, 1997; Ruzicka et al., 1997; Mandler and Elkins-Tanton., 2013; Toplis et al., 2013).

A range of processes have been proposed to explain this apparent paucity of olivine–rich materials: (i) olivine-rich asteroids are "disguised" by space weathering (Burbine et al., 1996; Hiroi and Sasaki, 2012), (ii) the meteoritic record provides a poor indication of the material present in the asteroid belt (Burbine et al., 2002a), (iii) olivine-rich samples may be preferentially destroyed by terrestrial weathering processes (Scott, 1977b), (iv) high viscosity and rapid heat loss in small planetesimals inhibits the formation of significant volumes of olivine cumulates (Elkins-Tanton et al., 2014), and (v) differentiated asteroids accreted in the terrestrial planet-forming region and were disrupted early in Solar System history, with the mechanically weaker olivine-rich material being effectively destroyed by continuous pulverization, the so called "battered-to-bits scenario (Burbine et al., 1996; Bottke et al., 2006; Scott et al., 2010; Greenwood et al., 2015a,b).

The abundance of olivine in the mantle of a differentiated asteroid would have been dependent on its bulk composition. Only planetesimals with carbonaceous chondrite bulk compositions would have developed true dunitic mantles with >90% olivine (Toplis et al., 2013), whereas bodies derived from ordinary chondrite precursors would have had harzburgitic mantles, with between about 55% to 80% olivine (Toplis et al., 2013; Mandler and Elkins-Tanton, 2013). In the case of enstatite chondrite bulk compositions, olivine would have been subordinate to pyroxene (Toplis et al., 2013). So an additional explanation for the great dunite shortage is compositional. If the precursor materials were predominantly enstatite chondrite-like, then olivine-rich mantle materials might be less abundant than suggested by models invoking melting of ordinary or carbonaceous chondrites. A recent survey suggests that A-type (olivine-rich) asteroids may be more common in the main belt than previously thought (DeMeo et al., 2014) and it has been suggested that there is in fact too much mantle material in the asteroid belt (Jacobson et al., 2016).

4.1.3.3. How representative is the achondrite record?. It is clear from the previous section that the achondritic samples in our meteorite collections are derived from parent bodies that were extensively modified by collisional processing in the early Solar System. In Section 4.1.1 we saw that meteorites derived from differentiated asteroids (irons, stony-irons and achondrites) can plausibly be sourced from approximately 95 parent bodies. However, this has to be set against the enormous number of differentiated bodies that must have contributed to the formation of the terrestrial planets. The combined mass of the inner planets is approximately 1.2×10^{25} kg. The mass of asteroid 4 Vesta is 2.6×10^{20} kg. This implies that at a minnimum at least 46,000 Vesta-sized asteroids are required to form the terrestrial planets. If the parent bodies that contributed differentiated material to our collections were Vesta-sized, these figures suggest that, at best, we have samples from about 0.2% of the protoplanetary population. In fact, as the parent bodies to the achondrites, stony-irons and irons-were generally much smaller than Vesta, this figure is a significant overestimate. In summary, the samples we have in our collections are highly unrepresentative, highly deformed remnants of the original protoplanetary population. With these caveats in mind we now look at what these samples can tell us concerning early Solar System processes.

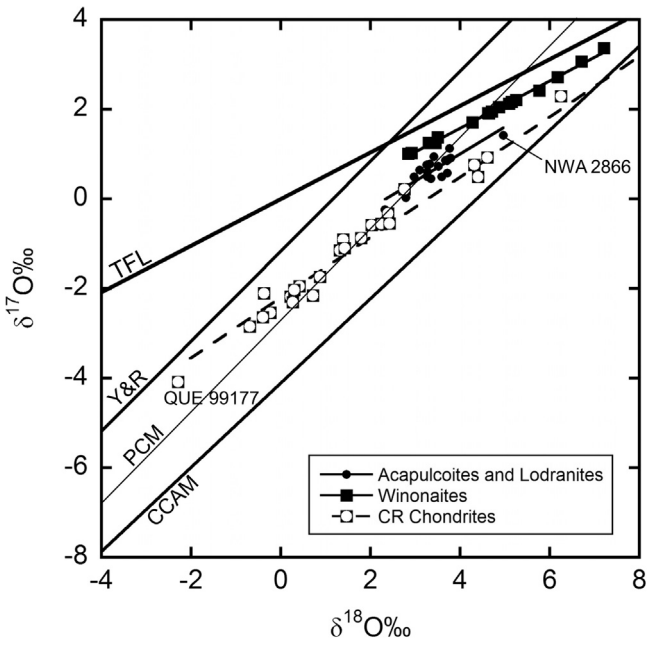

Fig. 24. Oxygen isotopic composition of acaplucoites, lodranites, winonaites and CR chondrites in relation to the Y&R, CCAM and PCM lines. Acapulcoite-lodranite and winonaite data: Greenwood et al., 2012; CR chondrite data: Schrader et al., 2011. (Key: TFL: Terrestrial Fractionation Line; Y&R: slope 1 line (Young and Russell, 1998); CCAM: Carbonaceous Chondrite Anhydrous Mineral line (Clayton et al., 1977; Clayton and Mayeda, 1999) PCM: Primitive Chondrule Minerals line (Ushikubo et al., 2012; Tenner et al., 2015).

4.2. The slope 1 oxygen isotope anomaly: an achondrite perspective

The origin of the mass-independent oxygen isotope variation displayed by Solar System materials remains controversial. While self-shielding of CO, either in the early solar nebula (Clayton, 2002; Lyons and Young, 2005), or precursor molecular cloud (Yurimoto and Kuramoto, 2004), appears to be a viable mechanism, alternative models have also been proposed (Dominguez, 2010). The oxygen isotope composition of achondrites provides additional constraints on the nature of the process involved, in particular, whether a single slope 1 line can be used to define the primordial oxygen isotope variation in the early solar nebula.

An important aspect of this problem relates to the interpretation of various reference lines on oxygen three-isotope diagrams (Fig. 24). The Carbonaceous Chondrite Anhydrous Mineral (CCAM) line, derived from analyses of Allende (CV3) refractory inclusions, is the most widely used reference and has a slope of 0.94 (Clayton et al., 1977; Clayton and Mayeda, 1999). However, the fundamental significance of the CCAM line has been questioned by Young and Russell (1998). Based on the results of a UV laser ablation study of an Allende CAI, these authors suggested that a line of exactly slope 1 was of more fundamental significance. They pointed out that almost all Solar System materials (with the exception of the R chondrites) plot either on or to the right of the slope 1 line. They went on to suggest that this variation could be explained if the primitive oxygen isotope composition of the Solar System was represented by the slope 1 line, with subsequent mass fractionation or isotopic exchange shifting compositions away from this line to the right. The fact that a highly ^{17,18}O-enriched phase (δ^{18}O and

$\delta^{17}O = \sim +180‰$) within the matrix of the primitive chondrite Acfer 094 (Sakamoto et al., 2007), as well as various IDPs (Starkey et al., 2014), plot closer to the extension of the slope 1 line than that of the CCAM line potentially lends additional support to the primordial significance of the former compared to the latter.

The slope 1 (Y&R line) and CCAM lines are shown in Fig. 24 along with oxygen isotope analyses for the winonaites, acapulcoites and lodranites, and CR chondrites (Clayton and Mayeda, 1999; Schrader et al., 2011; Greenwood et al., 2012). It is important to note that the Y&R and CCAM lines converge at a value of approximately $\delta^{18}O$ and $\delta^{17}O = -50‰$, a point that is more or less coincident with that of the most ^{16}O-rich phases analyzed in pristine CAIs (Krot et al., 2010). It has been suggested that the ^{16}O-rich composition measured in such CAIs may be close to that of the primordial Solar System (Clayton, 2002). This proposal is broadly consistent with measurements of captured solar wind from Genesis concentrator samples, which indicate that the Sun has a composition of $\delta^{18}O = -58.5‰$ and $\delta^{17}O = -59.1‰$ (McKeegan et al., 2011).

Both the acapulcoite-lodranite clan and the winonaites form distinct arrays that plot between the slope 1 and CCAM lines in Fig. 24. As noted in Section 3.2.4. (Fig. 12), chondrule-bearing winonaites, which may have a composition similar to that of the group's precursor material, plot closer to the slope 1 line than other more evolved winonaite samples. The CR chondrites display a similar relationship, with the least aqueously altered samples plotting close to the slope 1 line and progressively more altered ones further away (Schrader et al., 2011). In particular, the Antarctic CR chondrite QUE 99177, which contains abundant amorphous material and appears to have suffered relatively low levels of asteroidal aqueous alteration (Abreu and Brearley, 2006), plots immediately to the right of the slope 1 line in Fig. 24.

It was suggested by Greenwood et al. (2012) that the acapulcoites and lodranites may have experienced an early phase of aqueous alteration. On this basis it is possible that the precursor material to the acapulcoite-lodranite clan may originally have had a composition closer to the slope 1 line and this was subsequently shifted to the right during the aqueous alteration and later dehydration (Greenwood et al., 2012). Alternatively, the present bulk composition of the acapulcoite-lodranite clan, which lies between the slope 1 and CCAM lines, suggests that primordial oxygen isotope variation may have fluctuated somewhat between the two reference lines. However, the fact that the precursor material to the winonaites and CR chondrites appears to lie close to the slope 1 (Y&R) line provides strong evidence in favour of its underlying significance with respect to early Solar System oxygen isotope variation.

There is growing evidence that chondrules from relatively pristine carbonaceous chondrites (Acfer 094, MET 00426 and QUE 99177) define a distinct trend with a slope close to 1, termed the Primitive Chondrule Minerals (PCM) line, that lies between the CCAM and Y&R lines (Fig. 24) (Ushikubo et al., 2012; Tenner et al., 2015). As can be seen from Fig. 24, this line transects the acapulcoites and lodranites, winonaites and the bulk of primitive CRs. The relationship between the Y&R, PCM and CCAM lines remains unclear and is an area of active research.

CO photo-dissociation experiments (Chakraborty et al., 2008) and modelling studies (Lyons, 2011, 2014) yield slope values that diverge significantly from 1. Chakraborty et al. (2008) reported slope values that ranged from ~0.6 to 1.8, depending on the wavelength of radiation used. An alternative model to CO self-shielding proposed by Dominguez (2010) is that the $^{17,18}O$-enrichment took place by low temperature heterogeneous chemical processes, which form water ice around grains in the parent molecular cloud. Dominguez (2010) discounts the importance of CO self-shielding, but instead invokes a process analogous to the slope 1 ozone formation experiments of Thiemens and Heidenreich (1983). The mechanism proposed by Dominguez (2010) has yet to be experimentally verified.

Chromium isotope studies of both chondrites and achondrites provide a new and potentially important insight concerning the origin of the slope 1 anomaly. As noted in Section 3.2.3 ureilites plot on, or just to the left of, the CCAM line (Figs. 7 and 8). In view of the fact that the CCAM line was defined using analyses of materials from the CV chondrites (Clayton et al., 1977; Clayton and Mayeda, 1999), this relationship could be taken as evidence that the ureilites were derived from a CV3 precursor. Clayton and Mayeda (1996) were not in favour of such a direct link, merely noting that the ureilite precursor may have been C3 or CR-like. In fact, based on the relationships displayed on an $\varepsilon^{54}C$ vs. $\Delta^{17}O$ plot (Fig. 10), it is clear that the ureilites are unrelated to any group of carbonaceous chondrite (Warren, 2011b). This raises the question as to why, if they are unrelated, should both display oxygen isotope variation defined by the CCAM line? One explanation for this apparent co-variation is that it reflects the operation of secondary processes on both sets of parent bodies. As pointed out by Young and Russell (1998), secondary processes will always act to shift primary variation to the right on a three-isotope diagram. Alternatively, this coincidence indicates that the CCAM line is of more fundamental significance than indicated by the model of Young and Russell (1998). It is also possible that there is no single primordial line, but rather conditions fluctuated between two end-members defined by the CCAM and slope 1 Y&R line. The PCM line may therefore represent an intermediate stage between these end-members that was established while the bulk of chondrule formation was taking place. Such fluctuating conditions are broadly in keeping with the results of the experimental and modelling studies discussed above (Chakraborty et al., 2008; Lyons, 2011, 2014).

4.3. $\Delta^{17}O$ variation in solar system materials

4.3.1. Formation and preservation of primordial oxygen isotope anomalies

Solid particles collected from the Jupiter family comet 81P/Wild 2 by the NASA Stardust mission included chondrules and refractory inclusions that were most likely formed close to the early Sun and then subsequently transported to the cold outer regions of the Solar System (Brownlee, 2014). This suggests that there was relatively widespread mixing of materials within the early solar nebula (Boss, 2012). And yet, as is clear from the earlier sections of this review, oxygen isotope compositions were not homogenized by such mixing processes; a feature which allows oxygen to be such an effective tracer of early Solar System processes. So why did oxygen largely escape this early phase of mixing and homogenization?

As discussed in Section 2.1, part of the answer to this question relates to the fact that oxygen is an abundant element in Solar System materials and, depending on the physical conditions, would have been present simultaneously in various states i.e., within solids (silicates, ices), liquids (water) and vapor. Models of oxygen isotope fractionation in the early solar nebula suggest that the oxygen present in each of these different states would have had distinct isotopic compositions (Krot et al., 2010). According to the CO self-shielding hypothesis, UV photo-dissociation of CO would favour isotopologues containing heavy oxygen compared to those with the more abundant ^{16}O isotope (Clayton, 2002; Yurimoto and Kuramoto, 2004; Lyons and Young, 2005). The heavy oxygen atoms liberated by this process would have reacted with hydrogen to produce water that as a result would have been relatively enriched in ^{17}O and ^{18}O. In the scenario proposed by Yurimoto and Kuramoto (2004), self-shielding took place within the giant molecular cloud that was the precursor to the solar nebula. Yurimoto et al. (2007) suggest that self-shielding of CO, leading to heavy isotope enrich-

ments of water ice, is probably a common process in such diffuse, dark, giant molecular clouds and, if correct, this implies that the mass-independent variation in oxygen seen in meteorites is essentially a presolar process.

The model of Yurimoto and Kuramoto (2004) envisages the Solar System essentially forming from a three component mixture of ^{16}O-rich silicate grains coated by ^{16}O-poor water ice, surrounded by ^{16}O-rich nebular gas (Yurimoto et al., 2007). A fundamental question that arises from this model concerns the nature of the mechanism by which the oxygen isotope heterogeneities present in submicron grains came to be translated into the isotopic differences observed in asteroids and planets. This problem remains pertinent even if self-shielding took place within the solar nebula (Clayton, 2002; Lyons and Young, 2005), or if alternative mechanisms are invoked to explain the origin of oxygen isotope mass-independent fractionation (Thiemens and Heidenreich, 1983; Dominguez, 2010; Nittler and Gaidos, 2012).

The preservation and propagation of mass-independent oxygen isotope variation within Solar System materials is inextricably linked to thermal processing of gas and dust in the early nebula (Krot et al., 2010). Initial refractory solids (CAIs and AOIs) formed in the nebula 4567–4568 Myr ago (Amelin et al., 2002; Krot et al., 2009) and were most likely produced by multiple transient heating events, with high ambient temperatures and in fairly localized regions close to the Proto-Sun. At this early stage, ^{16}O-rich nebular gas would still have been present, swamping any contribution from vapourized ^{16}O-poor ices and ensuring that pristine CAIs remained close to the bulk Solar System composition (Clayton, 2002; McKeegan et al., 2011). As nebular gas dispersed, the influence of ^{16}O-poor ices would have increased, as seen in the transition from reduced Type-I (MgO and ^{16}O-rich) to oxidized type-II (FeO-rich and ^{16}O-poor) chondrules (e.g. Tenner et al., 2015). Accretion of planetesimals is now known to have occurred extremely early in Solar System history, possibly as little as 0.1–0.3 Myr after CAI formation (Kruijer et al., 2014) and may have preceded chondrule formation (Kleine et al., 2009). In fact, a number of studies have proposed that chondrule formation may have taken place as a result of impacts between such early-formed bodies (Sanders and Scott, 2012; Johnson et al., 2015).

At the accretion stage, planetesimals that formed beyond the snow line would have incorporated a significant fraction of ^{16}O-poor ice. This may subsequently have been lost from the body as it underwent heating due to the decay of short-lived radionuclides, principally ^{26}Al (Fu and Elkins-Tanton, 2014). However, prior to dehydration, heated fluids would almost certainly have interacted with the solid material through which they flowed. The exact nature of the processes involved in the hydrothermal alteration of chondritic parent bodies, and in particular whether this took place in an open or closed system environment, remain matters of ongoing debate (Young et al., 1999, 2003; Bland et al., 2009b; Fu et al., 2015, 2016). However, comparison between the oxygen isotope composition of chondrite groups that have experienced significant levels of aqueous alteration (e.g. CRs and CMs) and those which have not (e.g. COs) (Section 4.3.2, Fig. 25) demonstrates the efficacy of hydrothermal alteration in modifying the Δ^{17}O composition of meteorite parent bodies (Clayton and Mayeda, 1999; Young et al., 1999, 2003).

4.3.2. Δ^{17}O as an index of asteroidal differentiation

As discussed in various earlier sections of this review, there appears to be a general relationship between the level of Δ^{17}O homogeneity shown by individual meteorite groups and the degree of melting that they experienced (Table 1, Table S1) (Fig. 25). Not unsurprisingly, the carbonaceous chondrites (CV, CR, CM and CK) display the largest ranges in Δ^{17}O values of any of the major chondrite or achondrite groups (with the notable exception of the ureilites). In contrast, the COs display less Δ^{17}O variation, which is probably a reflection of a number of factors, including their lower levels of secondary alteration and more restricted lithological diversity compared to the other carbonaceous chondrite groups (Weisberg et al., 2006; Krot et al., 2014). The two enstatite chondrite groups (EH, EL) show somewhat differing levels of Δ^{17}O heterogeneity, whereas the ordinary chondrite groups (H, L, LL) show similar levels. An important implication of the Δ^{17}O variation displayed by all chondrite groups (Table 1, Table S1) (Fig. 25) is that achondritic asteroids would initially have been heterogeneous with respect to Δ^{17}O.

Following accretion, the primitive achondrites appear to have experienced variable, but generally low, degrees of partial melting, from a few degrees at best in the case of the acapulcoites (McCoy et al., 1997a), to a maximum of about 30% for the ureilites (Goodrich et al., 2007; Wilson et al., 2008). The particularly high levels of Δ^{17}O heterogeneity displayed by the ureilites, which is comparable to that seen in the CV chondrites, along with their distribution along the CCAM line (Figs. 7 and 8), might be taken as evidence that the two groups are genetically related. However, as discussed in Section 3.2.3, ^{54}Cr systematics appear to rule this out (Fig. 10). Despite this evidence, the level of Δ^{17}O heterogeneity seen in the ureilites suggests that their precursor materials displayed much higher levels of oxygen isotope heterogeneity than that of the other primitive achondrites (Clayton and Mayeda, 1996). This may indicate that some form of hydrothermal alteration took place on the ureilite parent body prior the onset of melting. During progressive radiogenic heating volatiles would have been efficiently removed from the body, leaving it essentially dry and creating a network of fractures that may have been used by later silicate melts (Wilson et al., 2008; Fu and Elkins-Tanton, 2014).

In comparison to the primitive achondrites, the differentiated achondrites (HEDs, main-group pallasites, mesosiderites, angrites and aubrites) are essentially homogeneous with respect to Δ^{17}O, a characteristic they share with larger bodies such as the Earth, Moon and Mars (Fig. 25). Estimates of the amount of melting of chondritic precursor materials involved in the formation of differentiated achondrites vary significantly. Based on the results of experimental studies it has been suggested that both HEDs and angrites could be formed by between approximately 15 to 30% melting of chondritic precursor materials (Stolper 1977; Jones, 1984; Jurewicz et al., 1993; Mikouchi et al., 2008). In contrast to these relatively low levels of melting, much higher values have been proposed based on evidence for efficient core formation on minor bodies (e.g. Righter and Drake, 1996). Thus, as discussed in Section 3.3.3, a range of evidence, including moderately (Ni, Co, Mo, W and P) and highly (Os, Ir, Ru, Pt, Pd, Re) siderophile element abundances in HED lithologies point to rapid, efficient, low-pressure core formation on Vesta in response to global-scale melting (Righter and Drake, 1996, 1997; Dale et al., 2012; Day et al., 2012b).

The magma ocean model for Vesta, developed by Righter and Drake (1997) invokes between 65% and 77% melting (1500–1530 °C), with turbulent convection during its initial stages. At such elevated temperatures, high degrees of partial melting and turbulent mixing, global-scale homogenization of oxygen isotopes would have taken place rapidly (Greenwood et al., 2005, 2014). The development of magma oceans has been proposed for other differentiated achondritic asteroids, including that of the angrites, aubrites and main-group pallasites (Taylor et al., 1993). Magma oceans are also implicated in the origin of the mesosiderites, based on the proposition that their silicate fraction was derived from the HED parent body (Scott et al., 2014; Greenwood et al., 2015a).

The fact that differentiated asteroids show levels of oxygen isotope homogenization comparable to that of larger bodies, such as the Moon, Mars and Earth, all of which had protracted high-

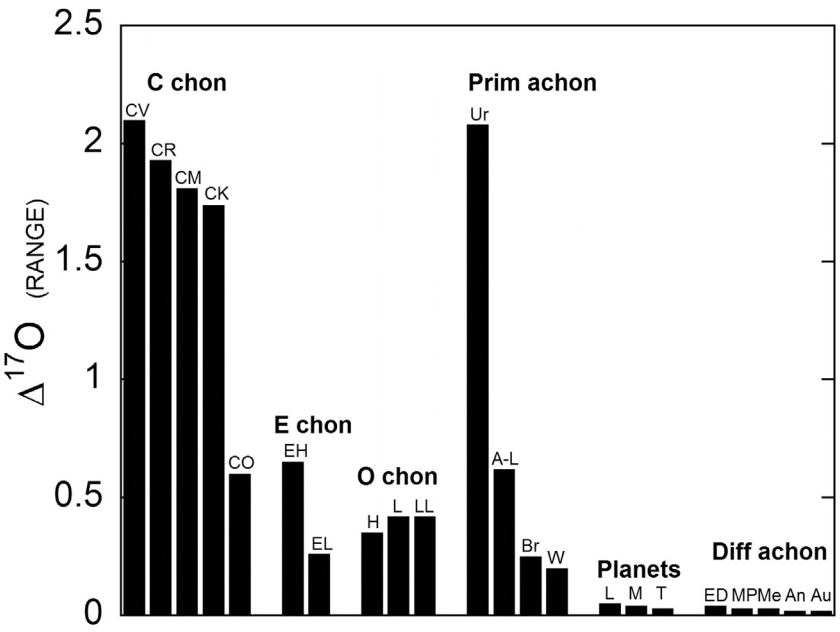

Fig. 25. $\Delta^{17}O$ variation in Solar System materials expressed in terms of the difference between the highest and lowest values for each major meteorite group (range). Abbreviations: C chon: carbonaceous chondrites; E chon: enstatite chondrites; O chon: ordinary chondrites; Prim achon: primitive achondrites (Ur: ureilites, A-L: acapulcoite-lodranite suite, Br: brachinites, W: winonaites); Planets (L: lunar rocks, M: martian meteorites, T: terrestrial high He-olivines); Diff achon: differentiated achondrites (ED: eucrites and diogenites, MP: main-group pallasites, Me: mesosiderites, An: angrites, Au: aubrites). Full data and references: Table S1.

temperature evolutions (e.g. Warren, 1985; Tonks and Melosh, 1993; Rubie et al., 2004; Wood et al., 2006; Halliday and Wood, 2010; Elkins-Tanton, 2012) demonstrates that isotopic homogenization was extremely efficient on these much smaller bodies. In keeping with the predictions of theoretical models of asteroidal heating through decay of short-lived radionuclides, such as ^{26}Al and ^{60}Fe (Hevey and Sanders, 2006; Sahijpal et al., 2007; Moskovitz and Gaidos, 2011), the most likely setting in which this equilibration took place was as a consequence of global-scale melting leading to the formation of magma oceans (Greenwood et al., 2005, 2014).

There is a clear hiatus in the $\Delta^{17}O$ range seen on Fig. 26, which may reflect a transition from bodies with low levels of melting, to those that experienced higher levels and were as a result isotopically well-mixed. However, within the group of bodies that display limited $\Delta^{17}O$ variation there are significant differences in the levels of alkali depletion, which may point to a diversity of origins. The angrites and HEDs show levels of alkali depletion similar to those displayed by lunar rocks. It has been suggested that such alkali depletion may have been caused by a process of volatile loss through evaporation into space from an essentially molten planet, or planetesimal (Ikeda and Takeda, 1985). Such a process is clearly not supported by the relatively high alkali content of the aubrites (Fig. 26). In addition, experimental studies indicate that had volatile loss taken place simply by evaporation into space, i.e. by Rayleigh distillation, significant mass fractionation of K isotopes should have occurred, with δ41K values of up to 90‰ under certain conditions (Yu et al., 2003). However, K isotope studies have failed to detect the presence of such large anomalies, either in the HEDs, or lunar rocks (Humayun and Clayton, 1995; Wang and Jacobsen, 2016). The recent detection of a 0.4-0.6‰ δ41K enrichment in lunar compared to terrestrial rocks, has been explained in terms of the formation of the Moon by partial condensation from the vapour disc produced by a giant impact event (Wang and Jacobsen, 2016). In the case of lunar rocks, volatile depletion appears to have been directly inherited from the Earth-orbiting disc formed following the giant impact, rather than as a consequence of subsequent processes in the lunar magma ocean (Canup et al., 2015; Lock et al., 2016). The parent bodies of the differentiated achondrites had complex formational histories, as is clear from the recent detailed studies of Vesta by the Dawn mission (Russell et al., 2012; McSween et al., 2013). The fact that alkalis and oxygen isotopes appear to be decoupled is a reflection of this complex formational history. Thus, while oxygen isotopic homogeneity probably results from early global-scale melting, alkali depletion may have been caused by a variety of mechanisms including: (i) 'hot' nebular processes prior to accretion (Wasson and Chou, 1974; Cassen, 1996; Bland and Ciesla, 2010), (ii) parent body hydrothermal processes (Delaney, 2009; Young et al., 2003; Fu and Elkins-Tanton, 2014, 2016), or (iii) by impact-related processes (Asphaug et al., 2006, 2011; Canup et al., 2015; Lock et al., 2016).

The angrites are even more alkali depleted than the HEDs (Fig. 26), perhaps indicating that their parent body experienced a similarly complex evolution to Vesta. A speculative possibility is that both Vesta and the angrite parent body are derived from asteroids that accreted from the debris produced during relatively high-energy collisional events that took place in the terrestrial planet region and were then ejected into the asteroid belt. Alkali depletion in these bodies may have taken place by a mechanism similar to that proposed for the Moon (Canup et al., 2015).

4.4. The relationship between chondrites and achondrites

As noted by Weisberg et al. (2006): "the chondrites are among the most primitive Solar System materials available for laboratory study" and their components (CAIs, AOAs, chondrules, matrix) "are ground truth for astrophysical models of nebular evolution". The "primitive" nature of chondrites in general and carbonaceous chondrites in particular, is supported by a large body of evidence. This includes the fact that they are the host to CAIs, the oldest dated Solar System solids, (MacPherson, 2014), contain presolar grains (Zinner, 2014), display a wide range of isotopic anomalies (Meyer and Zinner, 2006; MacPherson and Boss, 2011) and include an organic component that probably originated in the interstellar medium (Alexander et al., 2007, 2010). In contrast, achondrites are thermally processed materials that experienced variable degrees of melting in an asteroidal environment (Weisberg

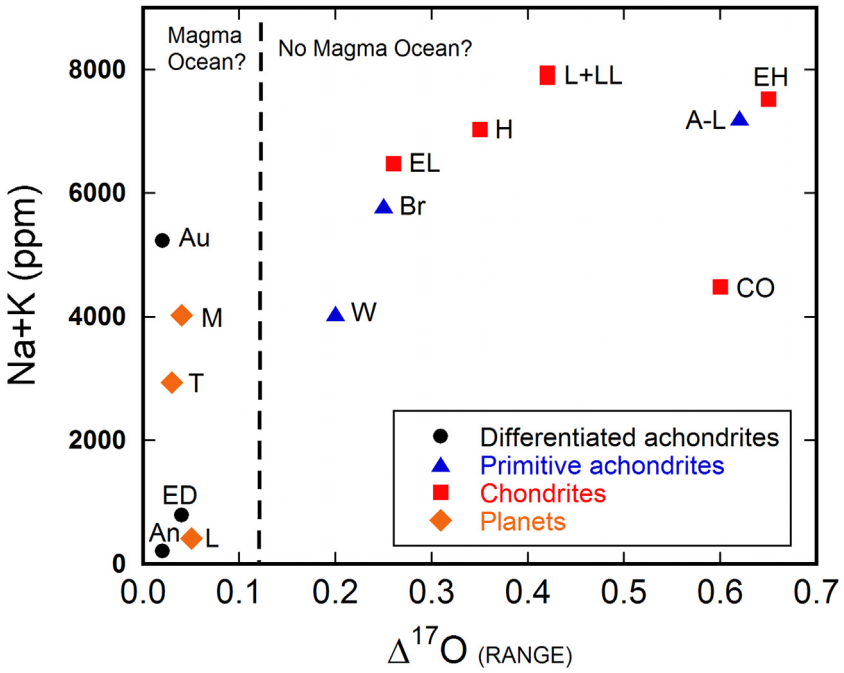

Fig. 26. $\Delta^{17}O$ vs. total alkalis for selected chondrite and achondrite groups. Abbreviations as Fig. 25.

et al., 2006). The primitiveness of chondrites in comparison to the thermally processed character of achondrites is suggestive of a parent-daughter relationship between these two major meteorite subdivisions. However, while such a relationship may be accurate on the macro scale i.e. chondrite-like materials were the precursors to the achondrite parent bodies, in detail the picture is extremely complex.

Aubrites are the group of achondrites which show the clearest link with a chondritic precursor and it is almost certain that they represent the differentiation products of enstatite chondrite-related materials (Barrat et al., 2016b). Both aubrites and enstatite chondrites have closely similar mineral and average bulk oxygen isotope compositions (Section 3.3.2). A close relationship between the aubrites and enstatite chondrites is also supported by the similar isotopic variation they display for a range of other elements, including Ca, Ti and Cr (Dauphas et al., 2014).

CR chondrite-like precursors have been proposed in the case of the acapulcoite-lodranite clan (Rubin, 2007) and for members of the winonaite-IAB-IIICD suite (Rubin et al., 2002). However, while the oxygen isotope composition of both of these primitive achondrite groups, like that of the primitive CRs (e.g. QUE 99177) (Fig. 24) lies well to the left of the CCAM line, they are isotopically distinct. This suggests that, although the precursor materials to the winonaites and acapulcoite-lodranites probably resembled CRs, both mineralogically and isotopically, they were not an exact match.

Ureilites show a somewhat ambiguous relationship with carbonaceous chondrites. While oxygen isotope evidence suggests that the two groups may be genetically linked (Figs. 7 and 8), a close relationship between them appears to be excluded on the basis of ^{54}Cr isotope systematics (Fig. 10) (Warren, 2011b) (Section 3.2.3). In contrast, both oxygen isotope (Fig. 18) and ^{54}Cr data (Fig. 10) indicate that the Eagle Station pallasite group formed from a carbonaceous chondrite-like precursor. However, in the case of many achondrite groups, including the angrites, HEDs, main-group pallasites, mesosiderites, brachinites and also the majority of ungrouped achondrites, there appear to be no known chondrites with similar oxygen isotope compositions. This general lack of a close match between chondrite and achondrite groups may be a reflection of the fact that the known chondrite groups formed late (Kleine et al., 2009) and so are less representative of "primitive" Solar System solids than was once thought.

Dating studies using the extinct ^{182}Hf-^{182}W chronometer ($t_{½}$ = 8.9 Myr) have shown that the parent bodies of the magmatic iron meteorites accreted less than 1 Myr, and possibly as little as 100,000 years, after CAIs (Kleine et al., 2009; Kruijer et al., 2014). Such rapid timescales are broadly consistent with the predictions of dynamical models for planetesimal growth in the early solar nebula (Weidenschilling and Cuzzi, 2006). In contrast to the early accretion of magmatic irons, a number of dating studies indicate that the main phase of chondrule formation took place approximately 2 Myr after CAI formation (Amelin et al., 2002; Kleine et al., 2009; Budde et al., 2016). However, the existence of a distinct time gap between the CAI and chondrule forming events is disputed by Connelly et al. (2012). Based on U-corrected Pb–Pb data they suggest that CAIs formed in a brief time interval with an age of 4567 ± 0.16 Myr, whereas chondrule formation took place over a more protracted interval of ~3 Myr, but commenced at the same time as CAIs. Despite these differences in interpretation, it seems likely that the main phase of chondrule formation took place after the onset of planetesimal accretion. Thus, since chondrules are a major constituent of chondritic meteorites, it follows that these meteorites cannot be direct samples of the material from which these early planetesimals accreted.

Relatively late accretion of chondritic parent bodies is also supported by thermal evolution modelling of the H chondrite parent body, which indicates that it formed rapidly, 2 Myr after CAIs and so immediately after the main phase of ordinary chondrite chondrule formation (Henke et al., 2013). Carbonaceous chondrite parent bodies probably accreted even later. Schrader et al. (2016) estimate that the CR parent body accreted >4 Myr after CAIs. Late accretion of chondrites is further supported by palaeomagnetic evidence from Allende (CV3), which indicates that it was magnetized over several million years within the outer layers of a partially differentiated asteroid with a convecting metallic core (Carporzen et al., 2011). Based on this evidence, it has been proposed that at least some of the carbonaceous chondrites present in our meteorite col-

lections are essentially late accreting materials that formed the outer layers to internally differentiated, early-formed planetesimals (Elkins-Tanton et al., 2011; Weiss and Elkins-Tanton, 2013).

A potential difficulty for models invoking rapid, early accretion of achondritic parent bodies is that at "canonical" values of ^{26}Al ($^{26}Al/^{27}Al_0 = 5.3 \times 10^{-5}$) (MacPherson et al., 1995; Jacobsen et al., 2008), heating would have been too efficient and not have resulted in the formation of partial melt residues, as represented by the primitive achondrites (Larsen et al., 2016). Early, rapid planetesimal accretion may also be a problem for models invoking differentiated bodies with thick outer chondritic crusts (Elkins-Tanton et al., 2011; Weiss and Elkins-Tanton, 2013). The problem is essentially that early-formed, fast accreting bodies would have been too hot to permit the preservation of anything other than extremely tenuous chondritic crusts (Hevey and Sanders, 2006). However, accretion timescales were probably not constant throughout the protoplanetary disc and may have been more protracted at greater heliocentric distances (Bottke et al., 2006).

The accretion time of a planetesimal relative to CAI formation is a critical parameter for models invoking heating by decay of short-lived radionuclides, such as ^{26}Al and ^{60}Fe (Ghosh and McSween, 1998; Hevey and Sanders, 2006; Sahijpal et al., 2007). In the model of Ghosh and McSween (1998), a post CAI accretion age of 2.8 Myr for Vesta was assumed, as this was required in order to incorporate the requisite amount of ^{26}Al to furnish the heat needed to cause 25% melting; a value that was derived from the HED model of Stolper (1977). As pointed out by Ghosh and McSween (1998), accretion earlier than 2.8 Myr would have resulted in whole-mantle melting below a depth of 30 km. In the model of Hevey and Sanders (2006), a planetesimal accreting at 0.75 Myr after CAI formation would have been 50% molten 0.75 Myr later and after a further 0.5 Myr (2 Myr after CAIs) would have resembled "a globe of molten, convecting slurry inside a thin residual crust." Similar conclusions concerning the importance of accretion time on the extent of melting in early-formed planetesimals were reached by Sahijpal et al. (2007) and they suggest that such modelling studies are consistent with accretion of chondritic parent bodies more than 2–3 Myr after CAIs, i.e. significantly later than the accretion ages of the iron meteorite parent bodies derived from Hf-W dating studies (Kleine et al., 2009; Kruijer et al., 2014).

It was pointed out by Warren (2011a,b), based on data from earlier studies (e.g. Shukolyukov and Lugmair, 2006; Trinquier et al., 2007, 2009; Qin et al., 2010a,b), that Solar System materials display a bimodal distribution with respect to a range of stable nuclides, including ^{54}Cr, ^{50}Ti and ^{62}Ni. These two groupings consist of one that is enriched in such nuclides and comprises the carbonaceous chondrites plus related achondrites (NWA 011, Eagle Station pallasites) and a second cluster essentially made up of all other types of chondrites and achondrites that are relatively depleted in such nuclides (Fig. 10). Warren (2011a,b) speculated that this bimodality might represent an extreme reflection of heterogeneous accretion within the protoplanetary disc, with the carbonaceous group originating in the outer Solar System and the non-carbonaceous group in the inner Solar System. Such bimodal distributions have also been observed for ^{48}Ca (Dauphas et al., 2014), ^{84}Sr (Moynier et al., 2012; Paton et al., 2013), ^{97}Mo (Dauphas et al., 2002) and $\mu^{26}Mg^*$ (^{26}Mg resulting from in situ decay of ^{26}Al) (Larsen et al., 2011, 2016). There appears to be a general consensus that this bimodal distribution reflects preferential thermal processing of dust within the hot inner regions of the protoplanetary disc (Trinquier et al., 2009; Paton et al., 2013; Schiller et al., 2015a; Larsen et al., 2016). One possible consequence of this process is that dust within the hot inner region may have had a lower initial abundance of ^{26}Al due to preferential sublimation of its carrier phase (Schiller et al., 2015b; Larsen et al., 2016). A study of three angrites by Schiller et al. (2015b) indicates that they accreted from precursor material with an initial $(^{26}Al/^{27}Al)_0$ ratio of 1.33×10^{-5}, a value that is significantly lower than the CAI-derived canonical value of 5.3×10^{-5}. If decay of ^{26}Al was the chief heat source driving differentiation of the angrite parent body then such low initial levels indicate that accretion took place within 250,000 years of CAI formation and so was essentially contemporaneous with formation of the magmatic iron meteorites (Kleine et al., 2005, 2009; Kruijer et al., 2014).

In summary, with the possible exception of the aubrite/enstatite chondrite and Eagle Station pallasite/carbonaceous chondrite associations, oxygen isotope studies provide little evidence to support a parent/daughter relationship between the major groups of chondrites and achondrites. This is unsurprising if the majority of achondritic parent bodies essentially accreted early, within the more thermally processed inner regions of the protoplanetary disc, whereas chondrites are samples derived from later-formed asteroids, or are the late accreted rinds to differentiated bodies. Thus, rather than being the poor relation to chondrites, achondrites furnish essential information about the processes that took place during the very earliest stages of Solar System evolution.

5. Summary and conclusions

Oxygen isotope analysis of extraterrestrial materials has played, and continues to play, a major role in improving our understanding of early Solar System processes. Conventional techniques, employing externally heated Ni "bombs", have now been superseded by laser-assisted fluorination, which currently achieves the highest level of precision available for oxygen isotope analysis. Laser-assisted fluorination is at a mature stage in its development, but further analytical improvements are potentially available via refinements to the construction of sample chambers, cleanup lines and the use of ultra-high resolution mass spectrometers.

High-precision oxygen isotope analysis has been an extremely effective and powerful technique in furthering our understanding of early Solar System processes. In particular, it has provided unique insights into the interrelationships between various groups of both primitive and differentiated achondrites. Oxygen isotope analysis has shown that main-group pallasites, angrites and HEDs all originate from distinct asteroids, whereas mesosiderites may be from the same body as the HEDs. Oxygen isotope analysis provides an important means of assessing the extent to which the parent bodies to the achondrites underwent melting and subsequent isotopic homogenization. Oxygen isotope analysis is also important in deciphering possible relationships between the ungrouped achondrites and the more well-populated groups; a good example being the suggested link between the evolved GRA 06128/9 meteorites and the brachinites.

The evidence from oxygen isotopes, in conjunction with that from other techniques, indicates that we have samples of approximately 110 asteroidal parent bodies (~60 irons, ~35 achondrites and stony irons, and ~15 chondrites). However, compared to the likely size of the original protoplanetary asteroid population this value is extremely low and in addition, the samples we have in our collections appear to be almost exclusively derived from extensively deformed bodies. High-precision laser fluorination analysis of achondrites provides additional constraints on the origin of the mass-independent oxygen isotope variation in Solar System materials and suggests that both the slope 1 (Y&R) and CCAM lines may be of primordial significance. $\Delta^{17}O$ differences between water ice and silicates may originally have arisen either in the giant molecular cloud that was the precursor to the solar nebula, or alternately within the early nebula itself. The small-scale isotopic heterogeneities produced by this process were propagated into larger-sized bodies, such as asteroids and planets, as a result of early Solar System processes, including dehydration, aqueous alteration, melting and collisional interactions.

There is increasing evidence that the chondritic parent bodies accreted relatively late compared to the achondritic asteroids. This may account for the fact that with a few notable exceptions, such as the aubrite-enstatite chondrite association, known chondrite groups could not have been the direct parents to the main achondrite groups.

Acknowledgements

We would like to thank the Associate Editor Klaus Keil for soliciting and handling this Invited Review. He has shown throughout an extraordinary level of patience and understanding and there is no doubt that without his polite and tactful persistence this contribution would not have been completed. We owe him an immense debt of gratitude. The manuscript was significantly strengthened as the result of a thoughtful and constructive review provided by Ed Scott for which we are particularly grateful. We would like to thank an anonymous reviewer for his supportive comments. Jenny Gibson is thanked for her help with all aspects of sample preparation and oxygen isotope analysis. Our understanding of the topics covered in this review have benefitted greatly from discussions with a wide range of friends and colleagues In particular, we would like to thank Jean-Alix Barrat, Akira Yamaguchi, Ed Scott, Ian Sanders, Duck Mittlefehldt, Bob Clayton, Conel Alexander, Doug Rumble, Ed Young, Alan Rubin, John Wasson and Mark Thiemens for their help and guidance over many years.

Oxygen isotope studies at the Open University are funded by a consolidated grant from the UK Science and Technology Facilities Council (STFC) (Grant Number: ST/L000776/1). THB would like to thank the Remote, In Situ, and Synchrotron Studies for Science and Exploration (RIS^{4}E) Solar System Exploration Research Virtual Institute (SSERVI) for support in the writing of this paper.

Appendix A. Supplementary data

Supplementary data associated with this article can be found, in the online version, at http://dx.doi.org/10.1016/j.chemer.2016.09.005.

References

Abreu, N.M., Brearley, A.J., 2006. Early solar system processes recorded in the matrices of CR2 chondrites MET 00426 and QUE 99177 (abstract). Lunar Planet. Sci. 37 (#2395).

Adams, F.C., 2010. The birth environment of the solar system. Annu. Rev. Astron. Astrophys. 48, 47–85.

Agee, C.B., Muttik, N., Ziegler, K., McCubbin, F.M., Sanborn, M.E., Yin, Q.-Z., 2014. NWA 8186 an ungrouped achondrite from the CK/CV chondrite parent body (abstract). Meteorit. Planet. Sci. 49 (#5385).

Agee, C.B., Miley, H.M., Ziegler, K., Spilde, M.N., 2015. Northwest Africa 8535: Unique dunitic angrite (abstract). Lunar Planet. Sci. 46 (#2681).

Alexander, C.M.O.'D., Fogel, M., Yabuta, H., Cody, G.D., 2007. The origin and evolution of chondrites recorded in the elemental and isotopic compositions of their macromolecular organic matter. Geochim. Cosmochim. Acta 71, 4380–4403.

Alexander, C.M.O.'D., Newsome, S.D., Fogel, M.L., Nittler, L.R., Busemann, H., Cody, G.D., 2010. Deuterium enrichments in chondritic macromolecular materials-implications for the origin and evolution of organics, water and asteroids. Geochim. Cosmochim. Acta 74, 4417–4437.

Ali, A., Jabeen, I., Banerjee, N.R., Tait, K.T., Hyde, B.C., Nicklin, I., Gregory, D., 2013. Potential for bimodality in main group pallasites: an oxygen isotope perspective (abstract). Meteorit. Planet. Sci. 48 (#5243).

Ali, A., Jabeen, I., Banerjee, N.R., Osinski, G.R., Tait, K.T., Hyde, B.C., Nicklin, I., Ganderon, T., Gregory, D., 2014. Oxygen isotope variations in main group pallasites and HEDs (abstract). Lunar Planet. Sci. 45 (#2390).

Allègre, C.J., Poirier, J.-P., Hofmann, A.B., 1995. The chemical composition of the Earth. Earth Planet. Sci. Lett. 134, 515–526.

Amelin, Y., Krot, A.N., Hutcheon, I.D., Ulyanov, A.A., 2002. Lead isotopic ages of chondrules and calcium-aluminum-rich inclusions. Science 297, 1678–1683.

Ashcroft, H.O., Wood, B.J., 2015. An experimental study of partial melting and fractional crystallization on the HED parent body. Meteorit. Planet. Sci. 50, 1912–1924.

Asphaug, E., Agnor, C.B., Williams, Q., 2006. Hit-and-run planetary collisions. Nature 439, 155–159.

Asphaug, E., Jutzi, M., Movshovitz, N., 2011. Chondrule formation during planetesimal accretion. Earth Planet. Sci. Lett. 308, 369–379.

Baertschi, P., Silverman, S.R., 1951. The determination of relative abundances of the oxygen isotopes in silicate rocks. Geochim. Cosmochim. Acta 1, 317–328.

Baghdadi, B., Jambon, A., Barrat, J.-A., 2015. Metamorphic angrite Northwest Africa 3164/5167 compared to magmatic angrites. Geochim. Cosmochim. Acta 168, 1–21, http://dx.doi.org/10.1016/j.gca.2015.07.022.

Barrat, J.-A., Yamaguchi, A., 2014. Comment on the origin of eucrites, diogenites, and olivine diogenites: Magma ocean crystallization and shallow magma processes on vesta by B.E. Mandler and L.T. Elkins-Tanton. Meteorit. Planet. Sci. 49, 468–472.

Barrat, J.-A., Yamaguchi, A., Greenwood, R.C., Benoit, M., Cotten, J., Bohn, M., Franchi, I.A., 2008. Geochemistry of diogenites: Still more diversity in their parental melts. Meteorit. Planet. Sci. 43, 1759–1775.

Barrat, J.-A., Yamaguchi, A., Zanda, B., Bollinger, C., Bohn, M., 2010. Relative chronology of crust formation on asteroid Vesta: Insights from the geochemistry of diogenites. Geochim. Cosmochim. Acta 74, 6218–6231.

Barrat, J.-A., Greenwood, R.C., Verchovsky, A., BGillet, Ph., Bollinger, C., Langlade, J., Liourzou, C., Franchi, I.A., 2015. Crustal differentiation in the early solar system: clues from the unique achondrite Northwest Africa 7325 (NWA 7325). Geochim. Cosmochim. Acta 168, 280–292.

Barrat, J.-A., Jambon, A., Yamaguchi, A., Bischoff, A., Rouget, M.-L., Liorzou, C., 2016a. Partial melting of a C-rich asteroid: Lithophile trace elements in ureilites. Geochim. Cosmochim. Acta 194, 163–178.

Barrat, J.A., Greenwood, R.C., Keil, K., Rouget, M.L., Boesenberg, J.S., Zanda, B., Franchi, I.A., 2016b. The origin of aubrites: Evidence from lithophile trace element abundances and oxygen isotopic compositions. Geochim. Cosmochim. Acta 192, 29–48.

Bartoschewitz, R., Wlotzka, F., Clayton, R.N., Mayeda, T.K., 2003. NWA 1500: The first basaltic ureilite? (abstract). Meteorit. Planet. Sci. 38 (#5114).

Bell, J.F., Davis, D.R., Hartmann, W.K., Gaffey, M.J., 1989. Asteroids: The Big Picture. In: Binzel, R.P., Gehrels, T., Matthews, M.S. (Eds.), Asteroids II. University of Arizona Press, Tucson, pp. 921–945.

Benedix, G.K., McCoy, T.J., Keil, K., Bogard, D.D., Garrison, D.H., 1998. A petrologic and isotopic study of winonaites: Evidence for early partial melting, brecciation, and metamorphism. Geochim. Cosmochim. Acta 62, 2535–2553.

Benedix, G.K., McCoy, T.J., Keil, K., Love, S.G., 2000. A petrologic study of the IAB meteorites: Constraints on the formation of the IAB-winonaite parent body. Meteorit. Planet. Sci. 35, 1127–1141.

Benedix, G.K., McCoy, T.J., Lauretta, D.S., 2003. Is NWA 1463 the most primitive winonaite? (abstract). Meteorit. Planet. Sci. 38 (#5125).

Benedix, G.K., Lauretta, D.S., McCoy, T.J., 2005. Thermodynamic constraints on the formation conditions of winonaites and silicate-bearing IAB irons. Geochim. Cosmochim. Acta 69, 5123–5131.

Benedix, G.K., Bland, P.A., Friedrich, J.M., Mittlefehldt, D.W., Sanborn, M.E., Yin, Q.-Z., Greenwood, R.C., Franchi, I.A., Bevan, A.W.R., Towner, M.C., Perotta, G.C., 2014a. Bunburra Rockhole: Exploring the geology of a new differentiated basaltic asteroid (abstract). Lunar Planet. Sci. 45 (#1650).

Benedix, G.K., Haack, H., McCoy, T.J., 2014b. Iron and stony-iron meteorites. In: Davis, A.M. (Ed.), Meteorites and Cosmochemical Processes, Treatise on Geochemistry, vol. 1, second edition. Elsevier, Oxford, pp. 267–285.

Bild, R.W., 1977. Silicate inclusions in group IAB irons and a relation to the anomalous stones Winona and Mt. Morris (Wis.). Geochim. Cosmochim. Acta 41, 1439–1456.

Binzel, R.P., Xu, S., 1993. Chips off of asteroid 4 Vesta: Evidence for the parent body of basaltic achondrite meteorites. Science 260, 186–191.

Binzel, R.P., Gaffey, M.J., Thomas, P.C., Zellner, B.H., Storrs, A.D., Wells, E.N., 1997. Geologic mapping of Vesta from 1994 Hubble space telescope images. Icarus 128, 95–103.

Bischoff, A., Horstmann, M., Pack, A., Laubenstein, M., Haberer, S., 2010. Asteroid 2008 TC_3—Almahata Sitta: A spectacular breccia containing many different ureilitic and chondritic lithologies. Meteorit. Planet. Sci. 45, 1638–1656.

Bischoff, A., Horstmann, M., Barrat, J.-A., Chaussidon, M., Pack, A., Herwartz, D., Ward, D., Vollmer, C., Decker, S., 2014. Trachyandesitic volcanism in the early solar system. Proc. Natl. Acad. Sci. U. S. A. 111, 12689–12692.

Bland P.A., Ciesla F.J., 2010. The impact of nebular evolution on volatile depletion trends observed in differentiated objects. 41st Lunar and Planetary Science Conference, Abstract #1817.

Bland, P.A., Spurny, P., Towner, M.C., Bevan, A.W.R., Singleton, A.T., Bottke, W.F., Greenwood, R.C., Chesley, S.R., Shrbeny, L., Borovicka, J., Ceplecha, Z., McClafferty, T.P., Vaughan, D., Benedix, G.K., Deacon, G., Howard, K.T., Franchi, I.A., Hough, R.M., 2009a. An anomalous basaltic meteorite from the innermost main belt. Science 325, 1525–1527.

Bland, P.A., Jackson, M.D., Coker, R.F., Cohen, B.A., Webber, R.F., Lee, M.R., Duffy, C.M., Chater, R.J., Ardakani, M.G., McPhail, D.S., McComb, D.W., Benedix, G.K., 2009b. Why aqueous alteration in asteroids was isochemical: High porosity $\neq$ high permeability. Earth Planet. Sci. Lett. 287, 559–568.

Boesenberg, J.S., Delaney, J.S., Hewins, R.H., 2012. A petrological and chemical re-examination of main group pallasite formation. Geochem. Cosmochim. Acta 89, 134–158.

Boss, A.P., 2012. Mixing and transport of isotopic heterogeneity in the early solar system. Annu. Rev. Earth Planet. Sci. 40, 23–43.

Boss, A.P., Keiser, S.A., Ipatov, S.I., Myhill, E.A., Vanhalla, H.A.T., 2010. Triggering collapse of the presolar dense cloud core and injecting short-lived

radioisotopes with a shock wave. I. Variable shock speeds. Astrophys. J. 708, 1268–1280.
Bottke, W.F., Durda, D.D., Nesvorný, D., Jedick, R., Morbidelli, A., Vokrouhlický, D., Levison, H., 2005. The fossilized size distribution of the main belt asteroid belt. Icarus 175, 111–140.
Bottke, W.F., Nesvorný, D., Grimm, R.E., Morbidelli, A., O'Brien, D.P., 2006. Iron meteorites as remnants of planetesimals formed in the terrestrial planet region. Nature 439, 821–824.
Brand, W.A., 2011. New reporting guidelines for stable isotopes - an announcement to isotope users. Isot. Environ. Health Stud. 47, 535–536.
Brownlee, D., 2014. The stardust mission: Analyzing samples from the edge of the Solar System. Annu. Rev. Earth Planet. Sci. 42, 179–205.
Budde, G., Kleine, T., Kruijer, T., Thomas, S., Burkhardt, C., Metzler, K., 2016. Tungsten isotopic constraints on the age and origin of chondrules. Proc. Natl. Acad. Sci. U. S. A. 113, 2886–2891.
Bunch, T.T., Rumble, D., Wittke, J.H., Irving, A.J., 2005. Pyroxene-rich pallasites Zinder and NWA 1911: Not like the others (abstract). Meteorit. Planet. Sci. 40 (#5219).
Bunch, T.E., Irving, A.J., Wittke, J.H., Rumble, D., Aaronson, A.A., 2007. Northwest Africa 2993: A coarse-grained lodran-like achondrite with affinities to winonaites (abstract). Lunar Planet. Sci. 38 (#2211).
Bunch, T.E., Irving, A.J., Wittke, J.H., Rumble, D., Gellissen, M., Palme, H., 2008. Evidence for pervasive metamorphism on the CR chondrite parent body from highly equilibrated CR6 chondrites Northwest Africa 2994 and Northwest Africa 3100 (abstract). Lunar Planet. Sci. 39 (#1991).
Burbine, T.H., 2014. Asteroids. In: M. Davis, A. (Ed.), Meteorites and Cosmochemical Processes, Treatise on Geochemistry, vol. 2, second edition. Elsevier, Oxford, pp. 365–414.
Burbine, T.H., 2016a. Advances in determining asteroid chemistries and mineralogies. Chem. Erde Geochem. 76, 181–195.
Burbine, T.H., 2016b. How well does the Bus-DeMeo taxonomy classify meteorite spectra? (abstract). Lunar Planet. Sci. 47 (#2425).
Burbine, T.H., Meibom, A., Binzel, R.P., 1996. Mantle material in the main belt: Battered to bits? Meteoritics 31, 607–620.
Burbine, T.H., McCoy, T.J., Nittler, L.R., Bell III, J.F., 2001. Could 433 eros have a primitive achondritic composition? (abstract). Lunar Planet. Sci. 32 (#1860).
Burbine, T.H., McCoy, T.J., Meibom, A., Gladman, B., Keil, K., 2002a. Meteoritic parent bodies: their number and identification. In: Bottke, W.F., Cellino, A., Paolicchi, P., Binzel, R.P. (Eds.), Asteroids III. University of Arizona Press, Tucson, pp. 653–667.
Burbine, T.H., McCoy, T.J., Nittler, L.R., Benedix, G.K., Cloutis, E.A., Dickinson, T.L., 2002b. Spectra of extremely reduced assemblages: Implications for Mercury. Meteorit. Planet. Sci. 37, 1233–1244.
Burbine, T.H., McCoy, T.J., Hinrichs, J.L., Lucey, P.G., 2006. Spectral properties of angrites. Meteorit. Planet. Sci. 41, 1139–1145.
Burbine, T.H., Greenwood, R.C., Buchanan, P.C., Franchi, I.A., Smith, C.L., 2007. Reflectance spectra of mesosiderites: implications for asteroid 4 Vesta (abstract). Lunar Planet. Sci. 38 (#2119).
Burbine, T.H., Duffard, R., Buchanan, P.C., Cloutis, E.A., Binzel, R.P., 2011. Spectroscopy of O-type asteroids (abstract). Lunar Planet. Sci 42 (#2483).
Burns, R.G., 1993. Mineralogical Applications of Crystal Field Theory. Cambridge University Press, Cambridge (576 pp.).
Bus, S.J., Binzel, R.P., 2002a. Phase II of the small main-belt asteroid spectroscopic survey: The observations. Icarus 158, 106–145.
Bus, S.J., Binzel, R.P., 2002b. Phase II of the small main-belt asteroid spectroscopic survey: A feature-based taxonomy. Icarus 158, 146–177.
Buseck, P.R., 1977a. Pallasite meteorites mineralogy, petrology and geochemistry. Geochim. Cosmochim. Acta 41, 711–740.
Buseck, P.R., 1977b. Pallasite meteorites—mineralogy, petrology and geochemistry. Geochim. Cosmochim. Acta. 41, 711–721.
Ćuk, M., Gladman, B.J., Nesvorný, D., 2014. Hungaria asteroid family as the source of aubrite meteorites. Icarus 239, 154–159.
Canup, R.M., Visscher, C., Salmon, J., Fegley, B., 2015. Lunar volatile depletion due to incomplete accretion within an impact-generated disk. Nat. Geosci. 8, 918–921.
Carporzen, L., Weiss, B.P., Elkins-Tanton, L.T., Shuster, D.L., Ebel, D., Gattacceca, J., 2011. Magnetic evidence for a partially differentiated carbonaceous chondrite parent body. PNAS 108, 6386–6389.
Cassen, P., 1996. Models for the fractionation of moderately volatile elements in the solar nebula. Meteorit. Planet. Sci. 31, 793–806.
Chabot, N.L., Haack, H., 2006. Evolution of asteroidal cores. In: Lauretta, D.S., McSween, H.Y. (Eds.), Meteorites and the Early Solar System II. University of Arizona Press, Tucson, pp. 747–771, 943 pp.
Chakraborty, S., Ahmed, M., Jackson, T.L., Thiemens, M.H., 2008. Experimental: Test of self-shielding in vacuum ultraviolet photo-dissociation of CO. Science 321, 1328–1331.
Chambers, J.E., 2004. Planetary accretion in the inner Solar System, Earth Planet. Earth Planet. Sci. Lett. 223, 241–252.
Chapman, C.R., 1986. Implications of the inferred compositions of the asteroids for their collisional evolution. Mem. Soc. Astron. Ital. 57, 103–114.
Chenet, H., Jutzi, M., Barrat, J.-A., Asphaug, E.I., Benz, W., Gillet, P., 2014. A deep crust-mantle boundary in the asteroid 4 Vesta. Nature 511, 303–306.
Choi, B.-G., Ouyang, X., Wasson, J.T., 1995. Classification and origin of IAB and IIICD iron meteorites. Geochim. Cosmochim. Acta 59, 593–612.
Clark, B.E., Bus, S.J., Rivkin, A.S., McConnochie, T., Sanders, J., Shah, S., Hiroi, T., Shepard, M., 2004. E-type asteroid spectroscopy and compositional modeling. J. Geophys. Res. 109, E02001, 11 pp.
Clayton, R.N., 2002. Solar system: Self-shielding in the solar nebula. Nature 415, 860–861.
Clayton, R.N., 2003. Oxygen isotopes in meteorites. In: Davis, A.M. (Ed.), Treatise on Geochemistry, vol. 1. Elsevier, pp. 129–142.
Clayton, R.N., 2006. Meteorites and their parent asteroids. Science 313, 1743–1744.
Clayton, R.N., Mayeda, T.K., 1963. The use of bromine pentafluoride in the extraction of oxygen from oxides and silicates for isotopic analysis. Geochim. Cosmochim. Acta 27, 43–52.
Clayton, R.N., Mayeda, T.K., 1988. Formation of ureilites by nebular processes. Geochim. Cosmochim. Acta 52, 1313–1318.
Clayton, R.N., Mayeda, T.K., 1996. Oxygen isotope studies of achondrites. Geochim. Cosmochim. Acta 60, 1999–2017.
Clayton, R.N., Mayeda, T.K., 1999. Oxygen isotope studies od carbonaceous chondrites. Geochim. Cosmochim. Acta 63, 2089–2104.
Clayton, R.N., Onuma, N., Mayeda, T.K., 1971. Oxygen isotope fractionation in Apollo 12 rocks and soils. Proc. 2nd Lunar Sci. Conf. 2, 1417–1420.
Clayton, R.N., Hurd, J.M., Mayeda, T.K., 1972. Oxygen isotope abundances in Apollo 14 and 15 rocks and minerals (abstract). Lunar Planet. Sci. 3, 141–143.
Clayton, R.N., Grossman, L., Mayeda, T.K., 1973. A component of primitive nuclear composition in carbonaceous chondrites. Science 182, 485–488.
Clayton, R.N., Onuma, N., Grossman, L., Mayeda, T.K., 1977. Distribution of the pre-solar component in Allende and other carbonaceous chondrites. Earth Planet. Sci. Lett. 34, 209–224.
Clayton, R.N., Mayeda, T.K., Rubin, A.E., 1984. Oxygen isotopic compositions of enstatite chondrites and aubrites. J. Geophys. Res. 89, C245–C249.
Clayton, R.N., Mayeda, T.K., Goswami, J.N., Olsen, E.J., 1991. Oxygen isotope studies of ordinary chondrites. Geochim. Cosmochim. Acta 55, 2317–2337.
Cleeves, I.I., Bergin, E.A., Alexander, C.M.O.D., Du, F., Graninger, D., Oberg, K.I., Harries, T.J., 2014. The ancient heritage of water ice in the solar system. Science 345, 1590–1593.
Cloutis, E.A., Hudon, P., 2004. Reflectance spectra of ureilites: Nature of the mafic silicate absorption features (abstract). Lunar Planet. Sci. 35 (#1257).
Cloutis, E.A., Binzel, R.P., Burbine, T.H., Gaffey, M.J., McCoy, T.J., 2006. Asteroid 3628 Božněmcová: covered with angrite-like basalts? Meteorit. Planet. Sci. 41, 1147–1161.
Cloutis, E.A., Hudon, P., Romanek, C.S., Bishop, J.L., Reddy, V., Gaffey, M.J., Hardersen, P.S., 2010. Spectral reflectance properties of ureilites. Meteorit. Planet. Sci. 45, 1668–1694.
Cloutis, E.A., Sanchez, J.A., Reddy, V., Gaffey, M.J., Binzel, R.P., Burbine, T.H., Hardersen, P.S., Hiroi, T., Lucey, P.G., Sunshine, J.M., Tait, K.T., 2015. Olivine-metal mixtures: Spectral reflectance properties and application to asteroid reflectance spectra. Icarus 252, 39–82.
Connelly, J.N., Bizzarro, M., Krot, A.N., Nordlund, A., Wielandt, D., Ivanova, M.A., 2012. The absolute chronology and thermal processing of solids in the solar protoplanetary disk. Science 338, 651–655.
Consolmagno, G.J., Golabek, G.J., Turrini, D., Jutzi, M., Sirono, S., Svetsov, V., Tsiganis, K., 2015. Is Vesta an intact and pristine protoplanet? Icarus 254, 190–201.
Craig, H., 1961. Standard for reporting concentrations of deuterium and oxygen-18 in natural waters. Science 133, 1833–1834.
Dale, C.W., Burton, K.W., Greenwood, R.C., Gannoun, A., Wade, J., Wood, B.J., Pearson, D.G., 2012. Late accretion on the earliest planetesimals revealed by the highly siderophile elements. Science 336, 72–75.
Dauphas, N., Marty, B., Reisberg, L., 2002. Molybdenum evidence for inherited planetary scale isotope heterogeneity of the protosolar nebula. Astrophys. J. 565, 640–644.
Dauphas, N., Chen, J.H., Zhang, J., Papanastassiou, D.A., Davis, A.M., Travaglio, C., 2014. Calcium-48 isotopic anomalies in bulk chondrites and achondrites: evidence for a uniform isotopic reservoir in the inner protoplanetary disk. Earth Planet. Sci. Lett. 407, 96–108.
Day, J.M.D., Ash, R.D., Liu, Y., Bellucci, J.J., Rumble III, D., McDonough, W.F., Walker, R.J., Taylor, L., 2009. Early formation of evolved asteroidal crust. Nature 457, 179–183.
Day, J.M.D., Ash, R.D., Walker, R.J., Liu, Y., Rumble III, D., Irving, A.J., McDonough, W.F., Tait, K., Taylor, L.A., 2011. Volatile-rich asteroid differentiation and links between felsic meteorites Graves Nunataks 06128 and 06129 brachinites and 'brachinite-like' achondrites (abstract). Lunar Planet. Sci. 42 (#1456).
Day, J.M.D., Walker, R.J., Ash, R.D., Liu, Y., Rumble, D., Irving, A.J., Goodrich, C.A., Tait, K., McDonough, W.F., Taylor, L.A., 2012a. Origin of felsic achondrites Graves Nunataks 06128 and 06129, and ultramafic brachinites and brachinite-like achondrites by partial melting of volatile-rich primitive parent bodies. Geochim. Cosmochim. Acta 81, 94–128.
Day, J.M.D., Walker, R.J., Qin, L., Rumble, D., 2012b. Late accretion as a natural consequence of planetary growth. Nat. Geosci. 5, 614–617.
De Sanctis, M.C., Ammannito, E., Capria, M.T., Tosi, F., Capaccioni, F., Zambon, F., Carraro, F., Fonte, S., Frigeri, A., Jaumann, R., Magni, G., Marchi, S., McCord, T.B., McFadden, L.A., Mc Sween, H.Y., Mittlefehldt, D.W., Nathues, A., Palomba, E., Pieters, C.M., Raymond, C.A., Russell, C.T., Toplis, M.J., Turrini, D., 2012. Spectroscopic characterization of mineralogy and its diversity across Vesta. Science 336, 697–700.
DeMeo, F.E., Binzel, R.P., Slivan, S.M., Bus, S.J., 2009. An extension of the Bus asteroid taxonomy into the near-infrared. Icarus 202, 160–180.

DeMeo, F.E., Carry, B., Binzel, R.P., Moskovitz, N., Polishook, D., Burt, B.J., 2014. The distribution of mantle material among main-belt asteroids. American Astronomical Society Meeting #224, #321.09.
Delaney, J.S., 2009. The missing achondrites: Taking a pinch of salt with the nebula. 72nd Meteoritical Society Meeting. Abstract #5095.
Delaney, J.S., Nehru, C.E., Prinz, M., Harlow, G.E., 1981. Metamorphism in mesosiderites. Proc. Lunar Planet. Sci. 12B, 1315–1342.
Delaney, J.S., Zanda, B., Clayton, R.N., Mayeda, T., 2000. Zag (b): A ferroan achondrite intermediate between brachinites and lodranites (abstract). Lunar Planet. Sci. 31 (#1745).
Dominguez, G., 2010. A heterogeneous chemical origin for the ^{16}O-enriched and ^{16}O-depleted reservoirs of the early solar system. Astrophys. J. Lett. 713, L59–L63.
Downes, H., Mittlefehldt, D.W., Kita, N.T., Valley, J.W., 2008. Evidence from polymict ureilite meteorites for a disrupted and re-accreted single ureilite parent asteroid gardened by several distinct impactors. Geochim. Cosmochim. Acta 72, 4825–4844.
Dyl, K.A., Bischoff, A., Ziegler, K., Young, E.D., Wimmer, K., Bland, P.A., 2012. Early solar system hydrothermal activity in chondritic asteroids on 1-10-year timescales. PNAS 109, 18306–18311.
Elkins-Tanton, L.T., 2012. Magma oceans in the inner Solar System. Annu. Rev. Earth Planet. Sci. 40, 113–139.
Elkins-Tanton, L.T., Weiss, B.P., Zuber, M.T., 2011. Chondrites as samples of differentiated planetesimals. Earth Planet. Sci. Lett. 305, 1–10.
Elkins-Tanton, L.T., Mandler, B.E., Fu R.R., 2014. Placing Vesta in the range of planetesimal differentiation models. Conference item: Vesta in the light of Dawn: First exploration of a protoplanet in the asteroid belt. Abstract #2034.
Elsenheimer, D., Valley, J.W., 1992. In situ oxygen isotope analysis of feldspar and quartz by Nd:YAG laser microprobe. Chem. Geol. 101, 21–42.
Elser, S., Meyer, M.R., Moore, B., 2012. On the origin of elemental abundances in the terrestrial planets. Icarus 221, 859–874.
Farquhar, J., Rumble, D., 1998. Comparison of oxygen isotope data obtained by laser fluorination of olivine with KrF excimer laser and CO_2 laser. Geochim. Cosmochim. Acta 62, 3141–3149.
Fazio, A., D'Orazio, M., Folco, L., Gattacceca, J., 2013. The extremely reduced silicate-bearing iron meteorite Northwest Africa 6583: Implications on the variety of impact melt rocks of the IAB-complex parent body. Meteorit. Planet. Sci. 48, 2451–2468.
Fieber-Beyer, S.K., Gaffey, M.J., Kelley, M.S., Reddy, V., Reynolds, C.M., Hicks, T., 2011. The Maria asteroid family: Genetic relationships and a plausible source of mesosiderites near the 3:1 Kirkwood Gap. Icarus 213, 524–537.
Floss, C., Crozaz, G., Jolliff, B., Benedix, G., Colton, S., 2008. Evolution of the winonaite parent body: Clues from silicate mineral trace element distributions. Meteorit. Planet. Sci. 43, 657–674.
Franchi, I.A., Wright, I.P., Gibson, E.K.Jr., Pillinger, C.T., 1986. The laser microprobe: a technique for extracting carbon, nitrogen, and oxygen from solid samples for isotope measurements. J. Geophy. Res. 91 (b4), D514–D524.
Franchi, I.A., Sexton, A.S., Wright, I.P., Pillinger, C.T., 1998. Oxygen isotopic homogeneity in the ureilite population (abstract). Lunar Planet. Sci. 29 (#1685).
Franchi, I.A., Wright, I.P., Sexton, A.S., Pillinger, C.T., 1999. The oxygen-isotopic composition of Earth and Mars. Meteorit. Planet. Sci. 34, 657–661.
Franchi, I.A., Baker, L., Bridges, J.C., Wright, I.P., Pillinger, C.T., 2001. Oxygen isotopes and the early Solar Sytem. Phil. Trans. R. Soc. Lond. A 359, 2019–2035.
Franchi, I.A., Greenwood, R.C., Scott, E.R.D., 2013. The IIIAB-pallasite relationship revisited: the oxygen isotope perspective. Meteorit. Planet. Sci., supplement abstract #5326.
Franchi, I.A., 2008. Oxygen isotopes in asteroidal materials. Rev. Mineral. 68, 345–397.
Fu, R.R., Elkins-Tanton, L.T., 2014. The fate of magmas in planetesimals and the retention of primitive chondritic crusts. Earth Planet. Sci. Lett. 390, 128–137.
Fu, R.R., Young, E.D., Greenwood, R.C., Elkins-Tanton, L.T., 2015. Fluid migration in early-accreting planetesimals (abstract). Lunar Planet. Sci. 46 (#1591).
Fu, R.R., Young, E.D., Greenwood, R.C., Elkins-Tanton, L.T., 2016. Silicate melting and volatile loss during differentiation in planetesimals. In: Elkins-Tanton, L.T., Weiss, B.P. (Eds.), Planetesimals. Cambridge University Press, in press.
Gaffey, M.J., 1997. Surface lithological heterogeneity of asteroid 4 Vesta. Icarus 127, 130–157.
Gaffey, M.J., Bell, J.F., Brown, R.H., Burbine, T.H., Piatek, J., Reed, K.L., Chaky, D.A., 1993. Mineralogic variations within the S-type asteroid class. Icarus 106, 573–602.
Gardner-Vandy, K.G., Lauretta, D.S., Greenwood, R.C., McCoy, T.J., Killgore, M., Franchi, I.A., 2012. The Taffassasset primitive achondrite: Insights into initial stages of planetary differentiation. Geochim. Cosmochim. Acta 85, 142–159.
Gardner-Vandy, K.G., Lauretta, D.S., McCoy, T.J., 2013. A petrologic, thermodynamic and experimental study of brachinites: Partial melt residues of an R chondrite-like precursor. Geochim. Cosmochim. Acta 122, 36–57.
Ghosh, A., McSween, H.Y., 1998. A thermal model for the differentiation of asteroid 4 Vesta, based on radiogenic heating. Icarus 134, 187–206.
Goldstein, J.I., Scott, E.R.D., Chabot, N.L., 2009. Iron meteorites: Crystallization, thermal history, parent bodies, and origin. Chem. Erde 69, 293–325.
Goldstein, J.I., Yang, J., Scott, E.R.D., 2014. Determining cooling rates of irons and stony-iron meteorites from measurements of Ni and Co at kamacite-taenite interfaces. Geochim. Cosmochim. Acta 140, 297–320.
Goodrich, C.A., Van Orman, J.A., Wilson, L., 2007. Fractional melting and smelting on the ureilite parent body. Geochim. Cosmochim. Acta 71, 2876–2895.
Goodrich, C.A., Kita, N.T., Spicuzza, M.J., Valley, J.W., Zipfel, J., Mikouchi, T., Masamichi, M., 2010. The Northwest Africa 1500 meteorite Not a ureilite, maybe a brachinite. Meteorit. Planet. Sci. 45, 1906–1928.
Greenwood, R.C., Franchi, I.A., 2004. Alteration and metamorphism of CO3 chondrites: Evidence from oxygen and carbon isotopes. Meteorit. Planet. Sci. 39, 1823–1838.
Greenwood, R.C., Franchi, I.A., Jambon, A., Buchanan, P.C., 2005. Widespread magma oceans on asteroidal bodies in the early solar system. Nature 435, 916–918.
Greenwood, R.C., Franchi, I.A., Jambon, A., Barrat, J.A., Burbine, T.H., 2006. Oxygen isotope variation in stony-iron meteorites. Science 313, 1763–1765.
Greenwood, R.C., Franchi, I.A., Kearsley, A.T., Alard, O., 2010. The relationship between CK and CV chondrites. Geochim. Cosmochim. Acta 74, 1684–1705.
Greenwood, R.C., Franchi, I.A., Gibson, J.M., Benedix, G.K., 2012. Oxygen isotope variation in primitive achondrites: The influence of primordial, asteroidal and terrestrial processes. Geochim. Cosmochim. Acta 94, 146–163.
Greenwood, R.C., Barrat, J.-A., Yamaguchi, A., Franchi, I.A., Scott, E.R.D., Bottke, W.F., Gibson, J.M., 2014. The oxygen isotope composition of diogenites: Evidence for early global melting on a single, compositionally diverse, HED parent body. Earth Planet. Sci. Lett. 390, 165–174.
Greenwood, R.C., Barrat, J.-A., Scott, E.R.D., Haack, H., Buchanan, P.C., Franchi, I.A., Yamaguchi, A., Johnson, D., Bevan, A.W.R., Burbine, T., 2015a. Geochemistry and oxygen isotope composition of main-group pallasites and olivine-rich clasts in mesosiderites: Implications for the great dunite shortage and HED-mesosiderite connection. Geochim. Cosmochim. Acta 169, 115–136.
Greenwood, R.C., Zolensky, M.E., Buchanan, P.C., Franchi, I.A., 2015b. The oxygen isotope composition of dark inclusions in HEDs, ordinary chondrites and carbonaceous chondrites (abstract). Lunar Planet. Sci. 46 (#2975).
Grossman, L., 1972. Condensation in the primitive solar nebula. Geochim. Cosmochim. Acta 36, 597–619.
Haack, H., McCoy, T.J., 2005. Iron and stony-iron meteorites. In: Davis, A.M. (Ed.), Treatise on Geochemistry: Meteorites, Comets and Planets, vol. 1. Elsevier, pp. 325–345.
Haack, H., Scott, E.R.D., Love, S.G., Brearley, A.J., McCoy, T.J., 1996. Thermal histories of IVA stony-iron and iron meteorites: Evidence for asteroid fragmentation and reaccretion. Geochim. Cosmchim. Acta 60, 3103–3113.
Halliday, A.N., Wood, B.J., 2010. The composition and major reservoirs of the Earth around the time of the Moon-forming giant impact. In: Stevenson, D. (Ed.), Evolution of the Earth: Treatise on Geophysics, vol. 9. Elsevier., pp. 13–50.
Hallis, L.J., Anand, M., Greenwood, R.C., Miller, M.F., Franchi, I.A., Russell, S.S., 2010. The oxygen isotope composition, petrology and geochemistry of mare basalts: Evidence for large-scale compositional variation in the lunar mantle. Geochim. Cosmochim. Acta 74, 6885–6899.
Hardersen, P.S., Gaffey, M.J., Abell, P.A., 2004. Mineralogy of asteroid 1459 Magnya and implications for its origin. Icarus 167, 170–177.
Hassanzadeh, J., Rubin, A.E., Wasson, J.T., 1990. Composition of large metal nodules in mesosiderites: Links to iron meteorite group IIIAB and the origin of mesosiderite subgroups. Geochim. Cosmochim. Acta 54, 3197–3208.
Henke, S., Gail, H.-P., Trieloff, M., Schwarz, W.H., 2013. Thermal evolution model for the H chondrite asteroid-instantaneous formation versus protracted accretion. Icarus 226, 212–228.
Herrin, J.S., Zolensky, M.E., Cartwright, J.A., Mittlefehldt, D.W., Ross, D.K., 2011. Carbonaceous chondrite-like lithologies on the HED parent (abstract). Lunar Planet. Sci 42 (#2806).
Hevey, P.J., Sanders, I.S., 2006. A model for planetesimal meltdown by ^{26}Al and its implications for meteorite parent bodies. Meteorit. Planet. Sci. 41, 95–106.
Hewins, R.H., 1983. Impact versus intenal origins for mesosiderites. Proc. 14th Lunar Planet. Sci. Conf. J. Geophys. Res 88, B257–B266.
Hiroi, T., Sasaki, S., 2012. Asteroidal space weathering: Compositional dependency and influence on taxonomy. Asteroids Comets and Meteors, Conference Proceedings. Abstract #6109.
Hopfe, W.D., Goldstein, J.I., 2001. The metallographic cooling rate method revised: Application to iron meteorites and mesosiderites. Meteorit. Planet. Sci. 36, 135–154.
Horstmann, M., Bischoff, A., Pack, A., Albrecht, N., Weyrauch, M., Hain, H., Roggon, L., Schneider, K., 2012. Mineralogy and oxygen isotope composition of new samples from the Almahata Sitta strewn field (abstract). Meteorit. Planet. Sci. 47 (#5053).
Humayun, M., Clayton, R.N., 1995. Potassium isotope cosmochemistry: Genetic implications of volatile element depletion. Geochim. Cosmochim. Acta 59, 2131–2148.
Humayun, M., Weiss, B.P., 2011. A common parent body for Eagle Station pallasites and CV chondrites (abstract). Lunar Planet. Sci. 42 (#1507).
Humayun, M., Teplyakova, S.N., Lorenz, C.A., Ivanova, M.A., Korochantsev, A.V., 2014. Siderophile element abundances in Karavanoe: Implications for the origin of the Eagle Station Pallasites (abstract). Lunar Planet. Sci. 45 (#2293).
Hutchison, R., 2004. Meteorites: A Petrologic, Chemical and Isotopic Synthesis. Cambridge University Press, Cambridge.
Hyde, B.C., Tait, K.T., Nicklin, I., Gregory, D.A., Ali, A., Jabeen, I., Banerjee, N.R., 2013. Northwest Africa 7680: an ungrouped achondrite with affinities to primitive achondrite groups (abstract). Meteorit. Planet. Sci. 48 (#5207).
Ikeda, Y., Takeda, H., 1985. A model for the origin of basaltic achondrites based on th Yamato 7308 howardite. Proc. 15th Lunar Planet. Sci. Conf. J. Geophys. Res. 90 (Supplement), C649–C663.
Irving, A.J., Larson, T.E., Longstaffe, F.J., Rumble, D., Bunch, T.E., Wittke, J.H., Kuehner, S.M., 2004. A primitive achondrite with oxygen isotopic affinities to

CV chondrites: Implications for differentiation and size of the CV parent body. EOS Trans. AGU, 85 #P31C-02.
Irving, A.J., Kuehner, S.M., Rumble, D., 2006. A fresh plutonic igneous angrite containing grain boundary glass from Tamassint, Northwest Africa. AGU, Fall Meeting 2006, abstract #P51E-1245.
Irving, A.J., Rumble III, D., Kuehner, S.M., Gellissen, M., Hupé, G.M., 2009. Ultramafic achondrite Northwest Africa 5400: A unique brachinite-like meteorite with terrestrial oxygen isotopic composition (abstract). Lunar Planet. Sci. 40 (#2332).
Irving, A.J., Kuehner, S.M., Bunch, T.E., Ziegler, K., Chen, G., Herd, C.D.K., Conrey, R.M., Ralew, S., 2013. Ungrouped mafic achondrite Northwest Africa 7325: A reduced, iron-poor cumulate olivine gabbro from a differentiated planetary parent body (abstract). Lunar Planet. Sci. 44 (#2164).
Irving, A.J., Kuehner, S.M., Ziegler, K., 2015. Petrology and oxygen isotopic composition of orthopyroxenitic achondrite Northwest Africa 8777 and sodic ultramafic achondrite Northwest Africa 10132 (abstract). Meteorit. Planet. Sci. 50 (#5254).
Izidoro, A., Haghighipour, N., Winter, O.C., Tsuchida, M., 2014. Terrestrial planet formation in a protoplanetary disk with a local mass depletion: A successful scenario for the formation of mars. Astrophys. J. 782, 31.
Jacobsen, B., Yin, Q.-Z., Moynier, F., Amelin, Y., Krot, A.N., Nagashima, K., Hutcheon, I.D., Palme, H., 2008. ^{26}Al-^{26}Mg and ^{207}Pb-^{206}Pb systematic of Allende CAIs: Canonical solar initial ^{26}Al/^{27}Al ratio reinstated. Earth Planet. Sci. Lett. 272, 353–364.
Jacobson, S.A., DeMeo, F., Morbidelli, A., Carry, B., Frost, D., Rubie, D.C., 2016. There is too much mantle material in the asteroid belt (abstract). Lunar Planet. Sci. 47 (#1895).
Janots, E., Gnos, E., Hofmann, B., Greenwood, R.C., Franchi, I.A., Bermingham, K., Netwing, V., 2012. Jiddat al Harasis 556: A howardite impact breccias with an H chondrite component. Meteorit. Planet. Sci 47, 1558–1574.
Javoy, M., Kaminski, E., Guyot, F., Andrault, D., Sanloup, C., Moreira, M., Labrosse, S., Jambon, A., Agrinier, P., Davaille, A., Jaupart, C., 2010. The chemical composition of the Earth: Enstatite chondrite models. Earth Planet. Sci. Lett. 293, 259–268.
Javoy, M., 1995. The integral enstatite chondrite model of the Earth. Geophys. Res. Lett. 22, 2219–2222.
Jenniskens, P., Shaddad, M.H., Numan, D., Elsir, S., Kudoda, A.M., Zolensky, M.E., Le, L., Robinson, G.A., Friedrich, J.M., Rumble, D., Steele, A., Chesley, S.R., Fitzsimmons, A., Duddy, S., Hsieh, H.H., Ramsay, G., Brown, P.G., Edwards, W.N., Tagliaferri, E., Boslough, M.B., Spalding, R.E., Dantowitz, R., Kozubal, M., Pravec, P., Borovicka, J., Charvat, Z., Vaubaillon, J., Kuiper, J., Albers, J., Bishop, J.L., Mancinelli, R.L., Sandford, S.A., Milam, S.N., Nuevo, M., Worden, S.P., 2009. The impact and recovery of asteroid 2008 TC_3. Nature 458, 485–488.
Jenniskens, P., Vaubaillon, J., Binzel, R.P., DeMeo, F.E., Nesvorný, D., Bottke, W.F., Fitzsimmons, A., Hiroi, T., Marchis, F., Bishop, J.L., Vernazza, P., Zolensky, M.E., Herrin, J.S., Welten, K.C., Meier, M.M.M., Shaddad, M.H., 2010. Almahata Sitta (=asteroid 2008 TC_3) and the search for the ureilite parent body. Meteorit. Planet. Sci. 45, 1590–1617.
Johnson, B.C., Minton, D.A., Melosh, H.J., Zuber, M.T., 2015. Impact jetting as the origin of chondrules. Nature 517, 339–341.
Jones, R.H., Wasson, J.T., Larson, T., Sharp, Z.D., 2003. Milton: A new unique pallasite (abstract). Lunar Planet. Sci. 34 (#1683).
Jones, J.H., 1984. The composition of the mantle of the eucrite parent body and the origin of eucrites. Geochim. Cosmochim. Acta 48, 641–648.
Jurewicz, A.J.G., Mittlefehldt, D.W., Jones, J.H., 1993. Experimental: partial melting of the Allende (CV) and Murchison (CM) chondrites and the origin of asteroidal basalts. Geochim. Cosmomchim. Acta 57, 2123–2139.
Kaneda, K., Warren, P.H., 1998. iron-nickel metal bearing unique eucrite Elephant Morraine 92023 Siderophile concentrations, and petrogenesis (abstract). Meteorit. Planet. Sci. 33, p. A81.
Keil, K., Ntaflos, Th., Taylor, G.J., Brearley, A.J., Newson, H.E., Romig Jr., A.D., 1989. The Shallowater aubrite: evidence for origin by planetesimal impacts. Geochim. Cosmochim. Acta 53, 3291–3307.
Keil, K., 1989. Enstatite meteorites and their parent bodies. Meteoritics 24, 195–208.
Keil, K., 2010. Enstatite achondrite meteorites (aubrites) and the histories of their asteroidal parent bodies. Chem. Erde/Geochem. 70, 295–317.
Keil, K., 2012. Angrites, a small but diverse suite of ancient, silica-undersaturated volcanic-plutonic mafic meteorites, and the history of their parent asteroid. Chem. Erde/Geochem. 72, 191–218.
Keil, K., 2014. Brachinite meteorites: partial melt residues from an FeO-rich asteroid. Chem. Erde/Geochem. 74, 311–329.
Kita, N.T., Ikeda, Y., Togashi, S., Liu, Y., Morishita, Y., Weisberg, M.K., 2004. Origin of ureilites inferred from a SIMS oxygen isotopic and trace element study of clasts in the Dar al Gani 319 polymict ureilite. Geochim. Cosmochim. Acta 68, 4213–4235.
Kita, N.T., Ushikubo, T., Fu, B., Valley, J.W., 2009a. High precision SIMS oxygen isotope analysis and the effect of sample topography. Chem. Geol. 264, 43–57, ijer.
Kita, N.T., Goodrich, C.A., Spicuzza, M.J., Valley, J.W., 2009b. Oxygen isotopes in ungrouped achondrite NWA 1500 and comparison to brachinites (abstract). Lunar Planet. Sci. 40 (#1393).
Kleine, T., Mezger, K., Palme, H., Scherer, E., Münker, C., 2005. Asteroids and late accretion of chondrite parent bodies: Evidence from 182Hf–182W in CAIs, metal-rich chondrites, and iron meteorites. Geochim. Cosmochim. Acta 69, 5805–5818.
Kleine, T., Toubol, M., Bourdon, B., Nimmo, F., Mezger, K., Plame, H., Jacobsen, S.B., Yin, Q.-B., Halliday, A.W., 2009. Hf-W chronology of the accretion and early evolution of asteroidsand terrestrial planets. Geochim. Cosmochim. Acta 73, 5150–5188.
Kleine, T., Hans, U., Irving, A.J., Bourdon, B., 2012. Chronology of the angrite parent body and implications for core formation in protoplanets. Geochim. Cosmochim. Acta 84, 186–203.
Kong, P., Su, W., Li, X., Spettel, B., Palme, H., Tao, K., 2008. Geochemistry and origin of metal olivine clasts, and matrix in the Dong Ujimqin Qi mesosiderite. Meteorit. Planet. Sci. 43, 451–460.
Korochantsev, A.V., Lorenz, C.A., Ivanova, M.A., Teplyakova, S.N., Kononkova, N.N., Roshina, I.A., Borisovsky, S.E., Bychkova, Y.V., Franchi, I.A., Greenwood, R.C., 2013. Karavannoe: A new member of the Eagle Station pallasite grouplet (abstract). Lunar Planet. Sci. 44 (#2020).
Krot, A.N., Amelin, T., Bland, P., Ciesla, F.J., Connelly, J., Davis, A.M., Huss, G.R., Hutcheon, I.D., Makide, K., Nagashima, K., Nyquist, L.E., Russell, S.S., Scott, E.R.D., Thrane, K., Yurimoto, H., Yin, Q.-Z., 2009. Origin and chronology of chondritic components: A review. Geochim. Cosmochim. Acta 73, 4963–4997.
Krot, A.N., Nagashima, K., Ciesla, F.J., Meyer, B.S., Hutcheon, I.D., Davies, A.M., Huss, G.R., Scott, E.R.D., 2010. Oxygen isotopic composition of the Sun and mean oxygen isotopic composition of the protosolar silicate dust: Evidence from refractory inclusions. Astrophys. J. 713, 1159–1166.
Krot, A.N., Keil, K., Scott, E.R.D., Goodrich, C.A., Weisberg, M.K., 2014. Classification of meteorites and their genetic relationships. In: Davis, A.M. (Ed.), Meteorites and Cosmochemical Processes, Treatise on Geochemistry, vol. 1, second edition. Elsevier, Oxford, pp. 1–63.
Kruijer, T.S., Touboul, M., Fischer-Gödde, M., Bermingham, K.R., Walker, R.J., Kleine, T., 2014. Protracted core formation and rapid accretion of protoplanets. Science 344, 1150–1154.
Kuehner, S.M., Irving, A.J., Ziegler, K., Rumble, D., Hupé, G., 2013. Mineralogy & oxygen isotopic composition of Northwest Africa 7822: A unique dunitic achondrite with affinities to the Eagle Station pallasite grouplet and/or the CV chondrite parent body (abstract). Meteorit. Planet. Sci. 48 (#5269).
Kusakabe, M., Maruyama, S., Nakamura, T., Yada, T., 2004. CO2 laser-BrF5 fluorination technique for analysis of oxygen three isotopes of rocks and minerals. J. Mass Spectrom. Soc. Jpn. 52, 205–212.
Lane, N., 2002. Oxygen: The Molecule That Made the World. Oxford University Press, Oxford, England.
Larsen, K.K., Trinquier, A., Paton, C., Schiller, M., Wielandt, D., Ivanova, M.A., Connelly, J.N., Nordlund, A., Krot, A.N., Bizzarro, M., 2011. Evidence for magnesium isotope heterogeneity in the solar protoplanetary disk. Astrophys. J. 735, L37.
Larsen, K.K., Schiller, M., Bizzarro, M., 2016. Accretion timescales and style of asteroidal differentiation in an 26Al-poor protoplanetary disk. Geochim. Cosmochim. Acta 176, 295–315.
Larson, H.P., Fink, U., 1975. Infrared spectral observations of asteroid 4 Vesta. Icarus 26, 420–427.
Lazzaro, D., Michtchenko, T., Carvano, J.M., Binzel, R.P., Bus, S.J., Burbine, T.H., Mothé-Diniz, T., Florczak, M., Angeli, C.A., Harris, A.W., 2000. Discovery of a basaltic asteroid in the outer main belt. Science 288, 2033–2035.
Lock, S.J., Stewart, S.T., Petaev, M.I., Leinhardt, Z.M., Mace, M., Jacobsen, S.B., Ćuk, M., 2016. A new model for lunar origin: Equilibration with Earth beyond the hot spin stability limit (abstract). Lunar Planet. Sci. 47 (#2881).
Lodders, K., 2003. Solar system abundances and condensation temperatures of the elements. Astrophys. J. 591, 1220–1247.
Lorenz, C.A., Ivanova, M.A., Nazarov, M.A., Mayeda, T.K., Clayton, R.N., 2003. A new primitive ungrouped achondrite, Dhofar 500: Links to winonaites and silicate inclusions from IAB-IIICD irons (abstract). Meteorit. Planet. Sci. 38 (#5045).
Lorenz, C., Brandstätter, F., Franchi, I.A., Greenwood, R.C., 2007. NWA 4518: The metal-rich ungrouped achondrite (abstract). Meteorit. Planet. Sci. 42 (#5169).
Lorenz, C.A., Teplyakova, S.N., Humayun, M., Ivanova, M.A., Franchi, I.A., Greenwood, R.C., 2011. Origin of the ungrouped achondrite NWA 4518: Mineralogy and geochemistry of FeNi-metal (abstract). Lunar Planet. Sci. 42 (#1291).
Lyons, J.R., 2011. Modeling CO photolysis experiments and disk chemistry using line-by-line spectra for oxygen isotopologues of CO (abstract). Lunar Planet. Sci. 42 (#2780).
Lyons, J.R., 2014. Photodissociation of CO isotopologues: models of laboratory experiments and implications for the solar nebula. Meteorit. Planet. Sci. 49, 373–393.
Lyons, J.R., Young, E.D., 2005. CO self-shielding as the origin of oxygen isotope anomalies in the early solar nebula. Nature 435, 317–320.
MacPherson, G.J., Boss, A., 2011. Cosmochemical evidence for astrophysical processes during formation of our Solar System. PNAS 108, 19152–19158.
MacPherson, G.J., Davis, A.H., Zinner, E.K., 1995. The distribution of aluminium-26 in the early Solar System—A reappraisal. Meteoritics 30, 365–386.
MacPherson, G.J., 2014. Calcium-aluminum-rich inclusions in chondritic meteorites meteorites and cosmochemical processes. In: Andrew Davis, M. (Ed.), Treatise on Geochemistry, vol. 1, second edition. Elsevier, pp. 139–179.
Macaulay, C.I., Fallick, A.E., Haszeldine, R.S., Graham, C.M., 2000. Methods of laser based stable isotope measurements applied to diagenetic cements and hydrocarbon reservoir quality. Clay Miner. 35, 313–322.
Mandler, B.E., Elkins-Tanton, L.T., 2013. The origin of eucrites, diogenites, and olivine diogenites: Magma ocean crystallization and shallow magma chamber processes on Vesta. Meteorit. Planet. Sci. 48, 2333–2349, http://dx.doi.org/10.1111/maps12135.

Manian, S.H., Urey, H.C., Bleakney, W., 1934. An investigation of the relative abundance of the oxygen isotopes O^{16}:O^{18} in stone meteorites. J. Am. Chem. Soc. 56, 2601–2609.
Matsuhisa, Y., Goldsmith, J.R., Clayton, R.N., 1978. Mechanisms of hydrothermal crystallization of quartz at 250C and 15 kbar. Geochim. Cosmochim. Acta 42, 173–182.
Mattey, D., Macpherson, C., 1993. High-precision oxygen isotope microanalysis of ferromagnesian minerals by laser fluorination. Chem. Geol. 105, 305–318.
Mattey, D., Lowry, D., MacPherson, C., 1994. Oxygen isotope composition of mantle peridotite. Earth Planet. Sci. Lett. 128, 231–241.
McCord, T.B., Adams, J.B., Johnson, T.V., 1970. Asteroid Vesta: Spectral reflectivity and compositional implications. Science 168, 1445–1447.
McCord, T.B., Li, J.-Y., Combe, J.-P., McSween, H.Y., Jaumann, R., Reddy, V., Tosi, F., Williams, D.A., Blewett, D.T., Turrini, D., Palomba, E., Pieters, C.M., de Sanctis, M.C., Ammannito, E., Capria, M.T., Le Corre, L., Longbardo, A., Nathues, A., Mittlefehldt, D.W., Schroder, S.E., Hiesinger, H., Beck, A.W., Capaccioni, F., Carsenty, U., Keller, H.U., Denevi, B.W., Sunshine, J.M., Raymond, C.A., Russell, C.T., 2012. Dark material on Vesta from infall of carbonaceous volatile-rich material. Nature 491, 83–86.
McCoy, T.J., Keil, K., Clayton, R.N., Mayeda, T.K., Bogard, D.D., Garrison, D.H., Huss, G.R., Hutcheon, I.D., Wieler, R., 1996. A petrologic, chemical and isotopic study of monument draw and comparison with other acapulcoites: Evidence for formation by incipient partial melting. Geochim. Cosmochim. Acta 60, 2681–2708.
McCoy, T.J., Keil, K., Muenow, D.W., Wilson, L., 1997a. Partial melting and melt migration on the acapulcoite-lodranite parent body. Geochim. Cosmochim. Acta 61, 639–650.
McCoy, T.J., Clayton, R.N., Mayeda, T.K., Bogard, D.D., Garrison, D.H., Wieler, R., 1997b. A petrologic and isotopic study of lodranites: evidence for early formation as partial melt residues from heterogeneous precursors. Geochim. Cosmochim. Acta 61, 623–637.
McCoy, T.J., Walker, R.J., Goldstein, J.T., Yang, J., McDonough, W.F., Rumble, D., Chabot, N.L., Ash, R.D., Corrigan, C.M., Michael, J.R., Kotula, P.G., 2011. Group IVA irons: New constraints on the crystallization and cooling history of an asteroidal core with a complex history. Geochim. Cosmochim. Acta 75, 6821–6843.
McCoy, T.J., Beck, A.W., Prettyman, T.H., Mittlefehldt, D.W., 2015. Asteroid (4) Vesta II: Exploring a geologically and geochemically complex world with the Dawn Mission. Chem. Erde/Geochem. 75, 273–285.
McDermott, K., Greenwood, R.C., Scott, E.R.D., Franchi, I.A., Anand, M., 2016. Oxygen isotope and petrological study of silicate inclusions in IIE iron meteorites and their relationship with H chondrites Geochim. Cosmochim. Acta 173, 97–113.
McKeegan, K.D., Kallio, A.P., Heber, V., Jarzebinski, G., Mao, P.H., Coath, C.D., Kunihiro, T., Wiens, R.C., Nordholt, J.E., Moses Jr., R.W., Reisenfeld, D.B., Jurewicz, A.J.G., Burnett, D.S., 2011. The Oxygen isotopic composition of the Sun inferred from captured solar wind. Science 332, 1528–1532.
McKinney, C.R., McCrea, J.M., Epstein, S., Allen, H.A., Urey, H.C., 1950. Improvements in mass spectrometry for the measurement of small differences in isotope abundance ratios. Rev. Sci. Instrum. 21, 724–730.
McSween Jr., H.Y., Mittlefehldt, D.W., Beck, A.W., Mayne, R.G., McCoy, T.J., 2011. HED meteorites and their relationship to the geology of Vesta and the Dawn mission. Space Sci. Rev. 163, 141–174.
McSween, Harry, Y., Binzel, Richard, P., De Sanctis, M., Cristina, Ammannito, Eleonora, Prettyman, Thomas, H., Beck Andrew, W., Reddy, Vishnu, Corre, Lucille, Gaffey, Michael, J., McCord, Thomas, B., Raymond, Carol, A., Russell, Christopher, T., 2013. Dawn, the Vesta-HED connection, and the geological context for eucrites diogenites and howardites. Meteorit. Planet. Sci. 48 (11), 2090–2104, http://dx.doi.org/10.1111/maps.12108.
Meteoritical, Bulletin Database: http://www.lpi.usra.edu/meteor/.
Metzler, K., Bobe, K.D., Palme, H., Spettel, B., Stöffler, D., 1995. Thermal and impact metamorphism on the HED parent asteroid. Planet. Space Sci. 43, 499–525.
Meyer, B.S., Zinner, E., 2006. Nucleosynthesis. In: Lauretta, D.S., McSween, H.Y. (Eds.), Meteorites and the Early Solar System II. University of Arizona Press, Tucson, pp. 69–108, 943 pp.
Mikouchi, T., McKay, G., Jones, J., 2008. Petrogenesis and crystallization history of quenched angrites (abstract). Meteorit. Planet. Sci. 43, A98.
Miller, M.F., Franchi, I.A., Sexton, A.S., Pillinger, C.T., 1999. High precision $\delta^{17}O$ isotope measurements of oxygen from silicates and other oxides: Methods and applications. Rapid Comm. Mass Spectrom. 13, 1211–1217.
Miller, M.F., Greenwood, R.C., Franchi, I.A., 2015. Comment on The triple oxygen isotope composition of the Earth mantle and understanding $\Delta^{17}O$ variations in terrestrial rocks and minerals by Pack and Herwartz [Earth Planet. Sci. Lett. 390 (2014) 138–145]. Earth Planet. Sci. Lett. 418, 181–183.
Miller, M.F., 2002. Isotopic fractionation and the quantification of ^{17}O anomalies in the oxygen three-isotope system: An appraisal and geochemical significance. Geochim. Cosmochim. Acta 66, 1881–1889.
Mittlefehldt, D.W., 1980. The composition of mesosiderite olivine clasts and implications for the origin of pallasites. Earth Planet. Sci. Lett. 51, 29–40.
Mittlefehldt, D.W., 2005a. Achondrites. In: Davis, A.M. (Ed.), Treatise on Geochemistry: Meteorites, Comets and Planets, vol. 1. Elsevier, pp. 291–324.
Mittlefehldt, D.W., 2005b. Ibitira—a basaltic achondrite from a distinct parent asteroid and implications for the Dawn mission. Meteorit. Planet. Sci. 40, 665–677.
Mittlefehldt, D.W., 2008, Meteorites —A brief tutorial. Rev. Mineral. Geochem. 68, Mineralogical Society of America, pp. 571–590.
Mittlefehldt, D.W., 2015. Asteroid 4 Vesta: I. Mineralogy: petrology and geochemistry of the HED meteorites. Chem. Erde/Geochem. 75, 155–183.
Mittlefehldt, D.W., Lindstrom, M.M., 1996. Antarctic Stannern and Nuevo Laredo trend eucrites, cumulates and others. Meteorit. Planet. Sci. 31, A90.
Mittlefehldt, D.W., McCoy, T.J., Goodrich, C.A., Kracher, A., 1998. Non-chondritic meteorites from asteroidal bodies. In: Papike, J.J. (Ed.), Planetary Materials. Reviews in Mineralogy, vol. 36. Mineralogical Society of America, 4. 1–4.195.
Mittlefehldt, D.W., Bogard, D.D., Berkley, J.L., Garrison, D.H., 2003. Brachinites: Igneous rocks from a differentiated asteroid. Meteorit. Planet. Sci. 38, 1601–1625.
Miura, Y.N., Hikada, H., Nishiizumi, K., Kusakabe, M., 2007. Noble gas and oxygen isotope studies of aubrites: a clue to origin and histories. Geochim. Cosmochim. Acta 71, 251–270.
Moskovitz, N., Gaidos, E., 2011. Differentiation of planetesimals and the thermal consequences of melt migration. Meteorit. Planet. Sci. 46, 903–918.
Mothé-Diniz, T., Carvano, J.M., 2005. 221 Eos: a remnant of a partially differentiated parent body? Astron. Astrophys. 442, 727–729.
Moynier, F., Day, J.M., Okui, W., Yokoyama, T., Bouvier, A., Walker, R.J., Podosek, F.A., 2012. Planetary-scale strontium isotopic heterogeneity and the age of volatile depletion of early solar system materials. Astrophys. J. 758, 45.
Nathues, A., et al., 2015. Exogenic olivine on Vesta from Dawn Framing Camera color data. Icarus 258, 467–428.
Nehru, C.E., Prinz, M., Delaney, J.S., Dreibus, G., Palme, H., Spettel, B., Wänke, H., 1983. Brachina: A new type of meteorite, not a chassignite. Proc. Lunar Planet. Sci. Conf. 14th J. Geophys. Res. 88, B237–B244.
Nehru, C.E., Prinz, M., Weisberg, M.K., Ebihara, M.E., Clayton, R.N., Mayeda, T.K., 1992. Brachinites: A new primitive achondrite group (abstract). Meteoritics 27, 267.
Nehru, C.E., Weisberg, M.K., Boesenberg, J.S., Kilgore, M., 2003. Tafassasset: A metal-rich primitive achondrite with affinities to brachinites (abstract). Lunar Planet. Sci. 34 (#1370).
Nehru, C.E., Boesenberg, J.S., Ebel, D.S., Weisberg, M.K., 2010. The Tafassasset primitive achondrite and relationship to chondrites. Meteorit. Planet. Sci. 45, #5305 (abstr.).
Neumann, W., Breuer, D., Spohn, T., 2012. Differentiation and core formation in accreting planetesimals. Astron. Astrophys. 543, A141, http://dx.doi.org/10.1051/0004-6361/201219157.
Newton, J., Franchi, I.A., Pillinger, C.T., 2000. The oxygen-isotopic record in enstatite meteorites. Meteorit. Planet. Sci. 35, 689–698.
Nittler, L.R., Gaidos, E., 2012. Galactic chemical evolution and the oxygen isotopic composition of the Solar System. Meteorit. Planet. Sci. 47, 2031–2048 (#5305).
Nyquist, L.E., Reese, Y., Wiesmann, H., Shih, C.-Y., Takeda, H., 2003. Fossil 26Al and 53 Mn in the Auska 881394 eucrite: evidence of the earliest crust on asteroid 4 Vesta Earth Planet. Sci. Lett. 214, 11–25.
O'Brien, D.P., Walsh, K.J., Morbidelli, A., Raymond, S.N., Mandel, A.M., 2014. Water delivery and giant impacts in the 'Grand Tack' scenario. Icarus 239, 74–84.
Onuma, N., Clayton, R.N., Mayeda, T.K., 1972. Oxygen isotope cosmothermometer. Geochim. Cosmochim. Acta 36, 169–188.
Pack, A., Herwartz, D., 2014. The triple oxygen isotope composition of the Earth mantle and understanding $\Delta^{17}O$ variations in terrestrial rocks and minerals. Earth Planet. Sci. Lett. 390, 138–145.
Pack, A., Toulouse, C., Przybilla, R., 2007. Determination of oxygen triple isotope ratios of silicates without cryogenic separation of NF_3-technique with application to analyses of technical O_2 gas and meteorite classification. Rapid Commun. Mass Spectrom. 21, 3721–3728.
Pack, A., Gehler, A., Süssenberger, A., 2013. Exploring the usability of isotopically anomalous oxygen in bones and teeth as palaeo-CO_2-barometer. Geochim. Cosmochim. Acta 102, 306–317.
Paton, C., Schiller, M., Bizzarro, M., 2013. Identification of an 84Sr-depleted carrier in primitive meteorites and implications for thermal processing in the solar protoplanetary disk. Astrophys. J. 763, L40.
Petaev, M.I., Barsukova, L.D., Lipschutz, M.E., Wang, M.-S., Ariskin, A.A., Clayton, R.N., Mayeda, T.K., 1994. The Divnoe meteorite: Petrology, chemistry, oxygen isotopes and origin. Meteoritics 29, 182–199.
Prettyman, T.H., Mittlefehldt, D.W., Yamashita, N., Lawrence, D.J., Beck, A.W., Feldman, W.C., McCoy, T.J., McSween, H.Y., Toplis, M.J., Titus, T.N., Tricarico, P., Reedy, R.C., Hendricks, J.S., Forni, O., Le Corre, L., Li, J.-Y., Mizzon, H., Reddy, V., Raymond, C.A., Russell, C.T., 2012. Elemental mapping by Dawn reveals exogenic H in Vesta's regolith. Science 338, 242–246.
Qin, L., Alexander, C.M.O'D., Carlson, R.W., Horan, M.F., Yokoyama, T., 2010a. Contributors to chromium isotope variation of meteorites. Geochim. Cosmochim. Acta 74, 1122–1145.
Qin, L., Rumble, D., Alexander, C.M.O'D., Carlson, R.W., Jenniskens, P., Shaddad, M.H., 2010b. The chromium isotope composition of Almahata Sitta. Meteorit. Planet. Sci. 45, 1771–1777.
Reddy, V., LeCorre, L., O'Brien, D.P., Nathues a. Cloutis, E.A., Durda, D.D., Bottke, W.F., Bhatt, M.U., Nesvorny, D., Buczkowski, D., Scully, J.E.C., Palmer, E.M., Sierks, H., Mann, P.J., Becker, K.J., Beck, A.W., Mittlefehldt, D., Li, J.-Y., Gaskell, R., Russell, C.T., Gaffey, M.J., McSween, H.Y., McCord, T.B., Combe, J.-P., Blewett, D., 2012. Delivery of dark material to Vesta via carbonaceous chondritic impacts. Icarus 221, 544–559.
Righter, K., Drake, M.J., 1996. Core formation in the earth's moon, mars and vesta. Icarus 124, 513–529.
Righter, K., Drake, M.J., 1997. A magma ocean on Vesta: Core formation and petrogenesis of eucrites and diogenites. Meteorit. Planet. Sci. 32, 929–944.

Righter, K., 2008. Siderophile element depletion in the angrite parent body (APB) mantle: due to core formation? (abstract). Lunar Planet. Sci. 39 (#1936).

Rivkin, A.S., Trilling, D.E., Thomas, C.A., DeMeo, F., Spahr, T.B., Binzel, R.P., 2007. Composition of the L5 mars trojans: neighbors, not siblings. Icarus 192, 434–441.

Roig, F., Gil-Hutton, R., 2006. Selecting candidate V-type asteroids from the analysis of the Sloan Digital Sky survey colors. Icarus 183, 411–419.

Roig, F., Nesvorný, D., Gil-Hutton, R., Lazzaro, D., 2008. V-type asteroids in the middle main belt. Icarus 194, 125–136.

Rosman, J.J.R., Taylor, P.D.P., 1998. Isotopic compositions of the elements 1997. Pure Appl. Chem. 70, 217–236.

Rubie, D.C., Gessman, C.K., Frost, D.J., 2004. Partitioning of oxygen during core formation on the Earth and Mars. Nature 429, 58–61.

Rubin, A.E., Mittlefehldt, D.W., 1993. Evolutionary history of the mesosiderite asteroid: A chronological and petrological synthesis. Icarus 101, 201–212.

Rubin, A.E., Kallemeyn, G.W., Wasson, J.T., 2002. A IAB-complex iron meteorite containing low-Ca clinopyroxene: Northwest Africa 468 and its relationship to lodranites and formation by impact melting. Geochim. Cosmochim. Acta 66, 3657–3671.

Rubin, A.E., 1983. Impact melt-rock clasts in the Hvittis enstatite chondrite breccias: implications for a genetic relationship between EL chondrites and aubrites. Proc. Lunar Planet. Sci. Conf. 14th J. Geophys. Res. 88 (Suppl), B293–B300.

Rubin, A.E., 2007. Petrogenesis of acapulcoites and lodranites: a shock-melting model. Geochim. Cosmochim. Acta 71, 2383–2401.

Rumble III, D., Hoering, T.C., 1994. Analysis of oxygen and sulphur isotope ratios in oxide and sulphide minerals by spot heating with a carbon dioxide laser in a fluorine atmosphere. Acc. Chem. Res. 27, 237–241.

Rumble, D., Farquhar, J., Young, E.D., Christensen, C.P., 1997. In situ oxygen isotope analysis with an excimer laser using F_2 and BrF_5 reagents and O_2 gas an analyte. Geochim. Cosmochim. Acta 61, 4229–4234.

Rumble, D., Miller, M.F., Franchi, I.A., Greenwood, R.C., 2007. Oxygen three-isotope fractionation lines in terrestrial silicate minerals: An inter-laboratory comparison of hydrothermal quartz and eclogitic garnet. Geochim. Cosmochim. Acta 71, 3592–3600.

Rumble, D., Irving, A.J., Bunch, T.E., Wittke, J.H., Kuehner, S.M., 2008. Oxygen isotopic and petrologic diversity among brachinites NWA 4872, NWA 4874, NWA 4882 and NWA 4969. How many ancient parent bodies? (abstract). Lunar Planet. Sci. 39 (#1974).

Rumble, D., Zolensky, M.E., Friedrich, J.M., Jenniskens, P., Shaddad, M.H., 2010. The oxygen isotope composition of Almahata Sitta. Meteorit. Planet. Sci. 45, 1765–1770.

Russell, C.T., Raymond, C.A., Coradini, A., McSween, H.Y., Zuber, M.T., Nathues, A., De Sanctis, M.C., Jaumann, R., Konopliv, A.S., preusker, F., Asmar, S.W., Park, R.S., Gaskell, R., Keller, H.U., Mottola, S., Roatsch, T., Scully, J.E.C., Smith, D.E., Tricarico, P., Toplis, M.J., Christensen, U.R., Feldman, W.C., Lawrence, D.J., McCoy, T.J., Prettyman, T.H., Reddy, R.C., Sykes, M.E., Titus, T.N., 2012. Dawn at Vesta: Testing the protoplanetary paradigm. Science 336, 684–686.

Ruzicka, A., Boynton, W.V., Ganguly, J., 1994. Olivine coronas, metamorphism, and the thermal history of the Morristown and Emery mesosiderites. Geochim. Cosmochim. Acta 58, 2725–2741.

Ruzicka, A., Snyder, G.A., Taylor, L.A., 1997. Vesta as the HED parent body: Implications for the size of a core and for large-scale differentiation. Meteorit. Planet. Sci. 32, 825–840.

Ruzicka, A., 2014. Silicate-bearing iron meteorites and their implications for the evolution of asteroidal parent bodies. Chem. Erde/Geochem. 74, 3–48.

Sahijpal, S., Soni, P., Gupta, G., 2007. Numerical simulations of the differentiation of accreting planetesimals with 26Al and 60Fe as the heat source. Meteorit. Planet. Sci. 42, 1529–1548.

Sakamoto, N., Seto, Y., Itoh, S., Kuramoto, K., Fujino, K., Nagashima, K., Krot, A.N., Yurimoto, H., 2007. Remnants of the early solar system water enriched in heavy oxygen isotopes. Science 317, 231–233.

Sanborn, M.E., Yin, Q.-Z., Irving, A.J., 2014. Isotope forensics utilizing $\triangle^{17}O$-ε ^{54}Cr systematic provide supporting evidence for differentiated parent bodies overlain by chondritic veneers (abstract). Lunar Planet. Sci. 45 (#2032).

Sanchez, J.A., Reddy, V., Kelley, M.S., Cloutis, E.A., Bottke, W.F., Nesvorný, D., Lucas, M.P., Hardersen, P.S., Gaffey, M.J., Abell, P.A., Corre, L.L., 2014. Olivine-dominated asteroids: Mineralogy and origin. Icarus 228, 288–300.

Sanders, I.S., Scott, E.R.D., 2012. The origin of chondrules and chondrites: Debris from low-velocity impacts between molten planetesimals. Meteorit. Planet. Sci. 47, 2170–2192.

Savage, P.S., Moynier, F., 2012. Silicon isotopic variation in enstatite meteorites: Clues to their origin and Earth-forming material. Earth Planet Sci. Lett. 361, 487–496.

Schiller, M., Paton, C., Bizzarro, M., 2015a. Evidence for nucleosynthetic enrichment of the protosolar molecular cloud core by multiple supernova events. Geochim. Cosmochim. Acta 149, 88–102.

Schiller, M., Connelly, J.N., Glad, A.C., Mikouchi, T., Bizzarro, M., 2015b. Early accretion of protoplanets inferred from a reduced inner solar system 26Al inventory. Earth Planet. Sci. Lett. 420, 45–54.

Schoenbeck, T.W., Kleine, T., Irving, A.J., 2006. Chemical and Hf-W compositions of CV metachondrite NWA 3133 (abstract). Lunar Planet. Sci. 37 (#1550).

Schrader, D.L., Franchi, I.A., Connolly Jr., H.C., Greenwood, R.C., Lauretta, D.S., Gibson, J.M., 2011. The formation and alteration of the Renazzo-like carbonaceous chondrites I: Implications of bulk-oxygen isotopic composition. Geochim. Cosmochim. Acta 75, 308–325.

Schrader, D.L., Nagashima, K., Krot, A.N., Ogliore, R.C., Yin, Q.-Z., Amelin, Y., Stirling, C.H., Kalenbach, A., 2016. Distribution of 26Al in the CR chondrite chondrule-forming region of the protoplanetary disk. Geochim. Cosmochim. Acta, http://dx.doi.org/10.1016/j.gca.2016.06.023.

Schultz, L., Palme, H., Spettel, B., Weber, H.W., Wänke, H., Michel-Levy, M.C., Lorin, J.C., 1982. Alan Hills A77081: An unusual stony meteorite. Earth Planet. Sci. Lett. 61, 23–31.

Scott, E.R.D., 1972. Chemical fractionation in iron meteorites and its interpretation. Geochim. Cosmochim. Acta 36, 1205–1236.

Scott, E.R.D., 1977a. Formation of olivine-metal textures in pallasite meteorites. Geochim. Cosmochim. Acta 41, 693–710.

Scott, E.R.D., 1977b. Geochemical relationships between some pallasites and iron meteorites. Min. Mag. 41, 265–272.

Scott, E.R.D., 2007. Impact origins for pallasites (abstract). Lunar Planet. Sci. 38 (#2284).

Scott, E.R.D., Taylor, G., 1990. Origins of pallasites at the core-mantle boundaries of asteroids (abstract). Lunar Planet. Sci. 21, 1119–1120.

Scott, E.R.D., Brearley, A.J., Haack, H., McCoy, T.J., 1994. Catastrophic fragmentation and reassembly of the parent body of the IVA iron and stony-iron meteorites. Meteoritics 29, 530–531.

Scott, E.R.D., Haack, H., Love, S.G., 2001. Formation of mesosiderites by fragmentation and reaccretion of a large differentiated asteroid. Meteorit. Planet. Sci. 36, 869–881.

Scott, E.R.D., Greenwood, R.C., Franchi, I.A., Sanders, I.S., 2009. Oxygen isotopic constraints on the origin and parent bodies of eucrites, diogenites, and howardites. Geochim. Cosmochim. Acta 73, 5835–5853.

Scott, E.R.D., Goldstein, J.I., Yang, J., Asphaug, E., Bottke, W.F., 2010. Iron and stony-iron meteorites and the missing mantle meteorites and asteroids (abstract). Meteorit. Planet. Sci. 45 (#5015).

Scott, E.R.D., Bottke, W.F., Marchi, S., Delaney, J.S., 2014. How did the mesosiderites form and do they come from Vesta or a Vesta-like body. Lunar Planet Sci., XLV. Lunar Planet. Inst., Houston #2260 (abstr.).

Scott, E.R.D., Keil, K., Goldstein, J.I., Asphaug, E., Bottke, W.F., Moskovitz, N.A., 2015. Early impact history and dynamical origin of differentiated meteorites and asteroids. In: Michel, P., DeMeo, F., Bottke, W.F. (Eds.), Asteroids IV. Univ. Arizona Press, Tucson, pp. 573–595.

Sharp, Z.D., 1990. A laser-based microanalytical method for the in situ determination of oxygen isotope ratios in silicates and oxides. Geochim. Cosmochim. Acta 54, 1353–1357.

Shearer, C.K., Burger, P.V., Neal, C., Sharp, Z., Spivak-Birndorf, L., Borg, L., Fernanded, V.A., Papike, J.J., Karner, J., Wadhwa, M., Gaffney, A., Shafer, J., Geisman, J., Atudorei, N.-V., Herd, C., Weiss, B.P., King, P.L., Crowther, S.A., Gilmour, J.D., 2010. Non-basaltic asteroidal magmatism during the earliest stages of solar system evolution: A view from Antarctic achondrites Graves Nunatak 06128 and 06129. Geochim. Cosmochim. Acta 74, 1172–1199.

Shirai, N., Humayan, M., Righter, K., 2009. Analysis of moderately siderophile elements in angrites: Implications for core formation of the angrite parent body (abstract). Lunar Planet. Sci. 40 (#2122).

Shukolyukov, A., Lugmair, G.W., 2006. Manganese-chromium isotope systematics of carbonaceous chondrites. Earth Planet. Sci. Lett. 250, 200–213.

Spicuzza, M.J., Valley, J.W., McConnell, V.S., 1998. Oxygen isotope analysis of whole rock via laser fluorination: An air-lock approach. Geol. Soc. Am. Abstr. Progr. 30, A80.

Spicuzza, M.J., Day, J.M.D., Taylor, L.A., Valley, J.W., 2007. Oxygen isotope constraints on the origin and differentiation of the Moon. Earth Planet. Sci. Lett. 253, 254–265.

Srinivasan, P., McCubbin, F.M., Agree, C.B., Ziegler, K., Sanborn, M.E., Yin, Q-Z., 2015. Petrologic and isotopic classifications of ungrouped achondrite NWA 8186: Implications for a CK/CV asteroidal origin. Lunar Planet. Sci. 46, Lunar Planet. Inst., Houston. #1472(abstr.).

Starkey, N.A., Franchi, I.A., Lee, M.R., 2014. Isotopic diversity in interplanetary dust particles and preservation of extreme ^{16}O-depletions. Geochim. Cosmochim. Acta 142, 115–131.

Starkey, N.A., Jackson, C.R.M., Greenwood, R.C., Parman, S., Franchi, I.A., Jackson, M., Fitton, J.G., Stuart, F.M., Kurz, M., Larsen, L.M., 2016. Triple oxygen isotopic composition of the high $^3He/^4He$ mantle. Geochim. Cosmochim. Acta 176, 227–238.

Stolper, E., 1977. Experimental: petrology of eucritic meteorites. Geochim. Cosmochim. Acta 41, 587–611.

Sunshine, J.M., Bus, S.J., Corrigan, C.M., McCoy, T.J., Burbine, T.H., 2007. Olivine-dominated asteroids and meteorites: distinguishing nebular and igneous histories. Meteorit. Planet. Sci. 42, 155–170.

Swindle, T.D., Kring, D.A., Burkland, M.K., Hill, D.H., Boynton, W.V., 1998. Noble gases, bulk chemistry, and petrography of olivine-rich achondrites Eagles Nest and Lewis Cliff 88763: Comparison to brachinites. Meteorit. Planet. Sci. 33, 31–48.

Tanaka, R., Nakamura, E., 2013. Determination of ^{17}O-excess of terrestrial silicate/oxide minerals with respect to Vienna Standard Mean Ocean Water (VSMOW). Rapid Commun. Mass Spectrom. 27, 285–297.

Tarduno, J.A., Cottrell, R.D., Nimmo, F., Hopkins, J., Voronov, J., Erickson, A., Blackman, E., Scott, E.R.D., McKinley, R., 2012. Evidence for a dynamo in the main group pallasite parent body. Science 338, 939–942.

Taylor, G.J., Keil, K., McCoy, T., Haack, H., Scott, E.R.D., 1993. Asteroid differentiation: Pyroclastic volcanism to magma oceans. Meteoritics 28, 34–52.

Taylor, G.J., 1992. Core formation in asteroids. J. Geophys. Res. 97, 14,717–14,726.

Tenner, T.J., Nakashima, D., Ushikubo, T., Kita, N.T., Weisberg, M.K., 2015. Oxygen isotope ratios of FeO-poor chondrules in CR3 chondrites: Influence of dust enrichment and H2O during chondrule formation. Geochim. Cosmochim. Acta 148, 228–250.
Thiemens, M.H., Heidenreich, J.E., 1983. The mass-independent fractionation of oxygen: a novel isotope effect and its possible cosmochemical implications. Science 219, 1073–1075.
Tholen, D.J., 1984. Asteroid Taxonomy from Cluster Analysis of Photometry PhD Thesis. University of Arizona.
Thomas, C.A., Binxel, R.P., 2010. Identifying meteorite source regions through near-earth object spectroscopy. Icarus 205, 419–429.
Tonks, W.B., Melosh, H.J., 1993. Magma ocean formation due to giant impacts. J. Geophys. Res. 98, 5319–5333.
Toplis, M.J., Mizzon, H., Monnereau, M., Forni, O., McSween, H.Y., Mittlefehldt, D.W., McCoy, T.J., Prettyman, T.H., De Sanctis, M.C., Raymond, C.A., Russell, C.T., 2013. Chondritic models of 4 Vesta: Implications for geochemical and geophysical properties. Meteorit. Planet. Sci., 1–16, http://dx.doi.org/10.1111/maps.12195.
Trinquier, A., Birck, J.-L., Allegre, C.J., 2007. Widespread ^{54}Cr heterogeneity in the inner solar system. Astrophys. J. 655, 1179–1185.
Trinquier, A., Elliot, T., Ulfbeck, D., Coath, C., Krot, A.N., Bizzarro, M., 2009. Origin of nucleosynthetic isotope heterogeneity in the solar protoplanetary disc. Science 324, 374–376.
Turrini, D., Combe, J.-P., McCord, T.B., Oklay, N., Vincent, J.-B., Prettyman, T.H., McSween, H.Y., Consolmagno, G.J., De Sanctis, M.C., Le Corre, L., Longobardo, A., Palomba, E., Russell, C.T., 2014. The contamination of the surface of Vesta by impacts and the delivery of the dark material. Icarus 240, 86–102.
Ueda, T., Yamashita, K., Kita, N., 2006. Chromium isotopic systematics of ureilite. In: 30th Antarctic Meteorite Symposium, National Institute of Polar Research, Tokyo (abstract), pp. 117–118.
Ulff-Møller, F., Choi, B.-G., Rubin, A.E., Tran, J., Wasson, J.T., 1998. Paucity of sulphide in a large slab of Esquel: New perspectives on pallasite formation. Meteorit. Planet. Sci. 33, 221–227.
Ushikubo, T., Kimura, M., Kita, N.T., Valley, J.W., 2012. Primordial oxygen isotope reservoirs of the solar nebula in chondrules in Acfer 094. Geochim. Cosmochim. Acta 90, 242–264.
Valley, J.W., Kita, N., 2005. Microanalysis of oxygen isotopes. Geochim. Cosmochim. Acta 69, Supplement 1, Goldschmidt Conference Abstracts A374.
Van Roosbroek, N., Debaille, V., Pittarello, L., Goderis, S., Humayun, M., Hecht, L., Jourdan, F., Spicuzza, M.J., Vanhaecke, F., Claeys, Ph., 2015. The formation of IIE iron meteorites investigated by the chondrule-bearing Mont Dieu meteorite. Meteorit. Planet. Sci. 50, 1173–1196.
Vernazza, P., Binzel, R.P., Thomas, C.A., DeMeo, F.E., Bus, S.J., Rivkin, A.S., Tokunaga, A.T., 2008. Compositional differences between meteorites and near-Earth asteroids. Nature 454, 858–860.
Vernazza, P., Zanda, B., Binzel, R.P., Hiroi, T., DeMeo, F.E., Birlan, M., Hewins, R., Ricci, L., Barge, P., Lockhart, M., 2014. Multiple and fast: The accretion of ordinary chondrite parent bodies. Astrophys. J. 791, 120 (22 pp.).
Walsh, K.J., Morbidelli, A., Raymond, S.N., O'Brien, D.P., Mandell, A.M., 2011. A low mass for Mars from Jupiter's early gas-driven migration. Nature 475, 206–209.
Wang, K., Jacobsen, S.B., 2016. Potassium isotopic evidence for a high-energy giant impact origin of the Moon. Nature, http://dx.doi.org/10.1038/nature19341.
Wang, P.-L., Rumble, D., McCoy, T.J., 2004. Oxygen isotopic compositions of IVA iron meteorites: Implications for thermal evolution derived from in situ ultraviolet laser microprobe analysis. Geochim. Cosmochim. Acta 68, 1159–1171.
Warren, P.H., Rubin, A.E., Isa, J., Brittenham, S., Ahn, I., Choi, B.-G., 2013. Northwest Africa 6693: A new type of FeO-rich, low Δ^{17}O poikilitic cumulate achondrite. Geochim. Cosmochim. Acta 107, 135–154.
Warren, P.H., 1985. The magma ocean concept and lunar evolution. Ann. Rev. Earth Planet. Sci. 13, 201–240.
Warren, P.H., 2011a. Stable-isotopic anomalies and the accretionary assemblage of the earth and mars: a subordinate role for carbonaceous chondrites. Earth Planet. Sci. Lett. 311, 93–100.
Warren, P.H., 2011b. Stable isotopes and the noncarbonaceous deriviation of ureilites: In common with nearly all the differentiated planetary materials. Geochim. Cosmochim. Acta 75, 6912–6926.
Wasson, J.T., 2013a. No magma ocean on Vesta (or elsewhere in the asteroid belt): Volatile loss from HEDs (abstract). Lunar Planet. Sci. 44 (#2836).
Wasson, J.T., 2013b. Vesta and extensively melted asteroids: why HED meteorites are probably not from Vesta. Earth Planet. Sci. Lett. 381, 138–146.
Wasson, J.T., Choi, B.-G., 2003. Main-group pallasites Chemical composition, relationship to IIIAB irons, and origin. Geochim. Cosmochim. Acta 67, 3079–3096.
Wasson, J.T., Chou, C.-L., 1974. Fractionation of moderately volatile elements in ordinary chondrites. Meteoritics 9, 69–84.
Wasson, J.T., Kallemeyn, G.W., 2002. The IAB iron-meteorite complex: A group, five subgroups, numerous grouplets, closely related, mainly formed by crystal segregation in rapidly cooling melts. Geochim. Cosmochim. Acta 66, 2445–2473.
Wasson, J.T., Rubin, A.E., 1985. Formation of mesosiderites by low-velocity impacts as a natural consequence of planet formation. Nature 318, 168–170.
Watters, T.R., Prinz, M., 1979. Aubrites: their origin and relationship to enstatite chondrites. Proc. Lunar Planet. Sci. Conf. 10, 1073–1093.
Weber, I., morlok, A., Bischoff, A., Hiesinger, H., Ward, D., Joy, K.H., Crowther, S.A., Jastrzebski, N.D., Gilmour, J.D., Clay, P.L., Wogelius, R.A., Greenwood, R.C., Franchi, R.C., Münker, C., 2016. Cosmochemical and spectroscopic properties of Northwest Africa 7325-A consortium study. Meteorit. Planet. Sci. 51, 3–30.
Weidenschilling, S.J., Cuzzi, J.N., 2006. Accretion dynamics and timescales: Relation to chondrites. In: Lauretta, D.S., McSween, H.Y. (Eds.), Meteorites and the Early Solar System II. University of Arizona Press, Tucson, p. 943 (pp 473–485).
Weidenschilling, S.J., 2011. Initial sizes of planetesimals and accretion of asteroids. Icarus 214, 671–684.
Weisberg, M.K., Prinz, M., Clayton, R.N., Mayeda, T.K., Grady, M.M., Pillinger, C.T., 1995. The CR chondrite clan. In: Proc. NIPR Symp. 8, NIPR, Toyko, pp. 11–32.
Weisberg, M.K., McCoy, T.J., Krot, A.N., 2006. Sytematics and evaluation of meteorite classification. In: Lauetta, D.S., McSween, H.Y. (Eds.), Meteorites and the Early Solar System II. University of Arizona press, Tucson, Arizona, pp. 19–52.
Weiss, B.P., Elkins-Tanton, L.T., 2013. Differentiated planetesimals and the parent bodies of chondrites. Annu. Rev. Earth Planet. Sci. 41, 529–560.
Weiss, B.P., Berdahl, J.S., Elkins-Tanton, L., Sabine, S., Lima, E.A., Carporzen, L., 2008. Magnetism on the angrite parent body and the early differentiation of planetesimals. Science 322, 713–716.
Wiechert, U., Hoefs, J., 1995. An excimer laser-based micro analytical preparation technique for in-situ oxygen isotope analysis of silicate and oxide minerals. Geochim. Cosmochim. Acta 59, 4093–4101.
Wiechert, U., Fiebig, J., Przybilla, R., Xiao, Y., Hoefs, J., 2002. Excimer laser isotope-ratio-monitoring mass spectrometry for in situ oxygen isotope analysis. Chem. Geol. 182, 179–194.
Wiechert, U.H., Halliday, A.N., Palme, H., Rumble, D., 2004. Oxygen isotope evidence for rapid mixing of the HED meteorite parent body. Earth Planet. Sci. Lett. 221, 373–382.
Wilson, L., Goodrich, C.A., Van Orman, J.A., 2008. Thermal evolution and physics of melt extraction on the ureilite parent body. Geochim. Cosmochim. Acta 72, 6154–6176.
Wood, B.J., Walter, M.J., Wade, J., 2006. Accretion of the Earth and segregation of its core. Nature 441, 825–833.
Yamaguchi, A., Clayton, R.N., Mayeda, T.K., Ebihara, M., Oura, Y., Miura, Y.N., Haramura, H., Misawa, K., Kojima, H., Nagao, K., 2002. A new source of basaltic meteorites inferred from North-west Africa 011 Science 296, 334–336.
Yamaguchi, A., Setoyanagi, T., Ebihara, M., 2006. An anomalous eucrite, Dhofar 007, and a possible genetic relationship with mesosiderites. Meteorit. Planet. Sci. 41, 863–874.
Yamaguchi, A., Barrat, J.-A., Greenwood, R.C., Shirai, N., Okamoto, C., Setoyanagi, T., Ebihara, M., Franchi, I.A., Bohn, M., 2009. Crustal partial melting on Vesta: Evidence from highly metamorphosed eucrites. Geochim. Cosmochim. Acta 73, 7162–7182.
Yamakawa, A., Yamashita, K., Makishima, A., Nakamura, E., 2010. Chromium isotope systematics of achondrites: Chronology and isotopic heterogeneity of the inner solar system bodies. Astrophys. J. 720, 150–154.
Yang, J., Goldstein, J.I., Scott, E.R.D., 2010. Main-group pallasites Thermal history, relationship to IIIAB irons, and origin. Geochim. Cosmochim. Acta 74, 4471–4492.
Young, E.D., Russell, S.S., 1998. Oxygen reservoirs in the early solar nebula inferred from an Allende CAI. Science 282, 452–455.
Young, E.D., Coutts, D.W., Kapitan, D., 1998. UV laser ablation and irm-GCMS microanalysis of ^{18}O/^{16}O and ^{17}O/^{16}O with application to a calcium-aluminim-rich inclusion from the Allende meteorite. Geochim. Cosmochim. Acta 62, 3161–3168.
Young, E.D., Ash, R.D., England, P., Rumble, D., 1999. Fluid flow in chondritic parent bodies: Deciphering the composition of planetesimals. Science 286, 1331–1335.
Young, E.D., Galy, A., Naghara, H., 2002. Kinetic and equilibrium mass-dependent isotope fractionation laws in nature and their geochemical and cosmochemical significance. Geochim. Cosmochim. Acta 66, 1095–1104.
Young, E.D., Zhang, K.K., Schubert, G., 2003. Conditions for pore water convection within carbonaceous chondrite parent bodies—implications for planetesimal size and heat production. Earth Planet. Sci. Lett. 213, 249–259.
Young, E.D., Kohl, I.E., Warren, P.H., Rubie, D.C., Jacobson, S.A., Morbidelli, A., 2016a. Oxygen isotopic evidence for vigorous mixing during the Moon-forming giant impact. Science 351, 493–496.
Young, E.D., Rumble, D., Freedman, P., Mill, M., 2016b. A large-radius high-mass-resolution multiple-collector isotope ratio mass spectrometer for analysis of rare isotopologues of O_2, N_2, CH_4 and other gases. Int. J. Mass spectrom. 401, 1–10.
Yu, Y., Hewins, R.H., Alexander, C.M.O'.D., Wang, J., 2003. Experimental: study of evaporation and isotopic mass fractionation of potassium in silicate melts. Geochim. Cosmochim. Acta 67, 773–786.
Yurimoto, H., Kuramoto, K., 2004. Molecular cloud origin for the oxygen isotope heterogeneity in the solar system. Science 305, 1763–1766.
Yurimoto, H., Kuramoto, K., Krot, A.N., Scott, E.R.D., Cuzzi, J.N., Thiemens, M.H., Lyons, J.R., 2007. Origin and evolution of oxygen isotopic compositions of the Solar System. In: Reipurth, V.V.B., Jewitt, D., Keil, K. (Eds.), Protostars and Planets. Univ. Arizona Press, pp. 849–862 (pp. 951).
Zellner, B., 1975. 44 Nysa: An iron-depleted asteroid. Astrophys. J. 198, L45–L47.
Zellner, B., Leake, M., Williams, J.G., Morrison, D., 1977. The E asteroids and the origin of the enstatite achondrites. Geochim. Cosmochim. Acta 41, 1759–1767.
Zhang, J., Dauphas n. Davis, A.M., Leya, L., Fedkin, A., 2012. The proto-Earth as a significant source of lunar material. Nat. Geosci. 5, 251–255.
Ziegler, K., Young, E.D., 2007. Pallasite, mesosiderite and HED Δ^{17}O signatures: the details (abstract). Lunar Planet. Sci. 38 (#2021).
Ziegler, K., Young, E.D., 2011. Oxygen isotope composition of main-group pallasites (abstract). Lunar Planet. Sci. 42 (#2414).

Zinner, E., 2014. Presolar grains. In: Holland, H.D., Turekian, K.K., Davis, A.M. (Eds.), Treatise on Geochemistry, vol. 1.4, 2nd edition. Elsevier Ltd., Oxford, pp. 181–213 (vol. ed.).

Zipfel, J., 2014. Merrilite in NWA 6901: Evidence for infiltration of a NWA 011-like melt (abstract). Meteorit. Planet. Sci. 49 (#5346).

Zolensky, M.E., Weisberg, M.K., Buchanan, P.C., Mittlefehldt, D.W., 1996. Mineralogy of carbonaceous chondrite clasts in HED achondrites and the Moon. Meteorit. Planet. Sci. 31, 518–537.

Zolensky, M., Herrin, J., Mikouchi, T., Ohsumi, K., Friedrich, J., Steele, A., Rumble, D., Fries, M., Sandford, S., Milam, S., Hagiya, K., Takeda, H., Satake, W., Kurihara, T., Colbert, M., Hanna, R., Maisano, J., Ketcham, R., Goodrich, C., Le, L., Robinson, G., Martinez, J., Ross, K., Jenniskens, P., Shaddad, M.H., 2010. Mineralogy and petrography of the Almahata Sitta ureilite. Meteorit. Planet. Sci. 45, 1618–1637.